TRAINING MANEUVER EVALUATION FOR REDUCED ORDER MODELING OF STABILITY & CONTROL PROPERTIES USING COMPUTATIONAL FLUID DYNAMICS

THESIS

Craig Curtis Porter, 2d Lt, USAF

AFIT-ENY-13-M-28

DEPARTMENT OF THE AIR FORCE
AIR UNIVERSITY

AIR FORCE INSTITUTE OF TECHNOLOGY

Wright-Patterson Air Force Base, Ohio

TRAINING MANEUVER EVALUATION FOR REDUCED ORDER MODELING
OF STABILITY & CONTROL PROPERTIES USING COMPUTATIONAL
FLUID DYNAMICS

THESIS

Presented to the Faculty

Department of Aeronautical Engineering

Graduate School of Engineering and Management

Air Force Institute of Technology

Air University

Air Education and Training Command

in Partial Fulfillment of the Requirements for the

Degree of Master of Science in Aeronautical Engineering

Craig Curtis Porter, BSAE

2d Lt, USAF

March 2013

AFIT-ENY-13-M-28

TRAINING MANEUVER EVALUATION FOR REDUCED ORDER MODELING
OF STABILITY & CONTROL PROPERTIES USING COMPUTATIONAL
FLUID DYNAMICS

Craig Curtis Porter, BSAE
2d Lt, USAF

Approved:

_____   _____

Christopher L. Martin, PhD (Chairman)   Date

_____   _____

Donald L. Kunz, PhD (Member)   Date

_____   _____

David Liu, PhD (Member)   Date

AFIT-ENY-13-M-28

Abstract

System identification has long been used as a tool for flight test engineers to characterize systems under test; however, the inputs to these characterization activities have previously been limited to wind tunnel and flight test data. There has been a recent effort to incorporate computational fluid dynamics (CFD) into the system identification process. An integral piece of the process is the simulation of training maneuvers utilizing CFD. Up until now, the suitability of particular training maneuvers has been assessed by comparing the reduced model to known results. This research strives to recommend a set of parameters to be used in determining *a priori* whether a training maneuver will be suitable under a particular set of flow conditions. As part of this study, regressor space parameters (RSPs) were proposed and evaluated for several maneuvers. Then, multivariate polynomial models for coefficient of lift, coefficient of drag and pitch moment coefficient were generated from the results of the training maneuvers simulated via CREATE-AV's flow solver, Kestrel. The resulting model-predicted coefficient values were then compared to CFD simulations of carefully selected comparison maneuvers, as measured by a set of suitable statistical metrics. Using the statistical analysis tool JMP$^{\circledR}$, the set of proposed RSPs were then analyzed in order to evaluate their utility in assessing the suitability of the training maneuvers. This research showed the reliability of certain RSPs to characterize training maneuver performance. Finally, lessons learned from this research were applied to improve upon current best practice training maneuvers.

iv

Acknowledgements

Table of Contents

List of Figures

Figure   Page

List of Tables

List of Symbols

List of Abbreviations

TRAINING MANEUVER EVALUATION FOR REDUCED ORDER MODELING OF STABILITY & CONTROL PROPERTIES USING COMPUTATIONAL FLUID DYNAMICS

I. Introduction

1.1   General Issue

Design changes late in the development cycle are a problem that have plagued military fighter aircraft for decades [15]. While analytical and numerical techniques can provide some insight into stability and control (S&C) characteristics at benign flight conditions, advanced flight conditions that include non-linearities are not easily calculated. Running the whole spectrum of dynamic maneuvers using a fully-turbulent Navier-Stokes solver in order to discover possible problems in the S&C characteristics is too costly.

Specific examples of costly late design changes are numerous. Consider the F-4, at high α (angle of attack); the aircraft lost directional stability. Over 200 F-4s were lost before a solution was found [14]. The 737NG had undesirable flaps-up stall characteristics; the aircraft experienced stick lightening during stall [14]. Northrop Grumman observed yaw departures and post stall lateral and directional instability with the F-5 which resulted in the loss of a flight test aircraft and large cost overruns and schedule delays [14].

There is a Department of Defense (DoD) and Air Force (AF) need to find and mitigate these risks earlier in the design cycle in order to save time, money and possibly human life.

1

1.2 Background

There are several avenues for obtaining the stability characteristics for an aircraft: analytical calculations, wind-tunnel testing, flight testing, and full computational simulations. System identification SID has been offered as methodology for utilizing computational simulations in order to produce simpler numerical calculations via reduced order models (ROMs) to calculate S&C characteristics. The paragraphs below will briefly discuss the benefits, challenges and limitations for each method.

Analytical results are useful in that the engineer can begin as early as desired in the design cycle. To some degree, analytical results guide aircraft designers early in the design; however, there is a limit to how much realism analytical techniques are able to incorporate. Non-linearities and complex configurations make analytical techniques an impractical choice.

Wind tunnel testing has the advantage of being able to produce a wide variety of aerodynamic results as soon as a configuration is determined. Unfortunately, there are also limitations to the results wind tunnel testing can obtain. A wind tunnel's testing parameters are unlikely to span the entire operational envelope of a fighter aircraft. Coefficients such as coefficient of lift (C_L) and coefficient of drag (C_D) are easy to obtain for static flight conditions; the ability to evaluate these coefficients for dynamic maneuvers is limited. This difficultly reduces the applicability of wind tunnel testing to obtaining derivatives such as $C_{N_{\dot{\alpha}}}$ which is the partial derivative of C_N, to $\dot{\alpha}$.

The benefits to flight testing are numerous. While the data provided by flight testing are absolutely invaluable, the downside is that a fully functional prototype must be used, and the prototype will likely only be available very near the end of the design process. At that point, considerable time, effort and money have been invested in the project. Major design changes at a late stage are detrimental to

the project, particularly on modern aircraft, where stealth characteristics are highly dependent on aircraft geometry. If sudden instabilities are found during the test, it can be dangerous for the aircraft as well as the pilot. Additionally, flight test has the downside of being the most expensive of all the methods.

Computational results also have the benefit of yielding results once a geometry is decided upon–after the necessary grid generation, grid refinement study and solution time. However, there are limitations to computational fluid dynamics (CFD) that need to be understood and taken into account in order to gain useful results. The quality of the outputs is heavily dependent upon the quality of the inputs. Grid and geometry need to be suitable; otherwise, no matter how highly accurate the solver may be, the results will be inaccurate or misleading. Also, while CFD has come a long way in the recent past, there is still no "perfect solution." Any computational simulation is going to include a variety of assumptions, the biggest of which will be the model used to simplify the turbulent structures in the flow. One benefit is that CFD has the capability to provide insight into aircraft behavior much earlier in the design cycle. Finally, there is also the benefit of having data everywhere in the flow, as opposed to a few select areas with sensors as in the case of wind tunnel and flight testing.

Put simply, SID is a process by which, using known inputs and measured outputs, a complex system is reduced to a simplified model. In this work, the known inputs are parameters such as α and Q. The measured outputs will be the stability coefficients: C_L, C_D and C_M. Previously, system identification had been considered a useful process only for flight test and wind tunnel testing data. From *System Identification, Theory and Practice*: "There are also analytic methods to find the aerodynamic function dependencies, such as computational fluid dynamics (CFD)...although these methods work well in some cases, typically for low angles of attack and low rotational

rates, the best aerodynamic predictions are obtained using experimental methods." [20] However, there has been a recent effort to incorporate the usefulness of the reduced order models obtained from the system identification process utilizing the early availability of solutions gained from high fidelity-CFD.

1.3   Research Objectives

This project seeks to further the current understanding of using CFD in the system identification process in order to gain S&C insight earlier in the design process and to refine the methods to do so. In order for CFD to be used in the system identification process, one must simulate an appropriate training maneuver. First, it is necessary to determine what makes a good training maneuver. Furthermore, is there a way to evaluate the suitability of a training maneuver *a priori*?

The focus of this project is to determine a set of parameters that will indicate if a training maneuver is suitable prior to simulating the maneuver. Previous research by Butler [5], has been conducted in order to find parameters to be used prior to running a maneuver. However, the parameters were not throughly evaluated. The objective of this research is to refine and create parameters in order to estimate future model prediction accuracy.

The path ahead for this project consists of several stages. The first stage is to take the proposed parameters from Butler [5] and use them to assess the suitability of benchmark maneuvers. The next stage is to simulate the different training maneuvers using CFD and create ROMs from the outputs using SID software. The next step is to conduct CFD simulations of the comparison maneuvers and compare the model-predicted coefficients to the CFD coefficients using selected metrics. Once that is completed, the next step is to evaluate how effectively the regressor space parameters (RSPs) measured the prediction capability of the models. If necessary, optimize

and generate new parameters to improve the prediction capability of the models. Once satisfied with the parameters, the final step is to create an ideal maneuver that optimizes those RSPs.

1.4 Road Map

Chapter I discussed a brief overview of the background and objectives to this research. Chapter II will discuss in more detail the background information for this research. Topics will include the governing equations, turbulence theory, turbulence modeling, stability & control, system identification, previous research and Kestrel. Chapter III will discuss the overall methodology used in the research. Topics in Chapter III include the grid convergence study method, initial regressor space parameters, training maneuvers, comparison maneuvers, reduced order model generation and analysis. Chapter IV will discuss the results of the methods employed in Chapter III, to include the grid convergence study, the regressor space parameters. Chapter IV will detail the comparison of the reduced order model predictions vs the CFD simulated results, and how those results motivated the design of two additional training maneuvers. Chapter V will tie all the results together to make conclusions.

II. Background

This chapter will present a discussion of necessary background material for this research. Computational fluid dynamics is a major component of this research, and as such, the background includes a discussion on the governing equations for CFD as well as turbulence modeling and the expected flow features to be modeled. Also, this chapter will include a discussion on system identification and the process by which a reduced order model is created. Finally, previous research in this area of study will be examined, and its application to this research will be discussed.

2.1 Computational Fluid Dynamics

Computational fluid dynamics is the combination of physics, numerical calculations, and computer science with the goal of simulating fluid flows. In its infancy, CFD was used to solve the 2-D Euler equations. With the increase in computing power and technology, the simulations have become more and more advanced. Using multigrid, multiblock, implicit time integration and unstructured grids, CFD has evolved to simulate highly unsteady, viscous flows around complex geometries. The following discussion will focus on the finite volume discretization of the Navier-Stokes equations with turbulence modeling, as that is the focus of this research.

2.1.1 Governing Equations

There are three governing relations for general CFD computations, which are further simplified depending on the fidelity of the solution. The three relations, as shown in Blazek [4], are the conservation of mass, conservation of momentum, and conservation of energy equations. In finite volume methods, the domain is discretized as cells, and the amount of the conserved quantities crossing the boundaries is known

as the flux. Taking the three conservation relations in integral form and combining them results in the integral form of the Navier-Stokes equations

$$\frac{\mathrm{d}}{\mathrm{d}t} \int \vec{W}\, \mathrm{d}\Omega \; + \; \oint (\vec{F}_c - \vec{F}_v)\, \mathrm{d}S \; = \; \int_\Omega \vec{Q} \mathrm{d}\Omega, \tag{2.1.1}$$

where $\vec{W}$ is a vector of conserved variables, $\vec{F}_c$ is a vector of convective fluxes, $\vec{F}_v$ is a vector of viscous fluxes, $\vec{Q}$ is a collection of source terms, $d\Omega$ is the differential volume and dS is the differential surface.

The conservative variables are given in the vector

$$\vec{W} = \begin{bmatrix} \rho \\ \rho u \\ \rho v \\ \rho w \\ \rho E \end{bmatrix}. \tag{2.1.2}$$

where ρ is the flow density, u is the x-direction velocity, v is the y-direction velocity, w is the z-direction velocity and E is the energy. The convective fluxes are represented by the vector

$$\vec{F}_c = \begin{bmatrix} \rho V \\ \rho u V \,+\, n_x p \\ \rho v V \,+\, n_y p \\ \rho w V \,+\, n_z p \\ \rho H V \end{bmatrix}, \tag{2.1.3}$$

7

where $V = \vec{U} \cdot \hat{n}$ and is the contravariant velocity. The viscous fluxes are given by

$$
\vec{F}_v = \begin{bmatrix} 0 \\ n_x \tau_{xx} + n_y \tau_{xy} + n_z \tau_{xz} \\ n_x \tau_{yx} + n_y \tau_{yy} + n_z \tau_{yz} \\ n_x \tau_{zx} + n_y \tau_{zy} + n_z \tau_{zz} \\ n_x \theta_x + n_y \theta_y + n_z \theta_z \end{bmatrix}, \tag{2.1.4}
$$

where

$$
\begin{aligned}
\theta_x &= u\tau_{xx} + v\tau_{xy} + w\tau_{xz} + k\frac{dT}{dx} \\
\theta_y &= u\tau_{yx} + v\tau_{yy} + w\tau_{yz} + k\frac{dT}{dy}. \\
\theta_z &= u\tau_{zx} + v\tau_{zy} + w\tau_{zz} + k\frac{dT}{dz}
\end{aligned} \tag{2.1.5}
$$

where τ_{ij} is the sheer stress tensor. Lastly, the source terms are given by

$$
\vec{Q} = \begin{bmatrix} 0 \\ \rho f_{e,x} \\ \rho f_{e,y} \\ \rho f_{e,z} \\ \rho \vec{f}_e \cdot \vec{v} + \dot{q}_h \end{bmatrix}. \tag{2.1.6}
$$

2.1.2 Turbulence Theory and Modeling

A rigorous definition of turbulence is hard to give; however, there are some distinct characteristics to help identify turbulent flow. Unsteady, irregular, and apparently random fluctuations are three distinct characteristics. Flow is likely to make the switch to turbulence when small perturbations are amplified. The sources of these

8

small perturbations can be free stream turbulence, surface roughness and vibrations. The transition to turbulence depends on the Reynolds number. At low Reynolds number, the viscous forces damp out the instabilities caused by turbulence. At high Reynolds numbers, inertial disturbances are sufficiently damped and none are amplified. Another characteristic of turbulent flow is the large range of length and time scales. This is due to the energy cascade in turbulence. At the largest scales, the inertial effects dominate the flow behavior, but then large scale vortices are stretched by the flow gradients which transfers energy to smaller scales. When the smallest scale is reached, the energy is dissipated as heat due to viscosity-dominated eddies. Kolmogorov assumed that the smallest scales are universal throughout different flows and that the equilibrium between energy states from the large turbulence scales can be modeled as

$$\epsilon = -\frac{dk}{dt},\tag{2.1.7}$$

where ϵ is the TKE dissipative rate and k is the turbulent kinetic energy. The Kolmogorov length scale is expressed as

$$\eta_k = \left(\frac{\nu^3}{\epsilon}\right)^{1/4}.\tag{2.1.8}$$

Close to the wall, the viscous effects dominate and $u^+ = y^+$, this relation is the law of the wall. While $y^+ < 5$ that region is known as the viscous sublayer. Then there is the log layer which is shown by equation (2.1.9).

The log law states that the average velocity of the flow is proportional to the log of the distance from the wall. The log wall is given by

$$u^+ = \frac{1}{\kappa}log(y^+) + \beta.\tag{2.1.9}$$

where κ is the Karman constant and β is another constant. The various sublayers are shown in Figure 1.
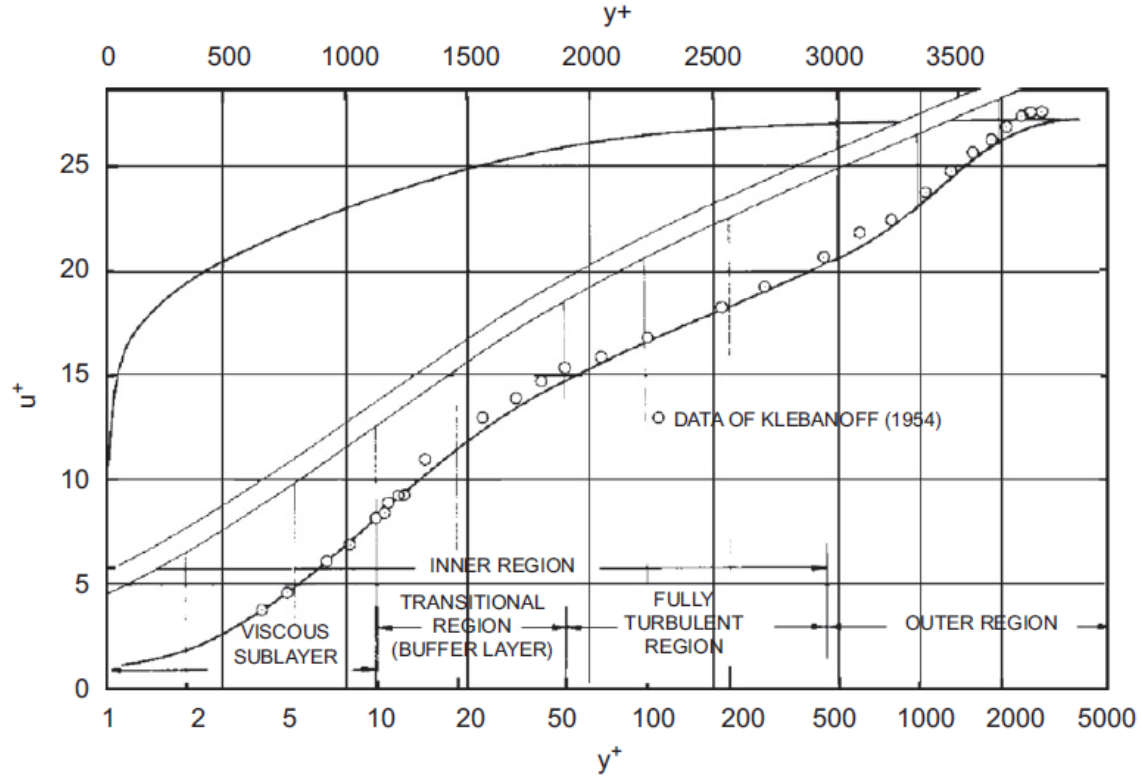
Figure 1. Mean velocity distribution across a turbulent boundary layer [6]

There are several different ways to model turbulence. Within these turbulence models there are several levels of approximation. The highest fidelity is direct numerical simulation (DNS). In decreasing order of fidelity, there are large eddy simulation (LES) methods, and there are Reynolds averaged Navier-Stokes (RANS) methods. Bridging the gap between RANS and LES are hybrid methods, the most popular being delayed detached eddy simulation (DDES). The range of turbulence modeling techniques is shown in Figure 2

DNS is the most accurate of all types of turbulence models, as it resolves all of the turbulent length scales. This direct simulation of the smallest turbulence scales requires that the grid must be able to resolve down to the Kolmogorov length scale
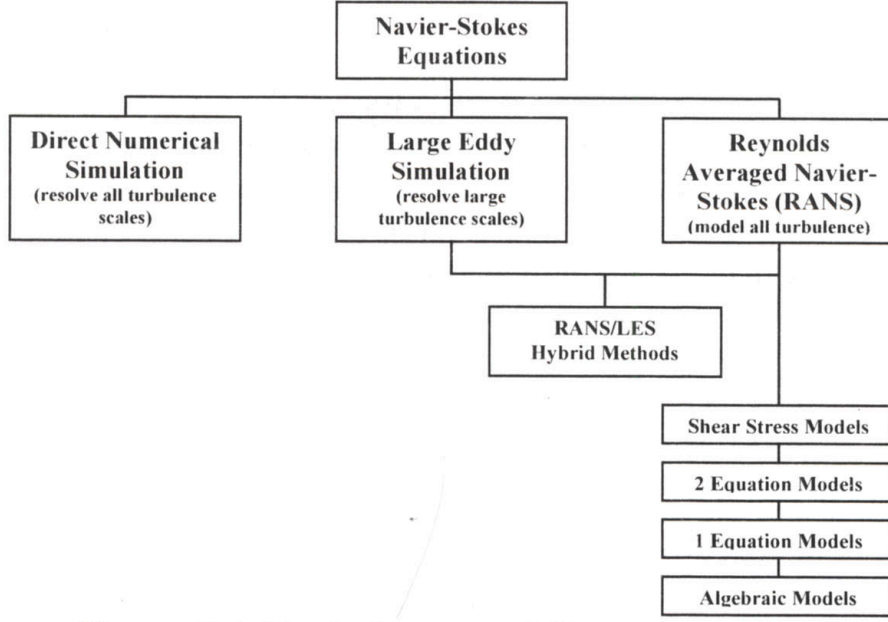
Figure 2. Turbulence modeling approaches [9]

shown in Equation (2.1.8) [4]. The small grid spacing that results translates to an extremely large computational cost, which causes DNS to be unpractical for most uses. [9]

In LES, the flow is split into two categories, small and large length scales. LES will model the small scales, or subgrid-scales, while simulating the large length scales. Since LES does not simulate the small length scales, it does not have the same computational costs as DNS. However, in order to accurately resolve the boundary layer, the grid spacing must be small. The grid scales must be so small that it currently drives the computational costs of LES solutions out of general engineering use. [9]

RANS models substitute an average and a fluctuating value into the N-S equations and then make some qualifying assumptions. An example of the decomposed values for incompressible flow is

$$u_i = \bar{u}_i + u'. \qquad (2.1.10)$$

After the substitution is made, the resulting equations are simplified. The Reynolds

11

stresses are the terms that arise in the Navier-Stokes equations when Reynolds-averaging the momentum equations. The term is given by $\tau_{ij}^{Re} = \bar{\rho}\overline{u_i' u_j'}$. The Reynolds stresses add six new unknowns into the equations that represent the transfer of momentum due to turbulent fluctuation.

Within the scope of RANS turbulence models there are several different methods. The least complex model is known as a 0-equation model. It is an algebraic model that calculates μ based solely on local flow conditions. A 1/2-equation model solves an ODE only in space to model the transport of turbulence. A 1-equation model solves one partial differential equation (PDE) of the transport of turbulence. The Spalart-Allmaras (SA) is an example of a 1-equation model. Two-equation models use two turbulence quantities which are modeled by two conservation equations. Examples of 2-equation models are $k - \epsilon$ and $k - \omega$.

The Boussinesq gradient transport hypothesis, also known as the eddy-viscosity hypothesis, is an example of a 0-equation model. The hypothesis assumes that the fluxes due to the turbulent fluctuations could be solved in a similar manner to molecular transport [4]. It assumes that turbulent shear stress depends linearly on the mean rate of strain. These transport laws can then be defined by analogy from kinetic principles. By applying this hypothesis to the Reynolds-averaged stresses, the viscosity term is replaced by a sum of the laminar viscosity and the turbulent viscosity. Eddy-viscosity is not valid in flows with sudden change of mean strain rate, significant streamline curvature, rotation and stratification, ducts and turbomachinary and flows with boundary layer separation and reattachment.

The SA model solves the Reynolds-averaged Navier-Stokes equations and a transport equation for the turbulence model. The SA model has the benefit of being local, numerically forgiving, and rapid convergence to steady state [29]. Reynolds-averaged equations are the most simplified case for solving turbulence models, if not the most

widely used. The comparatively low computational cost make RANS methods applicable to engineering applications; however, RANS models have difficulty predicting transition to turbulence. [9]

A discussion on turbulence modeling would be incomplete without addressing DDES [28]. Detached eddy-simulation (DES) and its latest form, DDES (Delayed Detached eddy-simulation) are a hybrid of RANS and LES. DES and DDES depend upon a defined distance to the wall. Near the wall the models act as a RANS model. When the distance is larger than a predefined distance, the model acts as an LES model. DDES has modifications to ensure that RANS turbulence modeling methods are utilized in the boundary even in situations with thick boundary layers as well as areas of shallow separation. The need for DDES is motivated by the grids in Figure 3, where the bottom grids would initiate a switch to LES methods before the edge of the boundary layer.

2.1.3 Expected Flow Features

It is important to determine what type of flow will result in the simulation. If the expected flow regime is nearly inviscid, it is prudent and responsible to run an Euler solver rather than a turbulent Navier-Stokes solver in order to save computation time, effort and resources. Flight conditions play an important role, as around Mach 0.8 the aircraft or airfoil will enter into the transonic regime. Likewise, at very high Mach numbers there is also the possibility for additional thermophysical considerations.

The angle of attack will play a large factor in the expected results. In high angle of attack (AoA) flows, highly separated turbulent flow is to be expected. In the case of this research, the SID process has risen out of the need to model the highly non-linear, separated flow regime. Therefore, highly separated flow is expected in this research.
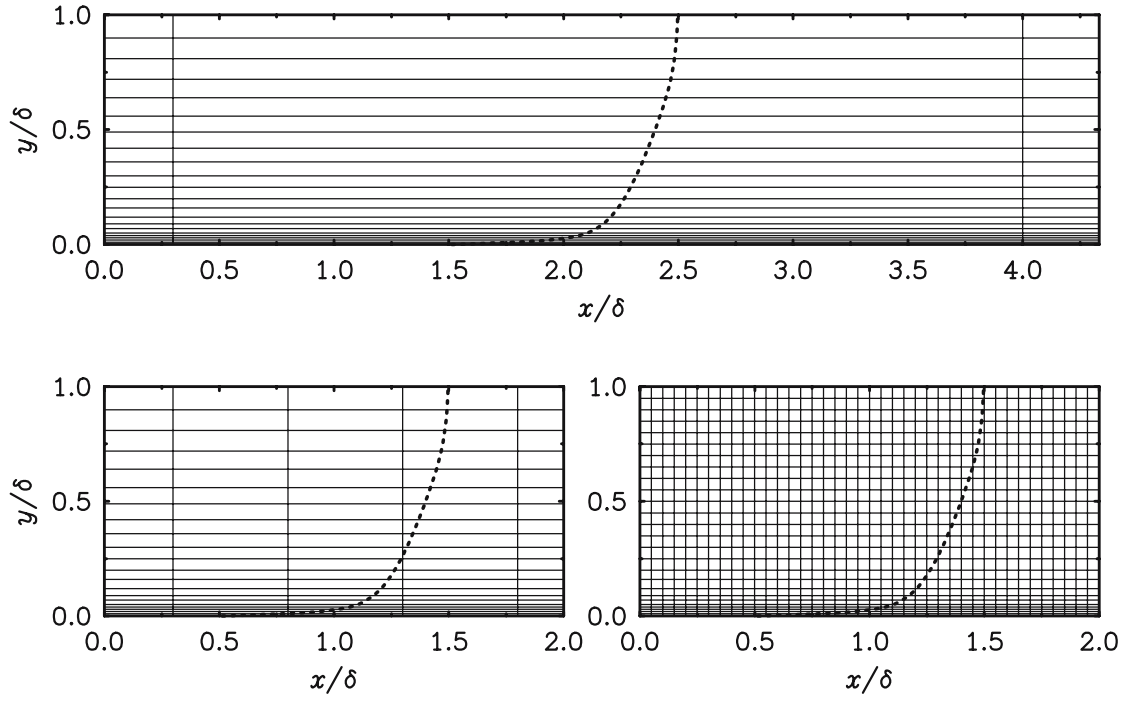
Figure 3. Grids in a boundary layer. *Top* natural DES; *left* ambiguous spacing; *right* LES. *Dotted lines* mean velocity. δ is the boundary-layer thickness [**27**]

Vorticity is a measure of the rotation that exists within a flow. One source for this rotation is viscosity. In the Navier-Stokes equations, viscous effects arise from the viscous stresses, given by Equation (2.1.4). It is viscosity that creates the flow phenomena necessary for flight, such as boundary layers. Viscosity also introduces simulation challenges such as turbulence and separation. For a high fidelity simulation, solving for viscous effects are very important.

Separation occurs as the boundary layer which forms on an airfoil can no longer remain attached and then separates from the airfoil. The point at which separation occurs is dependent on several factors, including angle of attack, Mach number and Reynolds number.

2.2   Stability and Control

Stability and control are fundamental to the successful flight of all aircraft. As this project aims to determine these important parameters, a brief introduction regarding the factors to be used will be presented here.

To say that an aircraft is stable in part means to say that the aircraft is statically stable. It is important that when an aircraft is perturbed, it returns to a trim position. This is shown in Figure 4. When the aircraft is trimmed, the static stability is measured in what the initial reaction of the system is to a perturbation. If there is a change in α, such as a gust, and there is no aerodynamic moment, it is said to be neutrally stable. If the aircraft returns to trim, it is said to be stable. If the aircraft diverges from the trim conditions it is said to be unstable.

While static stability is the initial tendency of a system to respond to a perturbation, dynamic stability is how the system responds to the perturbation over time. Dynamic stability is shown in Figure 5. Case A is positive static stability as it initially tends towards the pre-displacement state. Case A is also dynamically stable as over
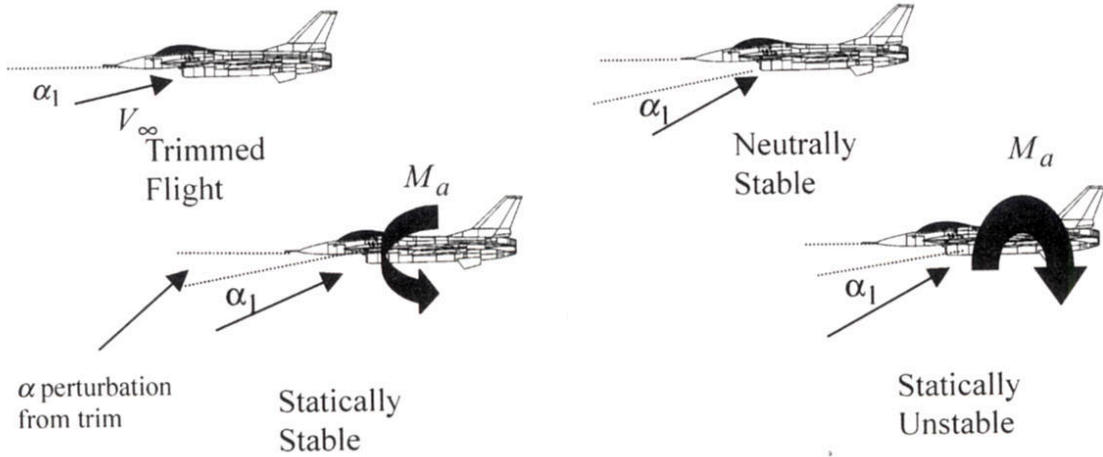
Figure 4. Stability conditions [31]

time it returns to the equilibrium state. Case B has neutral dynamic stability as over time it does not tend towards equilibrium nor does it diverge. Case C has negative dynamic stability because it diverges from the equilibrium state.

Insight into the static stability of an aircraft can be gained through the stability coefficients that are common to aeronautical engineering practices. The most commonly sought are the coefficient of lift (C_L), coefficient of drag (C_D), and the pitch moment coefficient (C_M). These coefficients are given by equation (2.2.1)

$$
\begin{aligned}
C_L &= \frac{L}{\frac{1}{2}\rho U_\infty^2 S}, \\
C_D &= \frac{D}{\frac{1}{2}\rho U_\infty^2 S}, \\
C_M &= \frac{M}{\frac{1}{2}\rho U_\infty^2 S L_{ref}}.
\end{aligned}
\tag{2.2.1}
$$

2.3 System Identification

System Identification is one of three main problems dealt with in aircraft dynamics and control. Referencing Figure 6, the three problems are [20]:

16
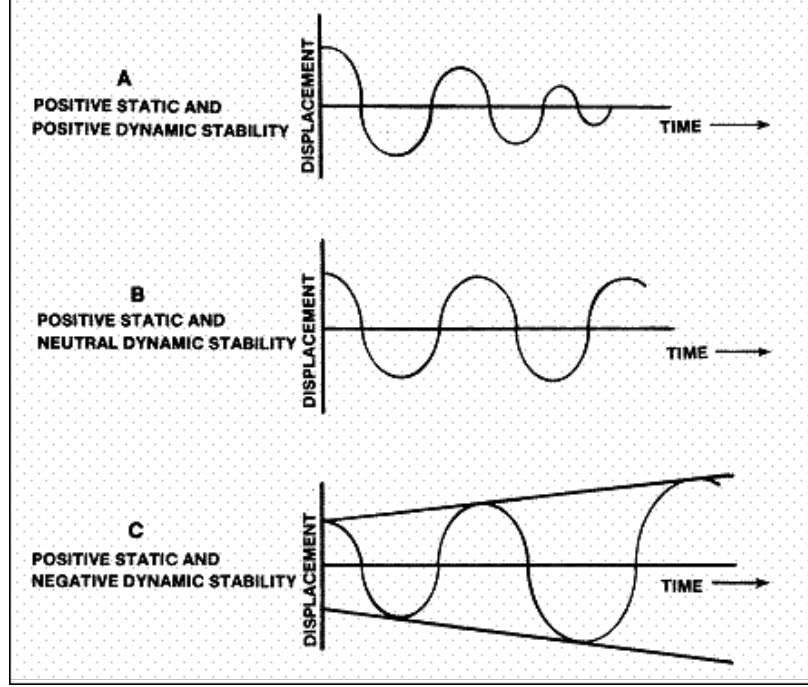
Figure 5. Dynamic stability [3]

1) Simulation: given input **u** and the system **S**, find the output y

2) Control: given the system **S** and the output **y**, find the input **u**

3) System Identification: given the input **u** and output **y**, find the system **S**

The methods used to determine the system are referred to as regression methods. Regression methods are a statistical technique for modeling the relationships between variables. For example, for this research a potential model could be

$$C_L = c_1 + c_2\alpha + c_3\alpha Q + c_4\alpha^2 Q \tag{2.3.1}$$

where c_n refers to a constant coefficient.

Multivariate orthogonal functions are used to decorrelate the modeling functions. Multivariate orthogonal functions are preferred over ordinary least-squares linear regression techniques as it is difficult to identify the difference between correlated
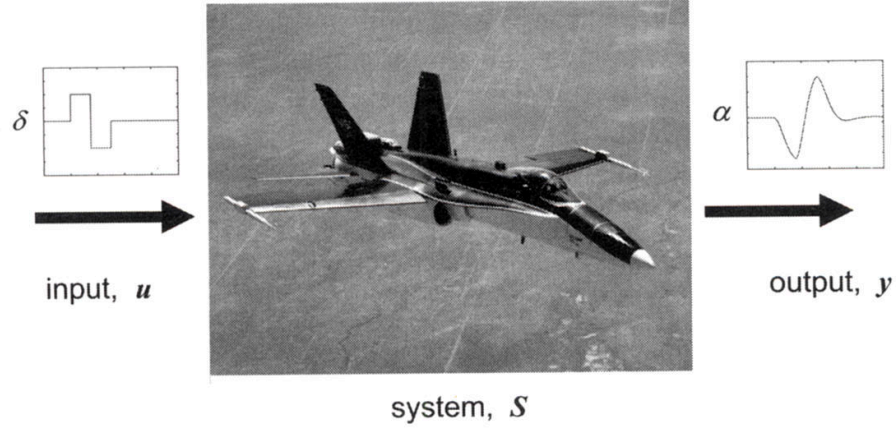
Figure 6. Aircraft dynamics and control [20]

polynomials obtained through ordinary least-squares. Once the regressors have been orthogonalized, the model output can be defined as [20]

$$\vec{z} = P\vec{a} + \vec{\nu} \tag{2.3.2}$$

where $\vec{z}$ is a vector of model output, $\vec{a}$ is a vector of unknown parameters, P is a matrix of orthogonal regressors and $\vec{\nu}$ is a vector of measurement errors.

Put simply, SID is a process by which using known inputs and measured outputs, a complex system is reduced to simplified model. In this work, the known inputs are parameters such as α and Q. The measured outputs ($\vec{z}$) will be the stability coefficients, C_L, C_D, and C_M. System identification is a method by which to create a mathematical model of a system using input data. This method with CFD incorporated is outlined in Figure 7.

There are three main steps of system identification: model training, model validation and model prediction. Model training is the act of creating the mathematical model in which a CFD simulation known as a training maneuver is conducted. A training maneuver is a dynamic computational run that spans a desired portion of the regressor space. The dynamic motion of the training maneuver is tailored such that

18
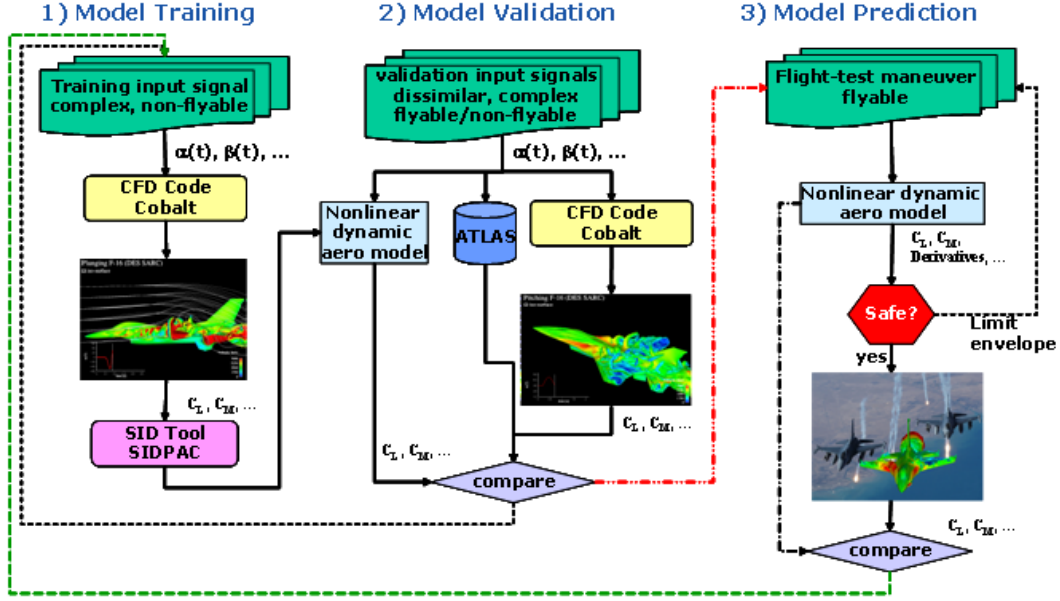
Figure 7. The system identification process [18]

the aircraft will experience a useful range of regressors $(\alpha, \dot{\alpha}, Q, \dot{Q}, \text{etc})$ values that the system is likely to experience in the comparison or virtual flight test maneuver stage.

After the dynamic computational run is conducted, the reduced order mathematical model is fashioned to the resulting data. This mathematical model is created by examining the stability characteristics calculated during the training maneuver. The model will predict the stability characteristics that are observed in a real-world flight test maneuver. There are several different methods that can be used to create the reduced order mathematical model. Two of these are multivariate polynomial and radial basis functions. Multivariate polynomial (MVP) models take the regressors and raise them to various powers along with coefficients for each regressor which must be uniquely determined for a given system. Radial basis functions (RBFs) are based on

the radius from an origin or center and generally take the form [25]

$$y(x) = \sum_{i=1}^{n} w_i \phi(||x - x_i||) \qquad (2.3.3)$$

where $y(x)$ is the approximate function, w_i is a weighted coefficient and x_i is a moving center.

Once the model is created, the SID process moves to Step 2, model validation. Model validation involves demonstrating that the reduced mathematical model gives the correct coefficient values. The reduced model is applied to a validation maneuver and compared against known data or comparison data such as validated CFD results.

If the model passes Step 2, it moves on to Step 3, model prediction. The model is then used to predict what will happen to an aircraft in a variety of maneuvers. This point in the process is also known as "virtual flight testing", as the model can be used to "fly" an aircraft. Using the developed model, time and money will be saved by reducing the amount of actual flight testing. Virtual flight testing can indicate to engineers which test points could be trouble for an aircraft and which ones will not be an issue.

In the past, wind tunnel testing and flight testing have been the sole inputs to system identification methods. A variety of tools have been developed based of this type of input, such as NASA's System Identification Programs for Aircraft (SIDPAC) [23]. These tools focus on the creation of the reduced model and generation of the resulting data, whereas the input data is up to the user. It is only recently that CFD has been explored as an approach for system identification.

2.4 Previous Research

This section will look into the research that has previously been conducted in this field and will consider the potential shortcomings of that research.

2.4.1 Computational Methods for Stability and Control and Early Attempts

The various problems discussed in Section 1.1 were taken from a NASA-sponsored symposium of S&C and CFD engineers known as Computational Methods for Stability and Control (COMSAC). The purpose of COMSAC was to foster the discussion between CFD and S&C engineers, fields that have traditionally has been considered two separate domains. The conclusions drawn from the symposium include [14]:

- The inaccurate prediction of aerodynamic S&C parameters have negative effects on the life-cycle costs of all types of aircraft. Generally, the inaccurate predictions lead developers to resort to "fly-and-try" fixes.

- Improved prediction of the impact of separated flow on the aircraft as well as the character of the separated flow should be a priority.

- There is an attitude of skepticism in using CFD for aircraft S&C issues in both the S&C and CFD communities.

- The success of advanced CFD methods will depend on the demonstration of success for generic as well as specific aircraft configurations.

- CFD shortfalls need to be high priority targets in encouraging the use of CFD for aircraft S&C tasks.

- There was immense value in sharing the experiences of CFD specialists and S&C specialists at the symposium.

- NASA Ames suggested that a "brute force" method be utilized [15] to fill a S&C database. However, it was determined to require "30 different angles-of-attack, 20 different Mach numbers, and 5 different side-slip angles, each for a number of different geometry configurations or control surface deflections [7]". Due to the large computational cost, this technique would need to rely on Euler solutions which was deemed undesirable.

2.4.2 Training Maneuvers

The training maneuver is the maneuver which will provide the model with the known inputs and the measured system outputs. In this case, the system is the mathematical model of the physical system utilized in the CFD solver. It is very important that the training maneuver be able to accurately excite the desired phenomena and be general enough to be accurate over a wide range of scenarios. Previous research has been conducted at Air Force Institute of Technology (AFIT) [5], United States Air Force Academy (USAFA) [19] [16], the Air Force Seek Eagle Office (AFSEO) [21] [12] [13], and by collaboration [15] [17].

McDaniel, et al. [15], examined a wide variety of training maneuvers and discussed how well the resulting SID models compared. The first maneuver examined was a pulse plunge. A pulse plunge is a maneuver designed to isolate the effects of α and $\dot{\alpha}$ by having the aircraft vertically drop in the flow. This maneuver highlights one of the benefits of using CFD as a training maneuver, the ability to simulate maneuvers that are un-flyable, meaning pilots in actual aircraft cannot command these maneuvers. Using an MVP model, the results were reasonably accurate to the validation maneuver. The next maneuver is the Schroeder sweep plunge maneuver, which is based off of the excitation of a specified bandwidth through the summation of discrete frequencies. Validated against a DC chirp maneuver, the Schroeder sweep

plunge ROM compared accurately. The model was also validated against a pitch plunge maneuver where the model less accurately followed the validation maneuver; however, it was noted to model unsteady behavior well. Then, the authors trained a model using the DC chirp maneuver previously run and compared it against sinusoidal pitch motions. The resulting models were comparable for a maneuver on the frequency of 2.0 Hz, but did not compare as well for 1.0 Hz or for 0.5 Hz. The conclusion was that using the DC chirp input the MVP model could model the system response. However, the predictive capability was limited by the range of phenomena excited by the training maneuver.

Dean, et al. [13], expanded the work done in McDaniel, et al. [15], above by then comparing the results against solutions obtained by Lockheed Martin's 6DOF simulator, ATLAS. Using the DC chirp maneuver as the input, the SID model was compared to a sinusoidal pitching maneuver at varying frequencies. At 1 Hz, the model had trouble predicting C_L but was accurate at predicting C_M. As the frequency was increased to 2 Hz and 3 Hz the model was able to better predict C_L. However, it was not able to correctly predict the shape of the hysteresis curve. It should be noted that the authors did state that the SID models take seconds to compute after the CFD training maneuver is complete and are able to offer a general idea of the flight characteristics, whereas ATLAS data is only available after significant testing.

Dean, et al. [12], again expanded upon previous work by comparing SID models created from CFD against a flight test maneuver conducted by a F-16C aircraft. The maneuver was a 2.5-g wind-up turn to the right. The authors used a pitch chirp maneuver to train the SID model. Lift was accurately predicted, while drag was observed to be inaccurate at low angles of attack. The cause was determined to be a lack inadequate training data with low Q. A combined training maneuver with

rotational and translational motion to cover the whole regressor space was devised. The results for drag were much better after using the combined training maneuver.

Some work has also been done by Lillian, et al. [21], to use proper orthogonal decomposition to recreate the pressure distribution on a wing which could then extract the stability coefficients.

Jeans, et al. [17], examined the ability of DDES simulations to predict a known non-linear aerodynamic effect on a generic fighter geometry. Then the group used SID techniques to created ROMs and noted how well the dynamic maneuvers and the ROMs compared. The DDES simulations could reliably predict the instability within a given frequency range and the SID models were able to reproduce constant frequency maneuvers. The SID techniques were also found to have worked better with higher frequency maneuvers. The authors then examined how the SID models faired using the chirp maneuver as the training maneuver. The group found that, using the SID model created from the chirp motion, it would be reasonable to extract the rolling moment for a dynamic roll maneuver with frequencies between 1.43 and 5.86 Hz. It was also found that the SID models indicate unwanted aerodynamic behavior at low frequencies which would alert an S&C engineer to investigate further.

Dean, et al. [11], used a multitude of chirp maneuvers on the F-22 and compared them to the Lockheed Martin AVTEST data. The training maneuver utilizes a chirp in three directions. The created models were then compared against a variety of maneuvers such as static data, wind-up turn to the right, and a pitch-up stall maneuver. On the whole, the reduced order models were shown to compare well with the validation data.

Jirasek, et al. [19], looked again to study which types of training maneuvers produced desirable results—specifically, the chirp, DC chirp, spiral, DC spiral, piecewise linear spirals, DC piecewise linear spirals, Schroeder, plunging, Fresnel integral, inte-

grated DC chirp, integrated spiral, integrated DC spiral, integrated piecewise linear spiral, integrated DC piecewise linear spiral, and integrated Schroeder maneuvers. The authors found that the spiral- and chirp-based maneuvers saw better lift and pitching moment predictions. Schroeder-based models resulted in favorable predictions at lower frequencies and unfavorable predictions at higher frequencies. For static data, the spiral maneuver gave the best results. Spiral-based models were unable to accurately predict sinusoidal motion while the chirp and Schroeder maneuvers were better suited to that task. The authors state that aside from static and very low frequency data, the chirp maneuvers resulted in the most robust and reliable models.

2.4.3   Model Generation

There has also been research into which type of models to use, as well as which regressors are important. Two models considered are MVP and RBF.

In addition to the training maneuvers discussed above, McDaniel, et al. [15], looked at several type of models, specifically multivariate polynomial, linear regression, and stepwise regression models. The results showed that a multivariate polynomial equation better compared with the CFD results using the pitch plunge maneuver.

Researchers at the United States Air Force Academy compared MVP models created from SIDPAC software and radial basis function models to wind tunnel data collected on site on the X-31 [18]. The conclusion of the authors was that the SIDPAC and RBF models were equally as good at predicting the static and dynamic pitching coefficients.

Dean, et al. [11], examined the use of Kestrel as a computational resource compared to Cobalt. The study also compared MVP and RBF models created using Kestrel as a input compared against Lockheed Martin performance data. C_L and C_D were found to compare well for both models, while C_M was found to be highly

25

inaccurate. Minor differences between the models can be seen in the results, however, the differences did not lead the authors to make a claim as to which model is more accurate.

2.4.4 Reduced Order Modeling of Fighter Aircraft

Butler [5] began to look into the objective of optimizing training maneuvers based upon a series of what he called "grid metrics." Another objective was to improve upon the chirp maneuver such that it was better suited for zero Q situations. The study was conducted using a full-scale F-16 grid. Two problems were encountered which did not enable him to reach any conclusions regarding the training maneuver parameters. First, the time required to run a full-scale F-16 grid in a dynamic maneuver is large, and requires a vast amount of computational resources. Running several maneuvers only compounds this problem. Thus, the work of Butler was only brought to partial completion. Second, the comparison and training maneuvers did not test the limits of the aircraft. The non-linear coefficients were not extremely complicated, making it hard for there to be much of a difference between the different models. Also, it was speculated in this study that the comparison maneuvers were too similar to the training maneuvers and that his training maneuvers were too long, giving the model more than ample amount of data.

Butler's work was invaluable to the author in the pursuit of this research and several scripts created as a result of that work were either used or adopted for the author's use. Also, the initial RSPs used in the present study were initially proposed as 'grid metrics' in Butler's work.

2.5 Kestrel

The CFD software chosen for use in this research is the product of the Computational Research and Engineering Acquisition Tools and Environments (CREATE) program known as Kestrel. Kestrel began as an initiative from the Department of Defense High Performance Computing Modernization Program (DoD HPCMP) [24]. The air vehicles portion of the CREATE program is known as CREATE-AV. The job of the CREATE-AV team was to determine where HPC can positively affect the acquisition process. It was determined that Kestrel, a virtual fixed wing aircraft simulation tool, could accomplish this goal.

Kestrel is a modular program, with the three most noteworthy modules or components being the Kestrel Infrastructure Executive (KIE), the Kestrel User Interface (KUI), and the flow solver, kAVUS, a derivative of the Air Vehicles Unstructured Solver (AVUS).

KIE is the executive component of Kestrel. It is the job of KIE to push data from one component to the next. KIE however does not ever actually utilize the data calculated from the other components. KIE is event based, and with each event, pushes the correct data pointer to the component. The tasks of KIE are outlined below [8].

a) Read the XML input file and parse the data out to each component

b) Initiate all of the components.

c) Connect all data consumers with producers.

d) Handle the publication and subscription of all events.

e) Handle all component exceptions.

f) Shut down all components.

The simplified architecture for Kestrel is shown in Figure 8.
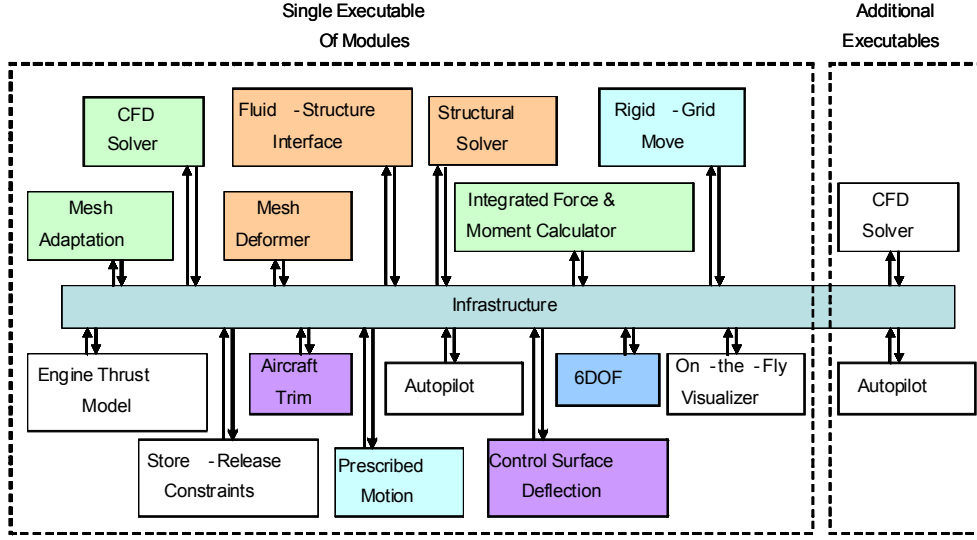
Figure 8. Kestrel architecture [24]

KUI is the interface utilized by the user for several functions. As of Kestrel v3.0, KUI has 6 modes including job input, boundary condition, mesh manipulation, post processing and preferences. The most utilized is the job input mode. Here the user can clearly see all the different 'knobs' that are used to set up a CFD simulation and does not have to interpret the meanings of various entries from a cryptic job file.

The most important component for this work is kAVUS, which is fundamentally a finite-volume, cell-centered, first-order in space and time, mesh-aligned exact Riemann solver of Godunov. kAVUS is modified to achieve second-order accuracy in time and space. Second-order accuracy in space is patterned after van Leers MUSCL scheme where the flow state is assumed to vary linearly within each cell [8]. First- and second- order temporal accuracy is achieved via the unconditionally stable point-implicit scheme as implemented by Tomaro et al [30]. Also, second-order accurate viscous terms are added such that kAVUS is a Navier-Stokes solver. For turbulence

28

modeling, kAVUS provides the following options: SA, SA + DDES, SARC, SARC + DDES, Mentor, Mentor + SST and Mentor + SST + DDES [8].

III. Methodology

3.1   Overview

The methodology of this thesis is organized into distinct stages. First, the grid to be used for the remainder of the research was created and validated. The initial RSPs were utilized from previous research conducted by Jed Butler [5]. These RSPs will be assessed against a known robust training maneuver and known low quality training maneuvers in order to determine which RSPs provide insight into the training maneuver development process. The analysis will be conducted according to the overarching process depicted in Figure 9.
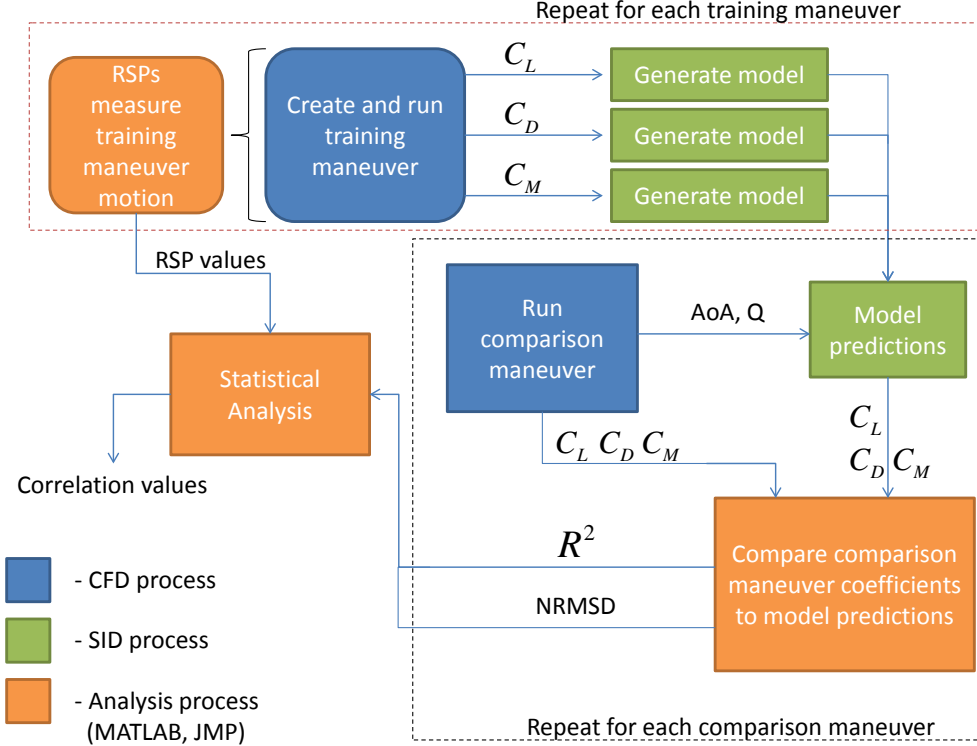
Figure 9. Methodology flow chart

First, the training maneuvers will be created and measured using the regressor space parameters. Then, the training maneuver will be simulated. The resulting co-

efficients will be used to generate the reduced order models. The process is repeated for each training maneuver; then, the comparison maneuvers are generated. The motion of the comparison maneuvers is fed into the ROMs to predict the comparison maneuver coefficients. That prediction is compared against the actual comparison maneuver CFD coefficients. The metrics R^2 and normalized root mean squared deviation (NRMSD) are then used to gage the accuracy of the predictions. The statistical analysis program JMP®is then used to examine the relationship between the metrics and the RSPs. All computation runs will be conducted at Mach 0.5 at 10,000 ft.

3.2   Computational Resources and Hours

This research was conducted using two computational resources. The first is the Nordic cluster on-site at AFIT. Nordic is a 12-node system comprised of 16 processors per node with two of the processors having 32 processors. The processors are 2.4 GHz Opteron with 64 (or 128) GB of RAM per node [1]. Jobs are submitted via the Portable Batch System (PBS).

The second computational resource, Raptor, is a cluster available through the U.S. Air Force Research Laboratory (AFRL) DSRC. Raptor has 2732 nodes with 32 cores per node. Each core is an AMD Opteron 64-bit running at 2.5 GHz with 64 GB of memory [2].

Table 1. Computational hours

Cluster	Total CPU-Hours	Grid Study
Raptor	402919	0
Nordic	14500	14500

Table 1 shows the number of computational hours used on each cluster.

3.3   Time Step and Grid Density Study

The geometry chosen for this project is a NACA 64A010 airfoil. The decision to utilize a 2-D case was made in order to reduce computational time and to allow for greater simplicity in the grid generation by removing difficulties associated with complex geometries. A C-Grid topology was chosen for ease of generation which allowed for a simple way to modify the grid refinement. The downside of a C-Grid topology is that there are very refined cells where there is no need for them. However, due to the already low computational expense of a 2-D airfoil case, the additional computational expense of these 'extra' cells is not a significant consideration. The coarse grid can be seen in Figure 10. The approach taken to conduct the time-step and grid density study is discussed in Cummings et al [10].
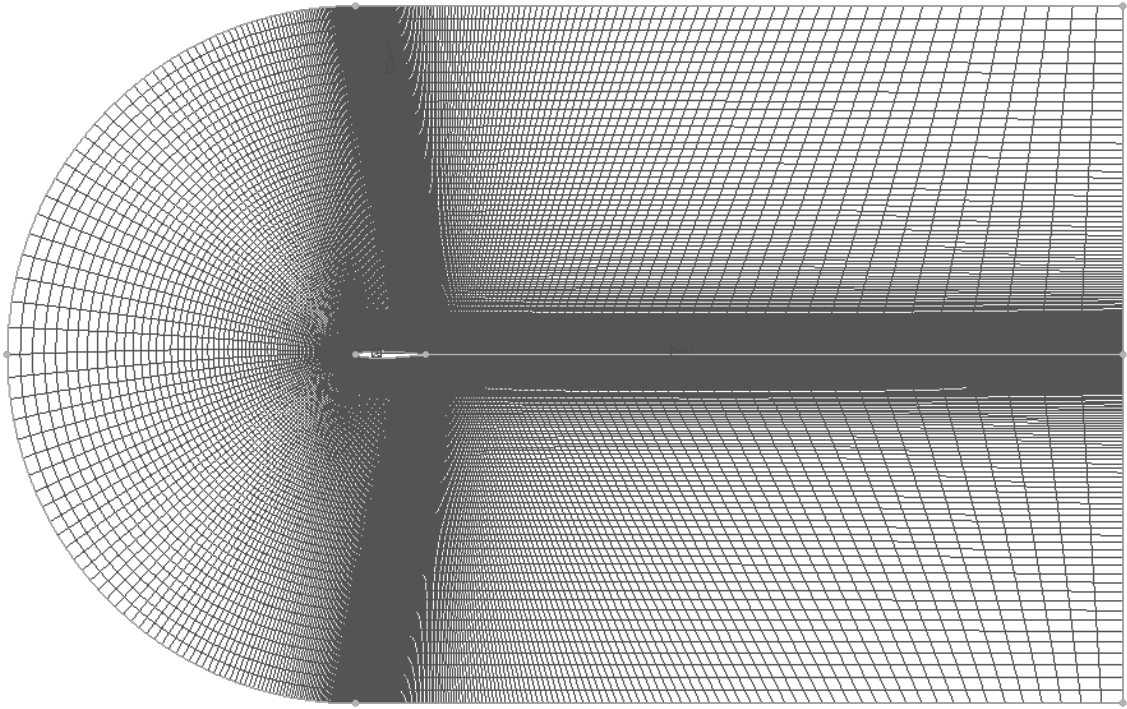
Figure 10. Coarse C-grid

The process above involves creating multiple grids of varying refinement. Likewise,

several time steps are also chosen using varied level of temporal refinement. The rule of thumb of $\Delta t^* = 0.01$ is a convenient medium or fine level of refinement, where

$$\Delta t^* = \frac{\Delta t U_\infty}{L} \ . \tag{3.3.1}$$

Then, the multiple grids are run in a systematic way using the different time steps. From the resulting data, a spectral analysis is conducted. Using the normal force coefficient, a single-sided amplitude spectrum is calculated from the frequencies observed in the simulation results. The dominant frequency is pulled from this analysis, and the Strouhal number is calculated by

$$St = \frac{fL}{U_\infty} \ , \tag{3.3.2}$$

where f is the frequency, L is a characteristic length and U_∞ is the flow velocity. In this study, L is taken as the chord length of 1 ft. The wave number is assumed to be the inverse of the Strouhal number and is plotted versus the time step. Ideally, a plot like Figure 11 will result.

Looking at Figure 11, it can be seen that the fine grid and the medium grid converge upon the same Strouhal number at a time step of 2.5e-05 seconds. It would be reasonable then to run either of the grids at this time step, however for computational expense considerations, it would be wise to run with the lower grid density. The main takeaway from this graph, however, is the combined effect that grid density and time step had on the solution. If time step were only varied for a single grid density, one may find a converging Strouhal number, but in the case of the coarse grid in Figure 11, the convergence behavior would be inconsistent with a fine grid. If one were to vary grid density for a set time step, one may observe convergence, again for an incorrect value as is seen by the second largest time step in Figure 11. The coarse and

33
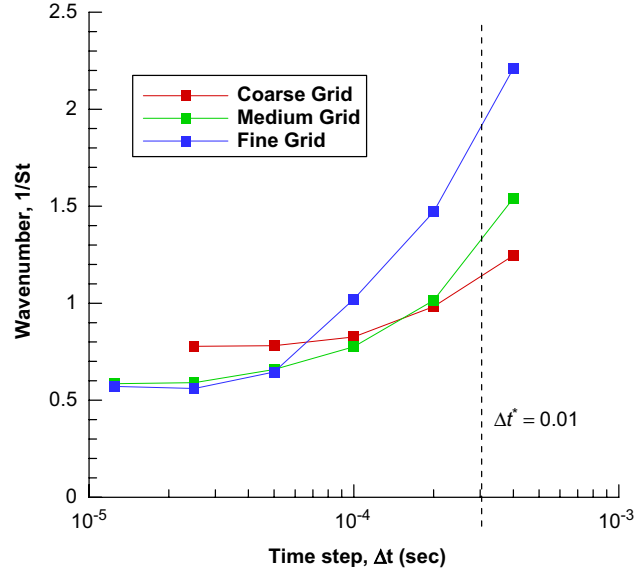
Figure 11. Time-step and grid convergence study for NACA 6512 airfoil [10]

Table 2. Grids used for NACA 64A010 airfoil

Grid Density	No. of Points	No. of Cells	No. of Faces on Surface
Coarse	124,125	123,504	248
Medium	298,850	297,804	498
Fine	802,575	801,054	498

medium grid converge on a Strouhal number, and a researcher may decide to run at that larger time step on the coarse grid which we can clearly see is insufficient, as proven by the data.

Table 2 shows summary data for the three grids created for the grid density study. Table 3 shows the different time steps and corresponding Δt^* and required number of iterations for 0.4 seconds of simulation time, solutions were obtained on each of the three grid densities from Table 3 to the required number of iterations for 0.4 seconds of runtime. Then, a spectral analysis was calculated from the resulting data in order to find the dominant frequency in the flow.

The spectral analysis was conducted using a fast Fourier transform on the fluctu-

34

Table 3. Time steps used for NACA 64A010 airfoil

Time Step (s)	Δt^*	Number of Iterations for 0.4 sec
5.0e-5	0.0260	8,000
2.5e-5	0.0134	16,000
1.25e-5	0.0060	32,000
6.25e-6	0.0030	64,000

ation of the coefficient of normal force from the time-averaged coefficient of normal force. The MATLAB®code used for the analysis has been placed in Appendix A.1 for the reader's reference

The results of the time step and grid density study are discussed in Section 4.1.

3.4   Initial Regressor Space Parameters

The basis for this research started with the "metrics" provided in Butler [5] which have been re-designated as regressor space parameters (RSPs) in this work. The RSPs are presented below and are calculated using the MATLAB®script contained in Appendix A.3.

The goal of the RSPs is to quantify how the training maneuver covers the regressor space. For this research the regressor space is considered to be the Q values between ±75 (deg/s) and AoA values between -5 and 20 degrees.

The RSPs require that the regressor space be discretized for the calculations. For some of the RSPs, the discretization refinement could have a large effect on the results. The question is how fine to discretize the regressor space. While pinpointing an exact number is not imperative (at the appropriate range the same trends should be seen in the data) finding the appropriate range is important. A large discretization of Q would result in inflated low or zero Q metrics. However, too small a discretization would exclude values from zero Q calculations that are practically zero. A value of

35

Q and AoA discretization of 0.1 was recommended by Jed Butler [5] and is used in the present work as well. The first RSP is an overall look at how well the maneuver covers the desired regressor space.

$$RSP_1 = \frac{\# \; of \; cells \; with \; data \; points}{Total \; \# \; of \; cells} \tag{3.4.1}$$

The second metric looks to measure the extent to which the extrema of the regressor space are captured by the maneuver.

$$RSP_2 = \frac{\# \; of \; cells \; on \; boundary \; with \; data \; points}{Total \; \# \; of \; cells \; on \; boundary} \tag{3.4.2}$$

The first two RSPs examine how many points total the TM covers. However, it could be important to know how well the data is spread throughout the regressor space. This is intended to be captured by Equation (3.4.3). In this RSP, each column of discretized AoA values is counted and then normalized by the column with the maximum number of points in it. Then, the standard deviation is taken across all the columns. In an evenly spaced training maneuver, the standard deviation would be large, as all columns would have the same number of points. The column and row descriptors refer to the format presented later on.

$$RSP_3 = std \left[\left(\begin{array}{l} \frac{\# \; cells \; with \; data \; points}{Total \; \# \; of \; cells} \Big|_{AoA \; column1} \\[2mm] \frac{\# \; cells \; with \; data \; points}{Total \; \# \; of \; cells} \Big|_{AoA \; column2} \\[1mm] \vdots \\[1mm] \frac{\# \; cells \; with \; data \; points}{Total \; \# \; of \; cells} \Big|_{last \; AoA \; column} \end{array} \right) \div max \; value \right] \tag{3.4.3}$$

A similar measure of evenness is calculated using the rows of Q values instead of columns of AoA values. This is shown in Equation (3.4.4).

$$RSP_4 = std \left[\left(\begin{array}{c} \frac{\# \, cells \, with \, data \, points}{Total \, \# \, of \, cells} \Big|_{Q \, row1} \\ \frac{\# \, cells \, with \, data \, points}{Total \, \# \, of \, cells} \Big|_{Q \, row2} \\ \vdots \\ \frac{\# \, cells \, with \, data \, points}{Total \, \# \, of \, cells} \Big|_{last \, Q \, row} \end{array} \right) \div max \, value \right] \qquad (3.4.4)$$

The next three RSPs focus on the region where there is zero pitch rate. The first metric shown in Equation (3.4.5) simply takes the percentage of AoA cells with zero Q rate.

$$RSP_5 = \frac{\# \, of \, cells \, at \, 0 \, Q \, with \, data \, points}{Total \, \# \, of \, cells \, at \, 0 \, Q} \times 100 \qquad (3.4.5)$$

The next RSP shown in Equation (3.4.6) attempts to give more weight to training maneuvers having more data points in zero Q states. This hopes to allow the solution a chance to dampen out dynamic effects and gives a more accurate steady state solution. However, it is possible to inflate this number by providing a large amount of zero Q data that does not add any more accuracy to the model. This RSP is also influenced by the timestep of the simulation.

$$RSP_6 = \frac{Total \, \# \, of \, data \, points \, at \, 0 \, Q}{Total \, \# \, of \, cells \, at \, 0 \, Q} \qquad (3.4.6)$$

Similar to the standard deviation RSPs above, this next RSP, shown in Equation (3.4.7), takes the standard deviation but only for AoA values with zero Q.

$$RSP_7 = std \left(\frac{cell_1, \, cell_2, \, cell_3, \, ...last \, cell}{Max \, Value} \right)_{@ \, 0 \, Q} \qquad (3.4.7)$$

The next set of three RSPs looks to capture the amount of low Q data. Low Q

data can be defined in many ways. In previous research, Bulter [5] looked at how different definitions affected the output of these RSPs. From his research, common results were seen when the cutoff was 5 deg/s, 10 deg/s and 20 deg/s whereas 50 deg/s seemed to show slightly different results. Based on that trend, the cutoff for this research will be 20 deg/s. The RSP for unique cells with low Q is shown in Equation (3.4.8).

$$RSP_8 = \frac{\#\ of\ cells\ at\ low\ (not\ 0)\ Q\ with\ data\ points}{Total\ \#\ of\ cells\ at\ low\ (not\ 0)\ Q} \times 100 \qquad (3.4.8)$$

The RSP that takes into account all the data points at low Q is shown in Equation (3.4.9)

$$RSP_9 = \frac{Total\ \#\ of\ data\ points\ at\ low\ (not\ 0)\ Q}{Total\ \#\ of\ cells\ at\ low\ (not\ 0)\ Q} \qquad (3.4.9)$$

The last of the low Q RSPs looks at the standard deviation in a similar fashion to the equations prior. This RSP is shown in Equation (3.4.10).

$$RSP_{10} = std \left(\frac{cell_1,\ cell_2,\ cell_3, ...last\ cell}{Max\ Value} \right)_{@\ low\ (not\ 0)\ Q} \qquad (3.4.10)$$

The last set of the initial RSPs look at the opposite side of the 20 deg/s cutoff, and are considered 'high' Q. These RSPs are computed using the same process as the last three RSPs, but using the high Q instead of the low Q values. These three RSPs are shown in Equations (3.4.11) - (3.4.13).

$$RSP_{11} = \frac{\#\ of\ cells\ at\ high\ Q\ with\ data\ points}{Total\ \#\ of\ cells\ at\ high\ Q} \times 100 \qquad (3.4.11)$$

$$RSP_{12} = \frac{Total\ \#\ of\ data\ points\ at\ high\ Q}{Total\ \#\ of\ cells\ at\ high\ Q} \qquad (3.4.12)$$

$$RSP_{13} = std \left(\frac{cell_1, \; cell_2, \; cell_3, \; ...last \; cell}{Max \; Value} \right)_{@ \, high \, Q} \tag{3.4.13}$$

3.5 Training Maneuvers

Unlike the previous research [5], the aim of this project is not to test out new training maneuvers. The focus of this work is the RSPs; therefore, the training maneuvers created for this work are simpler and fewer in number. The standard practice 'best' training maneuver, a DC chirp [19], was selected to be the baseline maneuver. Two other training maneuvers were created to be the 'bad' training maneuvers, designed to highlight the weak points in the initial RSPs and also the strong points.

Maneuvers that are sinusoidal in nature can be created using the same formula as the Kestrel software, and then can be input into Kestrel as arbitrary motion files. For the purposes of this discussion, the terms will be left in the form used by Kestrel. 'S' is given as either the roll, pitch or yaw angle, depending on the axis of prescribed sinusoidal motion.

$$S(t) = \tilde{s}(\hat{t}) cos \left[2\pi (\beta_f \hat{t}^{1+\lambda_f} + f_1 \hat{t} + \Phi/360) \right] \tag{3.5.1}$$

where

$$\tilde{s}(\hat{t}) = \beta_a \hat{t}^{1+\lambda_a} \tag{3.5.2}$$

$$\beta_a = \frac{a_2 - a_1}{(t_{max} - t_0)^{\lambda_a}} \tag{3.5.3}$$

$$\hat{t} = (t - t_0) \tag{3.5.4}$$

$$\beta_f = \frac{f_2 - f_1}{(t_{max} - t_0)^{\lambda_f}} \tag{3.5.5}$$

where the variable t is actual time, t_{max} is the maximum time of the motion, t_0 is the

39

initial time of the motion, a_2 and f_2 are the final amplitude and frequency, whereas a_1 and f_1 are the initial values. λ_f and λ_a are the shift parameters that define how the motion will be computed from the initial to the final values. A value of one in either λ parameter represents a linear change. Φ is the phase shift given in degrees [8].

Using MATLAB®, these equations can be calculated locally, and then the RSPs discussed in Section 3.4 can be calculated. From there the maneuver is transferred into an arbitrary motion file as described by the Kestrel User Guide [8]. The user guide specifies that there must be eight header lines followed by 13 columns. The first column is time. The next three columns are the rotated basis vector n_x, followed by the next three columns of n_y and three columns of n_z. The last three columns are the location of the center of rotation.

Three sinusoidal training maneuvers were created using Equations (3.5.1) - (3.5.5). The inputs for these training maneuvers can be seen in Table 4. It was quickly noticed that using an arbitrary motion file rather than the Kestrel inputs significantly increased the computational time per iteration. training maneuver 2, comparison maneuver 1a, comparison maneuver 3 and comparison maneuver 4 were computed using an arbitrary motion file, the rest of the maneuvers were run using the inputs in KUI. For the sinusoidal maneuvers such as training maneuver 1, training maneuver 3 and comparison maneuver 2, these inputs are identical. comparison maneuver 1b and comparison maneuver 1c required use of the constant rate pitch-and-hold motion in Kestrel. Comparison maneuver 6 used a series of constant rate pitch and hold maneuvers. Comparison maneuver 2 uses multiple sinusoidal inputs

The first maneuver is the best practice maneuver, it is known as a DC Chirp maneuver. The goal is to cover a large range of the regressor space. While the DC chirp produces the most robust models, it is known to have inaccuracies in the low

Table 4. Training maneuver input parameters

Input	TM1	TM2	TM3
λ_a	1	1	1
λ_f	1.9	1	1
a_1	14.7	12.5	10
a_2	0	12.5	10
f_1	0.75	1	0.75
f_2	1.6	1	0.5
$\Phi(degrees)$	-90	-90	-90
$AoA_i(degrees)$	6.5	7.5	7.5
Time(s)	4	1	3

and zero Q ranges. The first training maneuver (TM) is shown in Figure 12. By covering a greater portion of the regressor space, it is desired that the model will be more accurate with a greater understanding of the varying flow physics.

This training maneuver aims to span a large amount of the regressor space. To accomplish that task, the frequency is varied as is the amplitude of the wave. The result is seen in Figure 13.

Figure 14 shows a 3-D plot of the regressor space. Cells with greater spikes are cells that have data points more often in that particular cell. For visualization purposes, the cells for the 3-D plots are considered to be 1 (deg and deg/s) as smaller cells make the 3-D plots impossible to see. As can be seen with Figure 14, while the number of points centers around the initial AoA, as would be expected, the maneuver covers a variety of points and does not center on one particular region.

TM2 and TM3 are the maneuvers designed to produce less than optimal results. TM2 is a simple single oscillation sinusoid, as can be seen in Figure 15.

TM2 reaches the boundary of the regressor space during the maneuver, hitting the maximum and minimum Q and AoA. However, it does not make any effort to cover the large range of the regressor space as can be seen in Figure 16.

41

Figure 12. Training maneuver 1: AoA and Q vs time
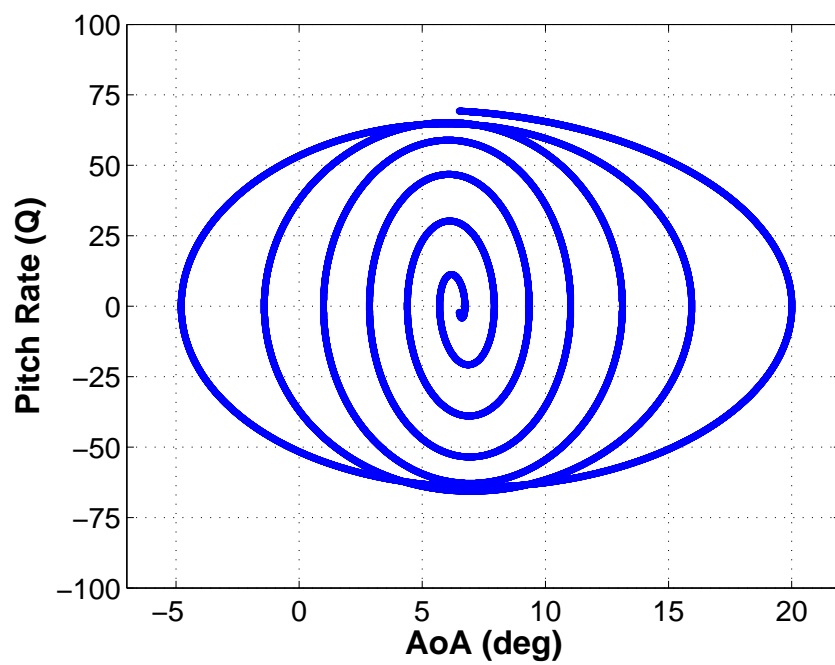
Figure 13. Training maneuver 1: Q vs AoA

42
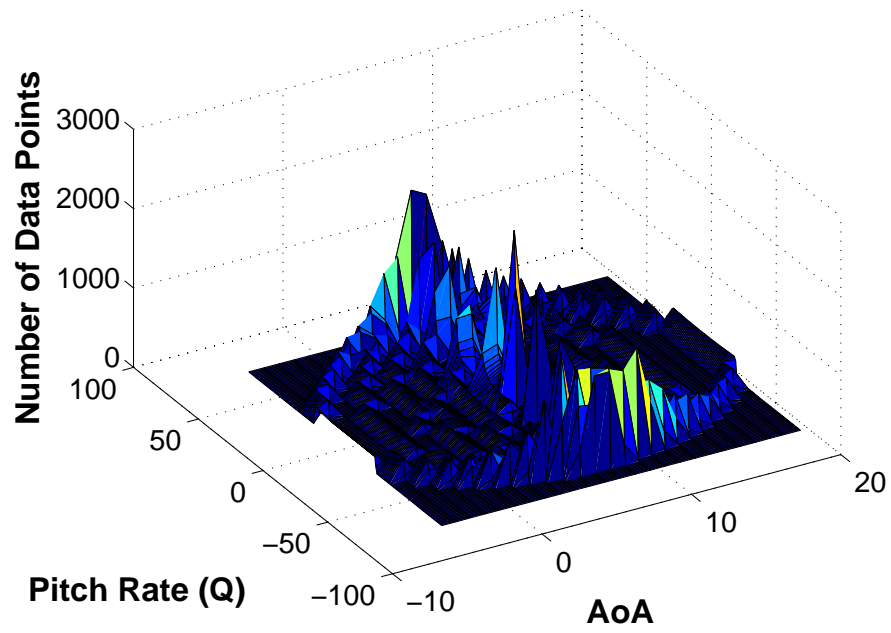
Figure 14. Training maneuver 1: discretized regressor space
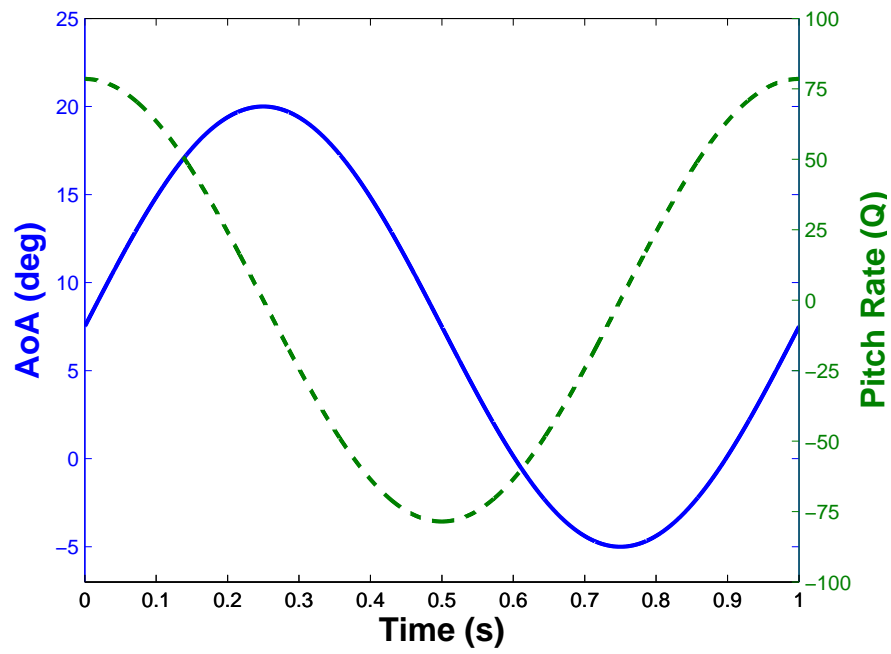
Figure 15. Training maneuver 2: AoA and Q vs time

43
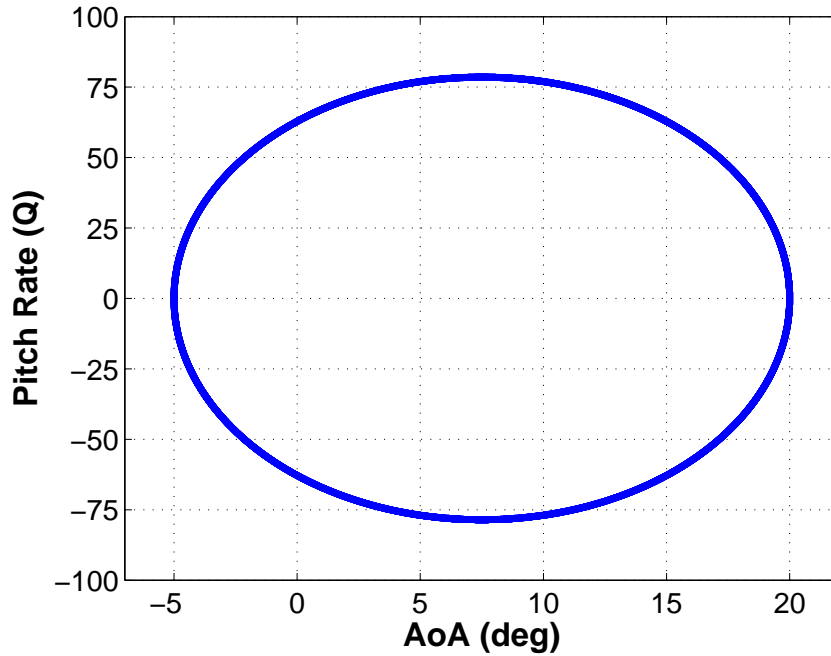
Figure 16. Training maneuver 2: Q vs AoA

The last plot shown in Figure 17 shows the amount of hits in the regressor space. As would be expected, there are many hits along the outskirts of the regressor space, however there are space the middle of the regressor space has no data points. The number of data points overall is less than seen in Figure 14 for TM1. The lower of points results from the shorter time period for TM2 (1 second) vs the time period for TM1 (4 seconds).

The last maneuver, TM3, attempts to cover slightly more of the regressor space while also covering more low Q data. However, it is also an aim of this training maneuver to miss the boundaries of the regressor space entirely as can be seen in Figure 18.

The emphasis around the low Q threshold of 20 deg/s can be seen in Figure 18 and Figure 19. The amount of hits in the regressor space can be seen in Figure 20. While TM3 shows a greater spread than TM2, it still does not cover as large a range as TM1.
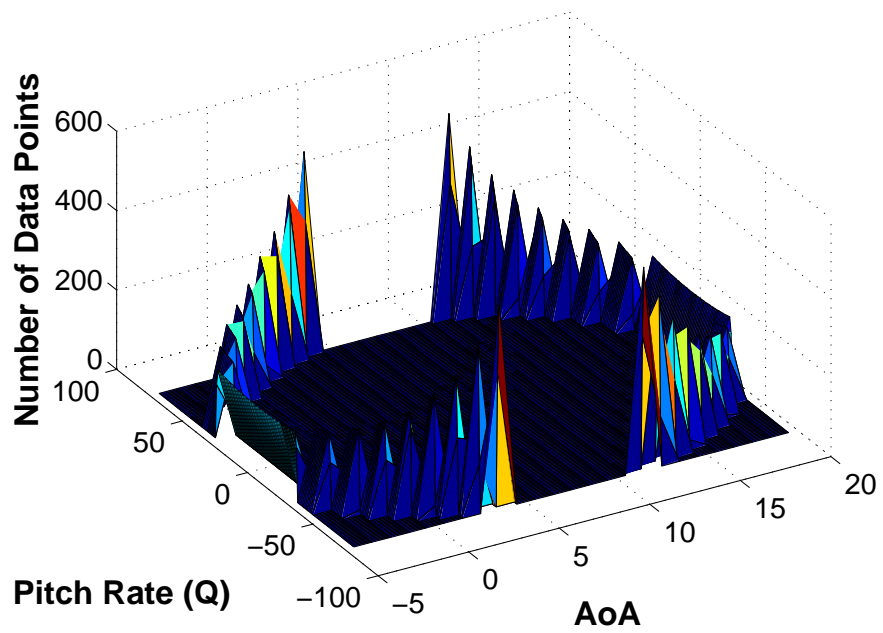
Figure 17. Training maneuver 2: discretized regressor space
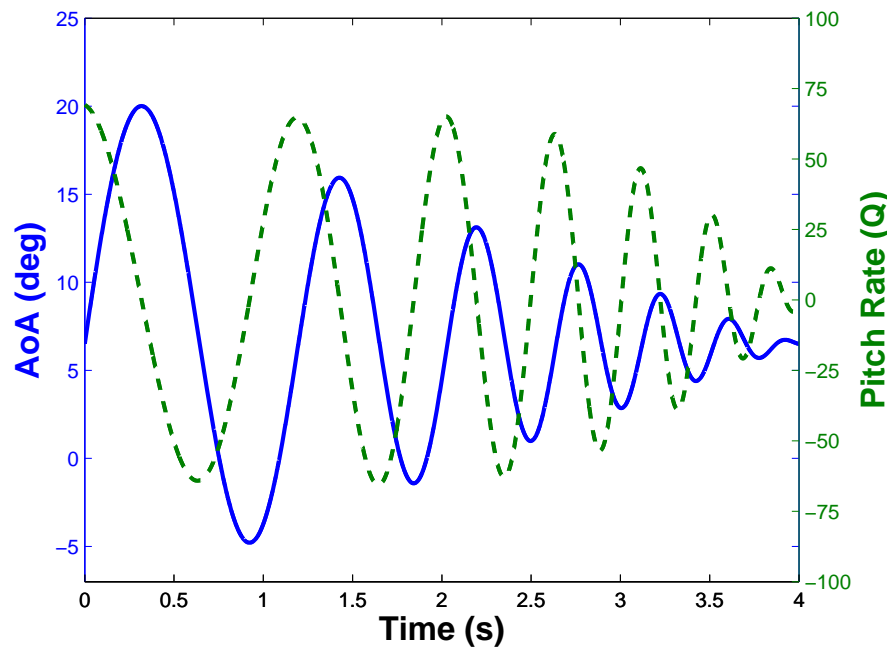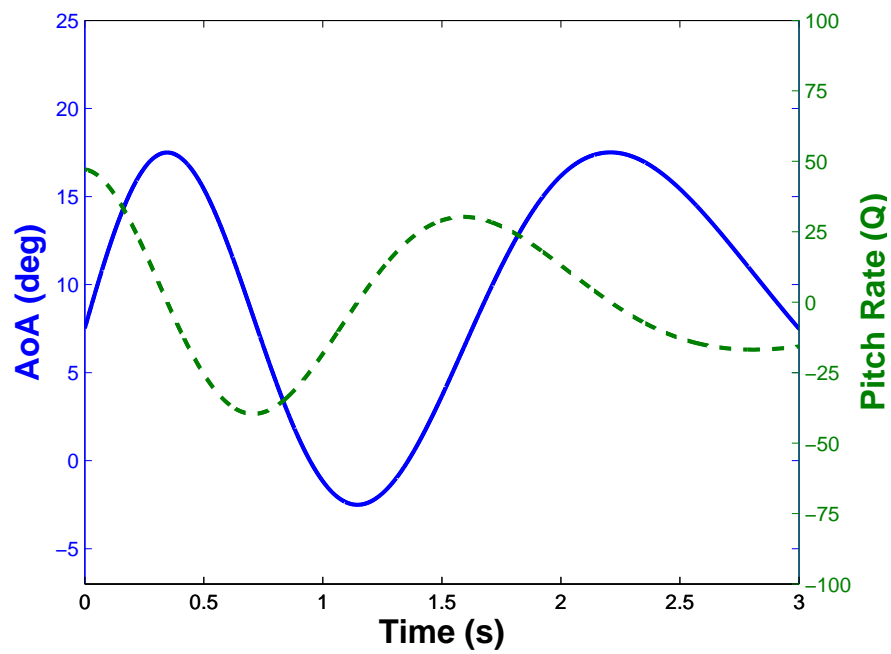

Figure 18. Training maneuver 3: AoA and Q vs time
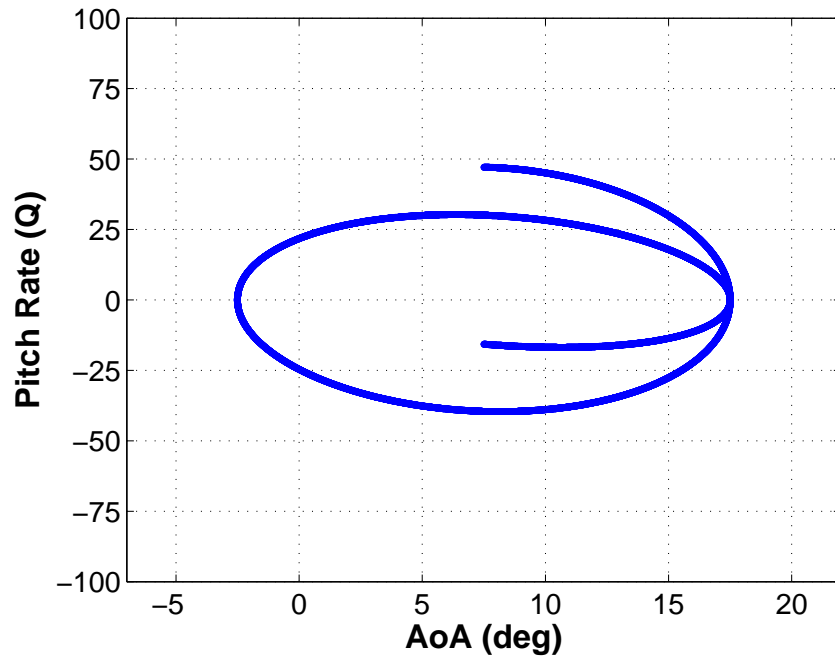
Figure 19. Training maneuver 3: Q vs AoA
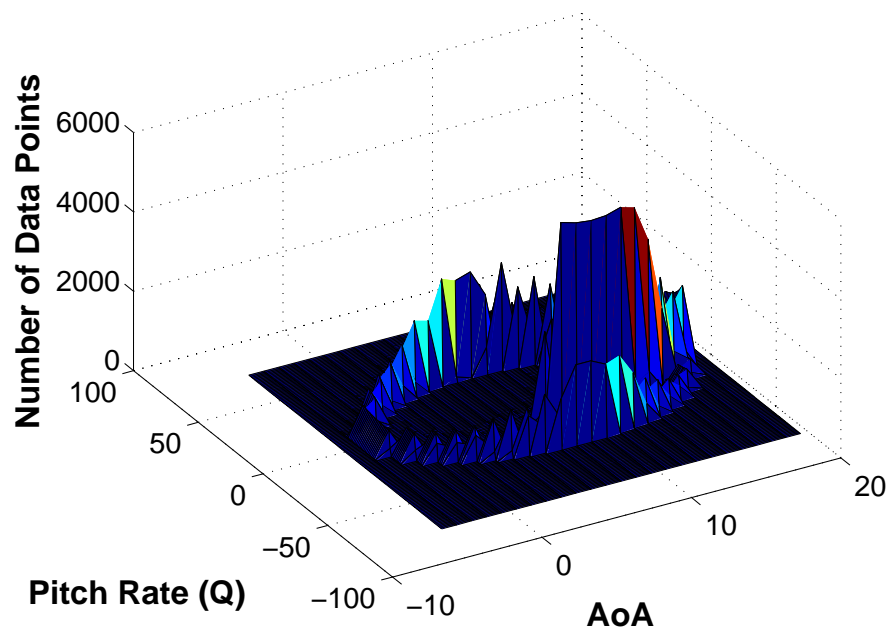
Figure 20. Training maneuver 3: discretized regressor space

Both TM2 and TM3 are distinguishable from TM1 in that the 3-D plots are much more sharply divided than the 3-D plot for TM1. The sharp contrast for TM2 and TM3 are because of the single sweep of the data regime. TM2 and TM3 make one pass and there is not much overlap in the points.

3.6   Comparison Maneuvers

The purpose of the comparison maneuvers is to provide the reduced order models generated from the training maneuvers a set of comparison data. That is, the comparison maneuvers are simulated using Kestrel. Instead of creating reduced order models from these maneuvers, the results of the comparison maneuver simulations are used as a basis of comparison for the ROMs.

The first comparison maneuver, abbreviated as COM1, is simple. COM1 is a linear sweep across the AoA regime. The goal of these maneuvers is to easily see how well the models can recreate the entire α range at a set Q value. Therefore, COM1 actually consists of three different maneuvers: COM1a, COM1b and COM1c. COM1a is set to a Q value of 25 deg/s, COM1b has a Q value of 10 deg/s and COM1c has a Q value of 50 deg/s. α and Q for the 3 maneuvers can be seen in Figures 21 - 23.

The goal of COM1 is to see if the ROMs can produce accurate C_L vs α curve and C_D and C_M curves. These are important curves which are the basis of much of aircraft design.

The next maneuver known as COM2 is more complicated. This maneuver attempts to cover a very large range of the regressor space and can be seen in Figure 24. While going through the oscillations shown in Figure 24, the maneuver also covers a large range of Q values, which can be seen in Figures 25 and 26.

The next two maneuvers strive to go through the AoA region for a range of Q
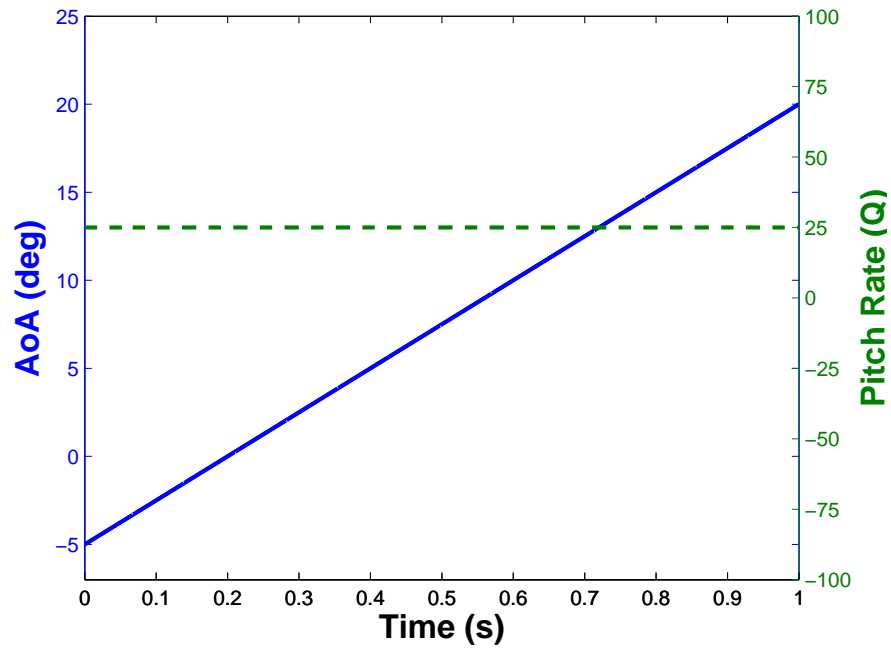
Figure 21. Comparison maneuver 1a (25 deg/s): AoA and Q vs time
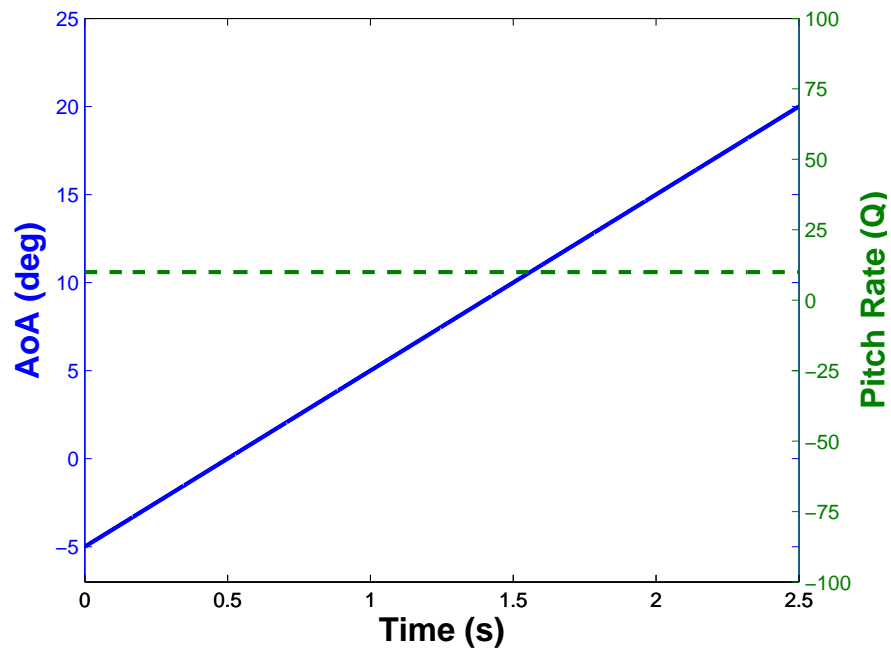
Figure 22. Comparison maneuver 1b (10 deg/s): AoA and Q vs time

48
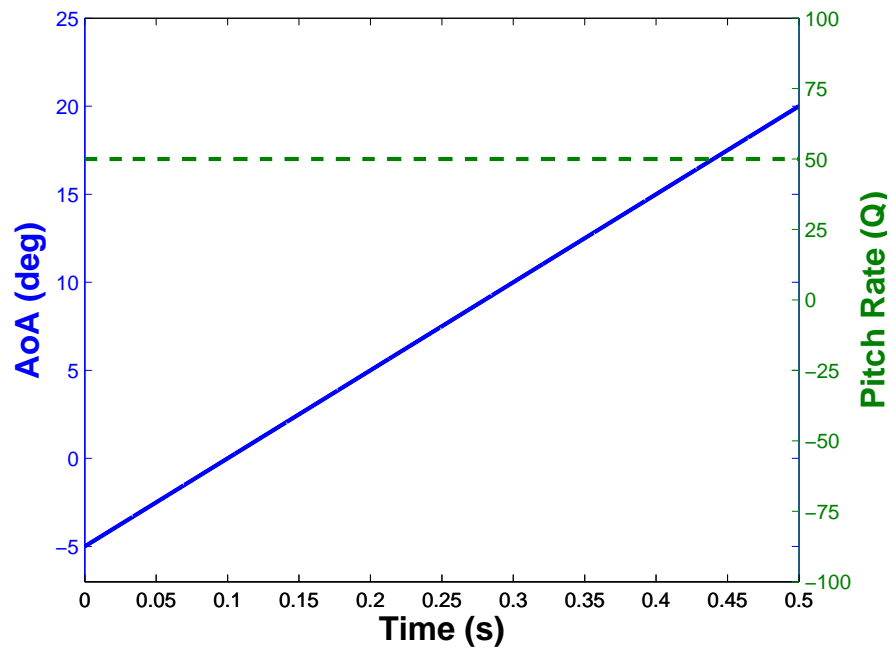
Figure 23. Comparison maneuver 1c (50 deg/s): AoA and Q vs time
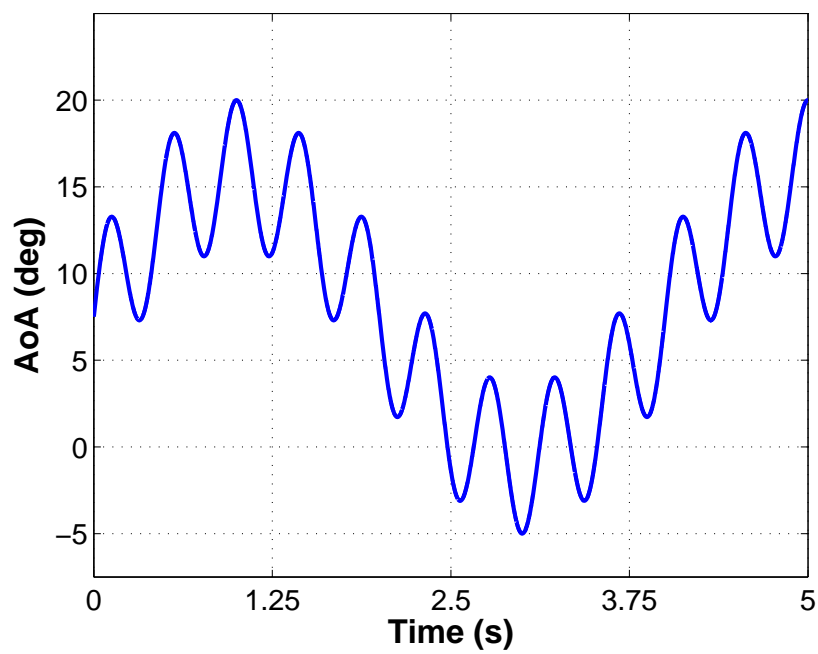
Figure 24. Comparison maneuver 2: AoA vs time

49
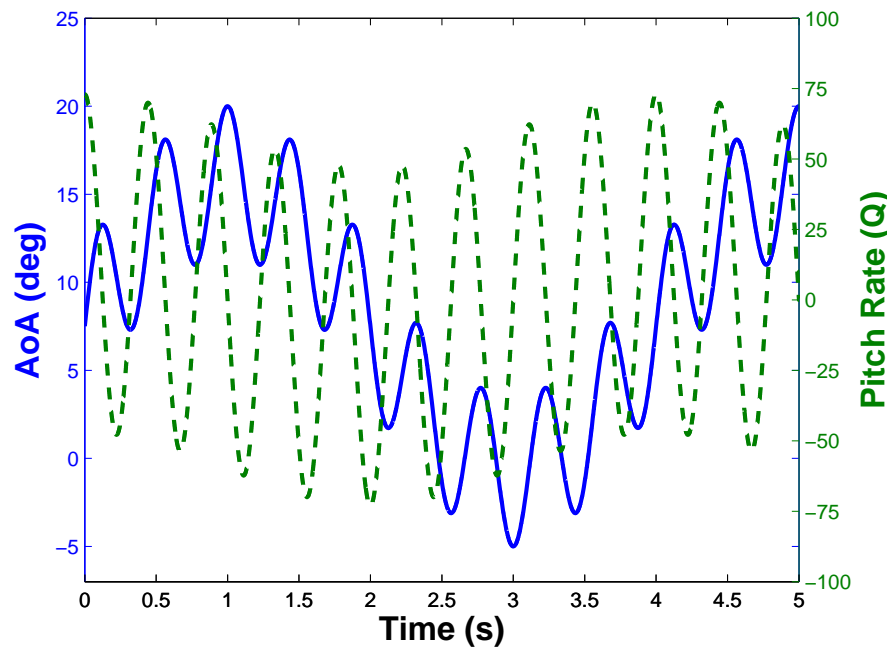
Figure 25. Comparison maneuver 2: AoA and Q vs time
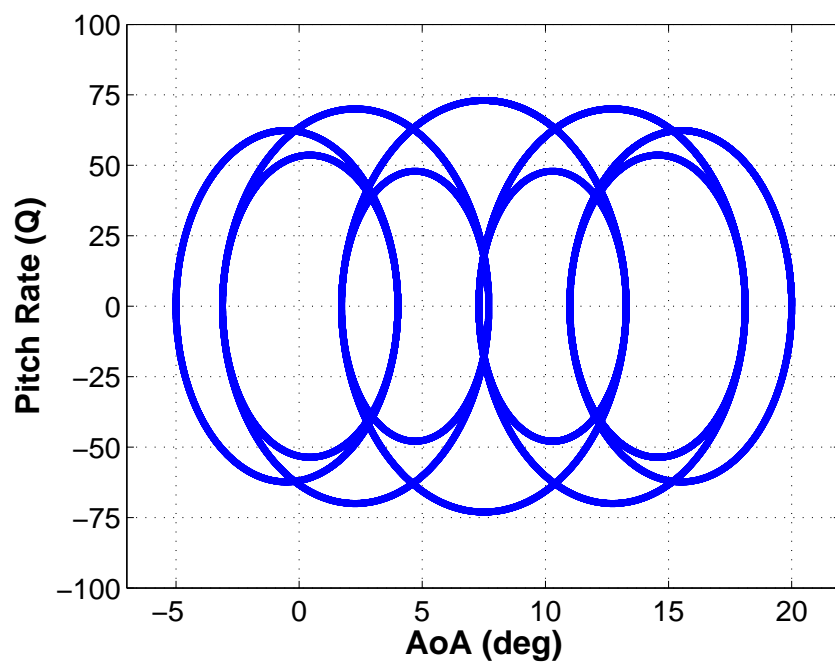
Figure 26. Comparison maneuver 2: Q vs AoA

values. COM3 uses an exponential change in angle of attack in order to provide a range of AoA and Q values. COM3 can be seen in Figure 27 and 28.
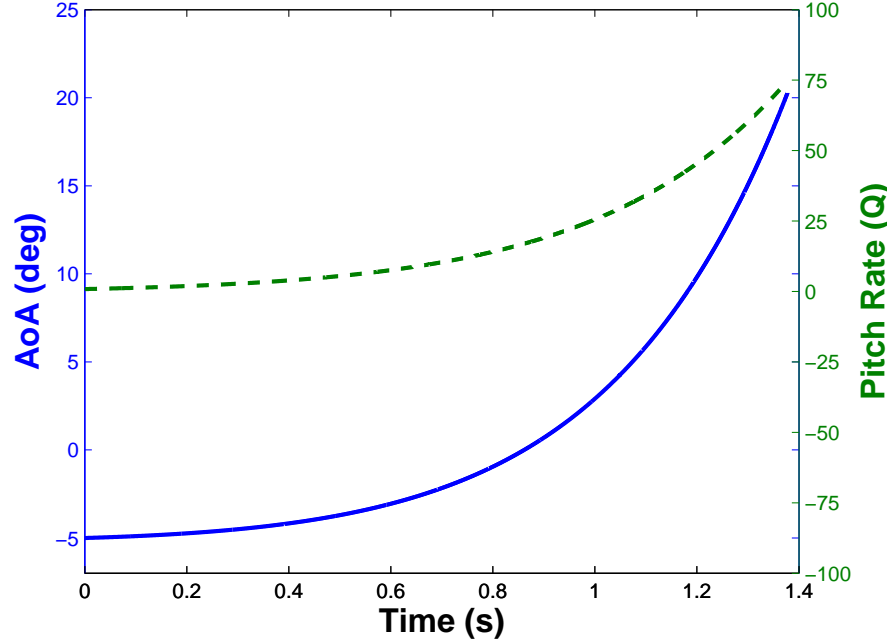
Figure 27. Comparison maneuver 3: AoA and Q vs time

While COM3 covers the range of positive Q-values, COM4 covers the negative Q-values and can be seen in Figures 29 and 30.

The final maneuver, known as COM5, is a series of constant rate pitch and hold maneuvers. The goal for COM3 is to show the weakness of the maneuvers at 0 Q values at several angles of attack. The maneuver can be seen in Figure 31.

3.7 Creating the Reduced Order Models

The reduced order models are created using methods discussed in 2.3. The software used to conduct this analysis is the System Identification Programs for Aircraft (SIDPAC) produced by NASA Langley. For the purposes of this research, it was decided to not use the built-in post-processing system identification tools implemented
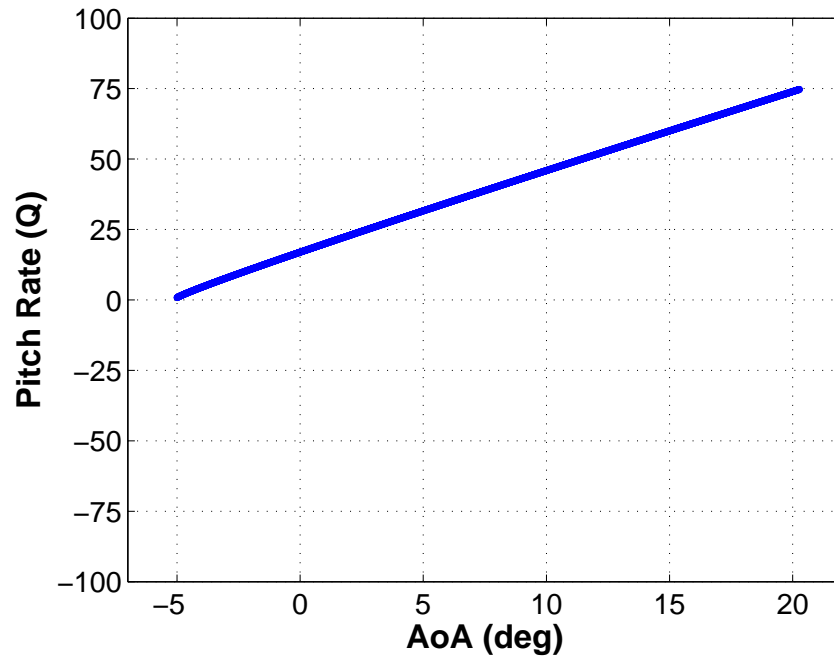
Figure 28. Comparison maneuver 3: Q vs AoA
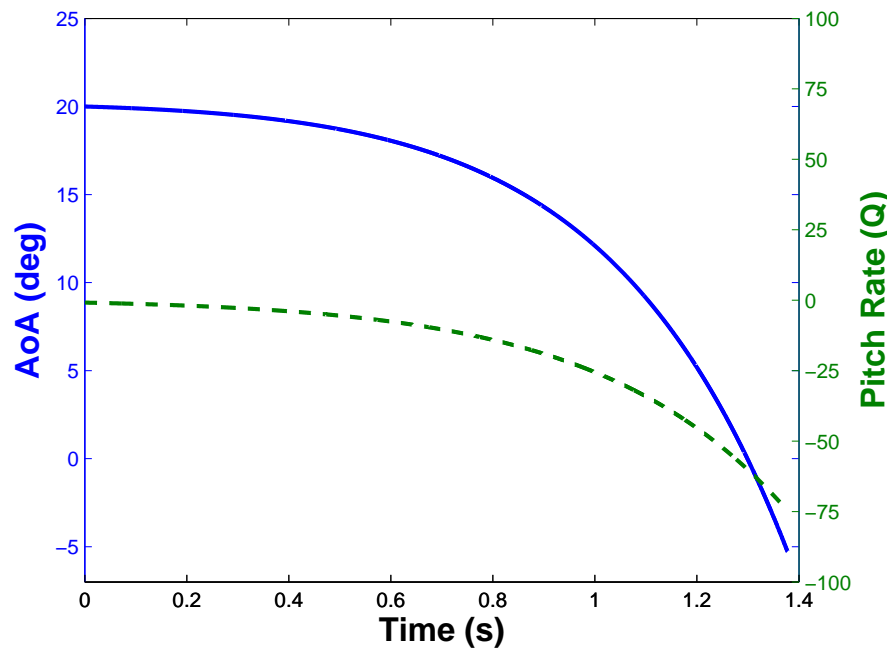
Figure 29. Comparison maneuver 4: AoA and Q vs time
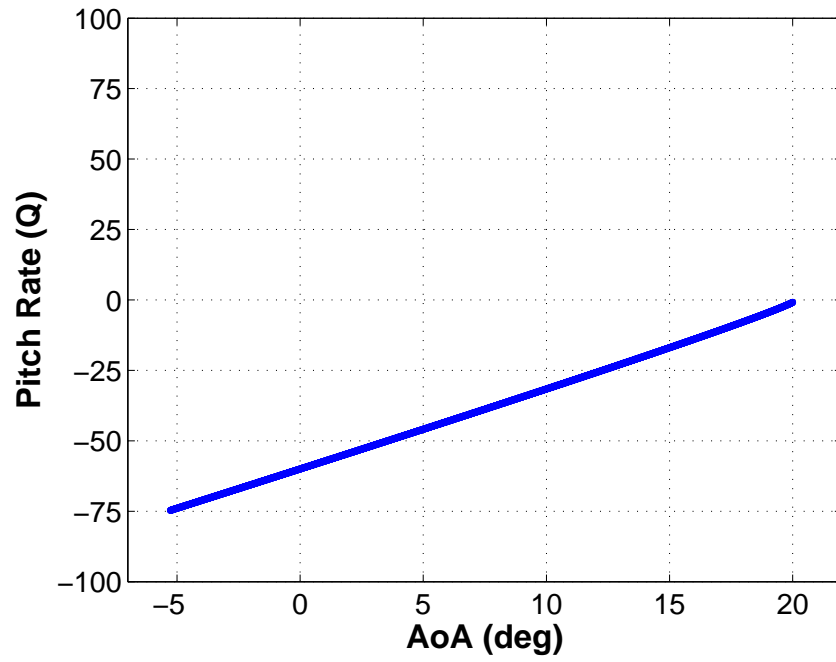
Figure 30. Comparison maneuver 4: Q vs AoA
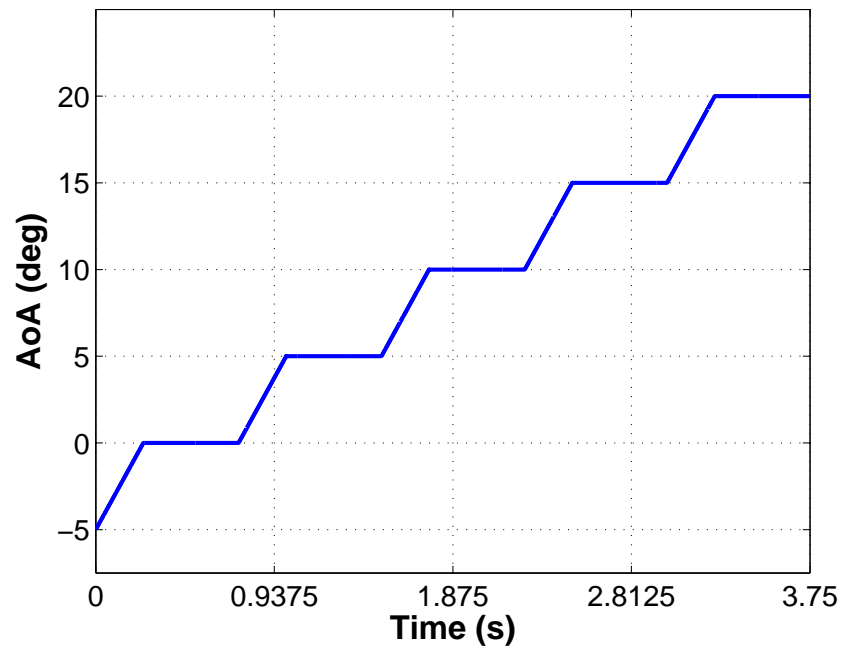
Figure 31. Comparison maneuver 5: AoA vs time

by Kestrel. This was done to ensure greater control and understanding of model creation. The SIDPAC software is a collection of MATLAB®functions, and the usefulness of each one is dependent upon the need of the user. For this research the code *mof.m* will be used. This file will map a multivariate polynomial model to the input data. The file does require some input from the user. The script used to call mof.m and input the necessary parameters is shown in Appendix A.2.

The first input is the variable *nord*, which is described as a vector of maximum independent variable orders. Each input variable, α and Q, is given a *nord* value. This value refers to maximum order of each independent variable in the final reduced order model. If a 4 is entered for α, the largest exponent on α is 4 in the ROM. However another term *maxord* restricts the total number of exponents for a given term. If *maxord* is defined to be 5, there could be a term with $\alpha^4 Q$ but not $\alpha^4 Q^2$ as 4+2=6 which is greater than 5. The final option is *maxopt* which sets the maximum number of terms in the final polynomial model.

For this work, the *maxord* is selected to be 5, as additional terms were seen to increase computational time significantly while not improving the ROM. The program orders the terms by significance to the model and ends where there is limited additional benefit to the model based on R^2 and predicted square error (PSE). From experience in this research, the maximum value was seen to be around 14 in most cases. However, the maximum number of terms was not limited by user input in this research. An example of the *mof.m* output is shown in Figure 32. The red dot in the figure represents the programs final choice for the number of terms in the model. This example is the output fit for TM1 C_L data. The R^2 value in this chart is the R^2 for the model fit to the raw CFD data. It is lower than the R^2 values shown in Chapter IV due to the fluctuations in the flow.

For each training maneuver, each regressor will have a *nord* value of 5, and *maxord*
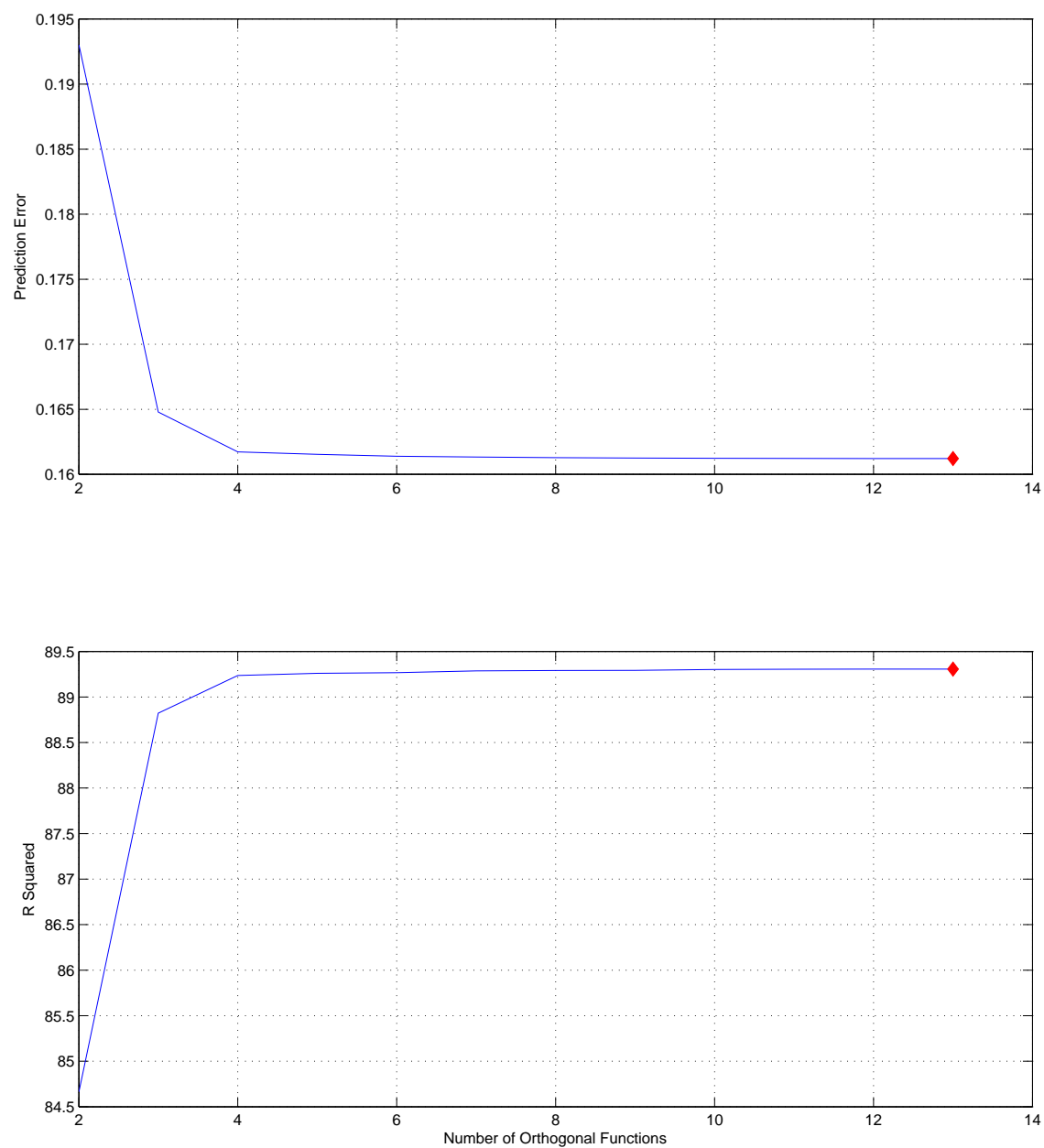
Figure 32. Model termination determination by SIDPAC software

will be defined as 5. Then a model will be generated using the *mof.m* program. The program will calculate the best model given the input data and input parameters. That reduced order model will then be used going forward.

In the highly constrained circumstances of CFD flow, $\dot{\alpha}$ is assumed to be equal to Q, as any other motion will not be introduced. However $\dot{Q}$ could also be a factor for the model. In order to provide $\dot{Q}$ as a regressor, the *deriv.m* function of SIDPAC will be used. This function calculates a locally smoothed numerical time derivative. However, $\dot{Q}$ was not selected as a regressor in any of the final reduced order models.

3.8 Analysis of Results

Once the reduced order models have been created, they will be compared to full CFD predictions of the comparison maneuver coefficients C_L, C_D and C_M. Because of the unsteady nature of the flow, a moving average is computed for the coefficients. The metrics for each ROM, as compared to the comparison maneuver moving-average coefficients, are calculated using the following relations:

$$\bar{z} = mean(Obs) \tag{3.8.1}$$

$$SSR = \sum \left(Model - \bar{z}\right)^2 \tag{3.8.2}$$

$$SSE = \sum \left(Obs - Model\right)^2 \tag{3.8.3}$$

$$SST = SSR + SSE \tag{3.8.4}$$

$$R^2 = \frac{SSR}{SST} \tag{3.8.5}$$

where R^2 is the coefficient of determination, $\bar{z}$ is the mean of the observed (CFD coefficient) data, *Model* refers to the ROM predicted coefficient, SSR is the regression

sum of squares, SSE is sum of squares of residuals and SST is total sum of squares.

$$NRMSD = \frac{\sqrt{\frac{\sum(Obs-Model)^2}{\# \, of \, observations}}}{max(Obs) - min(Obs)} \qquad (3.8.6)$$

NRMSD is the normalized root mean squared deviation. Each ROM, as derived from the various TMs, will have these two metrics associated with them for each comparison maneuver.

Two approaches will be used to analyze the results. The first is a more visual approach. An examination of the RSPs and the output metrics for each maneuver will be compared along with plots of the predicted and simulated coefficients to get a sense of which RSPs show a trend in the final data. The second approach, to add more scientific rigor, will incorporate the statistical program JMP®to investigate which inputs (RSPs) have an effect on the outputs (R^2 and NRMSD) for each coefficient using "contrasting" methods. It is important to note the combined effectiveness gained by using these two methods. While JMP®will be able to provide insight into the generic trend of the data, it will be the onus of the author to correlate trends within the data subsets such as low Q maneuvers or even low Q sections of maneuvers.

IV. Results

4.1 Time Step and Grid Density Study

Using the methodology discussed in Section 3.3, the time step and grid density study was conducted, Figure 33 shows the wave number converges between the fine and the medium grid at a time step of 2.5×10^{-5} seconds. However, at this point the two grids are still decreasing in wave number with respect to decreasing time step. At a time step of 1.25×10^{-5} seconds, both grids are stationary with respect to wave number and, are therefore, considered to be converged with respect to time. At this point, it can be said that the solution is grid and time step independent. $\Delta t^* = 0.01$ for these flow conditions is plotted for reference. It is desirable to run on the smallest grid possible to reduce computation expense; therefore, the medium grid at a time step of 1.25×10^{-5} seconds was chosen. Figure 34 is a graph of the time-averaged value for normal force coefficient. While not a great indicator of grid convergence, it does serve as a sanity check. The medium grid and the fine grid nearly converge upon a solution at the 1.25×10^{-5} second time step.

However, after the medium grid was selected and the training maneuver simulations began, the grid required additional refinement. Additional cells were needed approximately 0.1 ft above and below the trailing edge. The final grid can be seen in Figure 35 and the final grid statistics are given in Table 5.

Table 5. Final grid used for NACA 64A010 airfoil

Grid	Number of Points	Number of Cells	Number of Faces on Surface
Final	629,378	628,008	498

58
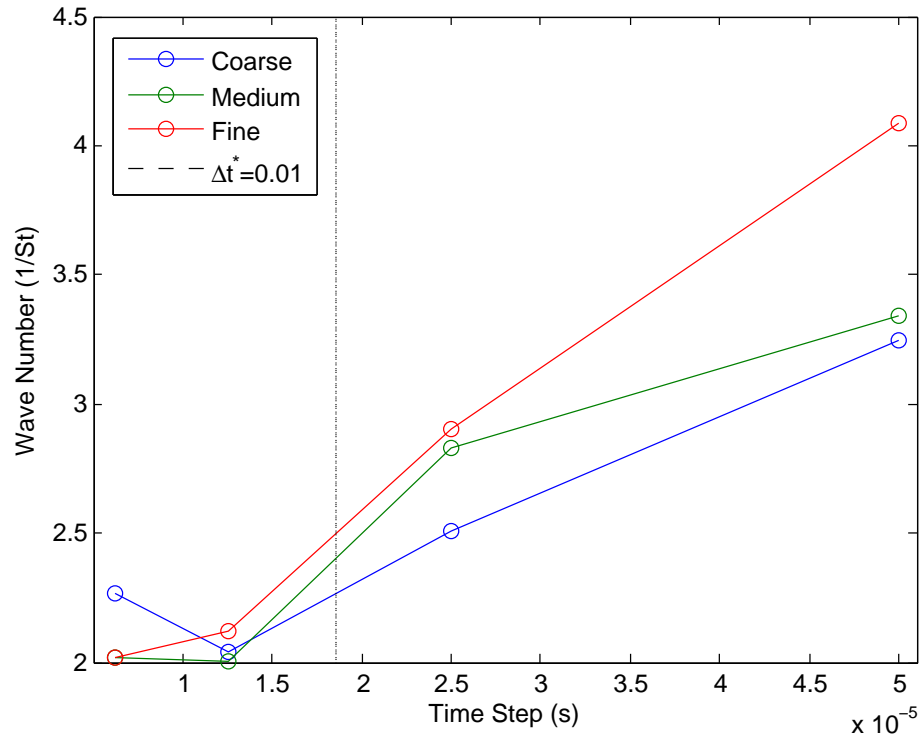
Figure 33. Grid sensitivity study results: wave number
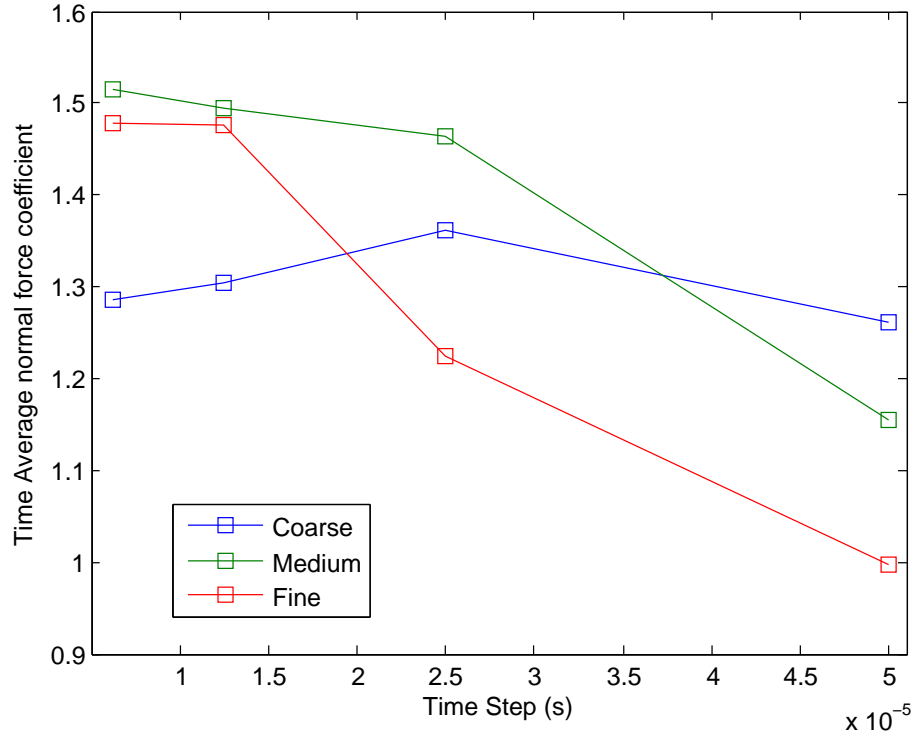
Figure 34. Grid sensitivity study results: time-averaged normal force
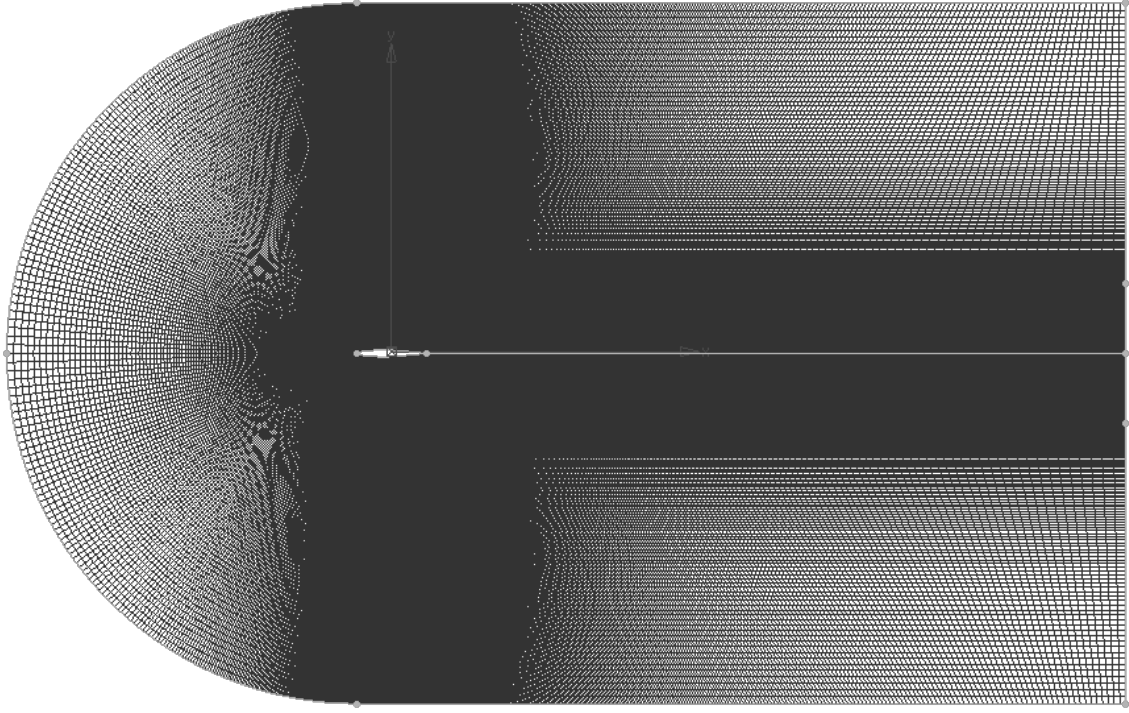
Figure 35. Final computational grid

4.2 Initial RSPs

The initial RSPs were computed for the three training maneuvers and the results are shown in Table 6 and Table 7. The first thing to note is the addition of a TM4. It was observed early on that it would help the statistical analysis if there was another point of comparison for the RSPs. Since the COM2 CFD results were readily available and COM2 was very similar in behavior to a training maneuver, the results of COM2 were used to create additional models and labeled as TM4. However, TM4 is not compared to COM2 as that would confound the results.

Looking at the RSPs can be useful for the purpose of gaining a better idea of what the maneuver is doing before looking at the output metrics. From the first seven RSPs it can be seen that TM4 and TM1 cover a larger amount of the regressor space, while TM2 and TM3 do not. This is to be expected, as these maneuvers were

60

Table 6. First seven RSPs

TM	Percent		Std on		0 Q Data		
	Whole	Boundary	α	Q	Percent	Per cell	Std
TM1	3.6691	4.7483	0.1951	0.2444	5.20	0.9720	0.1000
TM2	0.8851	11.556	0.1074	0.1532	0.80	0.1280	0.0892
TM3	0.6880	0.0000	0.1188	0.1105	0.80	0.9889	0.0671
TM4	5.0029	15.103	0.1605	0.1862	4.80	0.8320	0.1404

Table 7. Last six RSPs with 20 deg/s as cutoff

TM	Below 20 deg/s			Above 20 deg/s		
	Percent	Per cell	std	Percent	Per cell	std
TM1	4.9990	0.9586	0.1226	3.1866	0.8152	0.1053
TM2	0.8120	0.1311	0.0891	0.9115	0.1874	0.0903
TM3	1.3050	1.3431	0.0757	0.4650	0.3845	0.0336
TM4	4.2240	0.8766	0.1472	5.2843	1.1357	0.1404

not created to cover a wide range. With these high values it would be expected that TM1 and TM4 would correlate to an overall robust model.

The next RSP is the percent of the boundary. TM2 and TM4 both have large values for this RSP. This result may correlate to favorable results for coefficients that are more linear in nature.

The third and fourth RSPs are the standard deviation in AoA and Q. A high standard deviation would imply that the results are more evenly distributed throughout the regressor space. A small standard deviation would imply that a majority of the data set is located near the mean. TM1 provides the largest standard deviation in AoA and Q.

The next three RSPs focus on the zero Q data. The same thoughts above for the general case carry down into this data subset. TM1 hits the largest percent of the dataset as well as the largest per cell count and one of the largest standard deviations. Therefore, it is expected to produce the best results in a zero Q scenario.

The next set looks at the low Q data points. Looking at these RSPs, TM1 again returns the best values. However, for the high Q RSPs, TM4 returns the best values. Based on these values it would be expected that TM1 models will return the best low Q data while TM4 models will return the best high Q data.

4.3 Model Results

This section discusses the results gained from comparing the reduced order models to the results gained from the full CFD simulation of the comparison maneuvers. Again, TM4 is not compared against COM2 as that would just be a measure of how well the model fit the data and not a measure of the predictive capability of the model.

4.3.1 Coefficient of Lift

The results for C_L can be seen in Table 8. Looking at the table there are some surprising results. From the RSPs and the way the training maneuvers were designed, TM2 and TM3 were not expected to produce very good results. However it is clear from the metrics, and the results that this is not the case for coefficient of lift. To refresh the memory of the reader, COM1a is the medium Q maneuver at 25 deg/s, COM1b is the low Q maneuver at 10 deg/s and COM1c is the high Q maneuver at 50 deg/s.

First, reference Figure 36, it can be seen that the models all follow the trend of the comparison data well. At first glance, it would appear that all the models are a good prediction, with TM4 being the only model distinguishable from the rest of the data. Table 8 confirms that idea. The surprising result is that TM2 has the highest R^2 and the lowest NRMSD. Following that the best model is TM3. Linking back to the RSPs in Tables 6 and 7, TM2 is middle of the pack on everything but the

Table 8. R^2 and **NRMSD for all** C_L **models vs a moving average**

COM	TM1		TM2		TM3		TM4	
	R^2	NRMSD	R^2	NRMSD	R^2	NRMSD	R^2	NRMSD
COM1a	0.9920	0.0254	0.9941	0.0211	0.9936	0.0216	0.9891	0.0271
COM1b	0.9926	0.0237	0.9939	0.0211	0.9918	0.0256	0.9860	0.0305
COM1c	0.9919	0.0227	0.9905	0.0245	0.6674	0.1068	0.9917	0.0219
COM2	0.9774	0.0376	0.9826	0.0329	0.8064	0.1034	-	-
COM3	0.9950	0.0197	0.9941	0.0212	0.6487	0.1707	0.9947	0.0407
COM4	0.9619	0.0407	0.9809	0.0300	0.7761	0.0912	0.9823	0.0283
COM5	0.9901	0.0245	0.9904	0.0244	0.9852	0.0318	0.9822	0.0318

zero/low Q parameters in which it is the lowest, therefore there is no clear link from the metrics to the RSPs from this maneuver.

Next, reference Figure 37. The results for this case are very similar to the results for COM1a. Looking at the results in Figure 37 it is hard to distinguish the results and all the models agree well. Looking at the metrics in Table 8 it can be seen that TM2 has the largest R^2 and lowest NRMSD. Surprisingly, despite having a greater concentration in the low Q area, TM3 has worse values than TM1 if only by a small margin. Because of this, there is again no clear link between the output metrics and the RSPs.

The last constant-Q α sweep results are shown in Figure 38. This high Q case is where we start to see some separation between the models. For this maneuver it is easily seen that TM3 is wildly off point. The error is due to the fact that TM3 does not have a large amount of high Q data. The low amount of data is reflected in the high Q RSPs. TM2 also has low high Q RSP values, and in a switch from the previous lower Q maneuvers, TM2 now displays worse metrics than TM1 and TM4, both of which have better high Q RSPs. The better RSPs would suggest a link between the high Q metrics and performance of the maneuver at high Q.

Figure 39 shows the model results for COM2. Note that TM3 is omitted. The
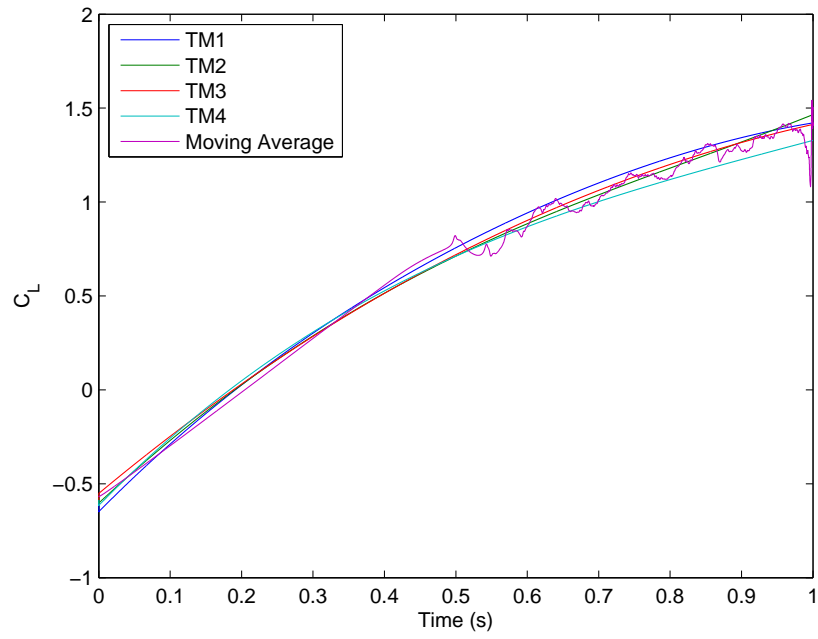
Figure 36. Model results COM1a C_L
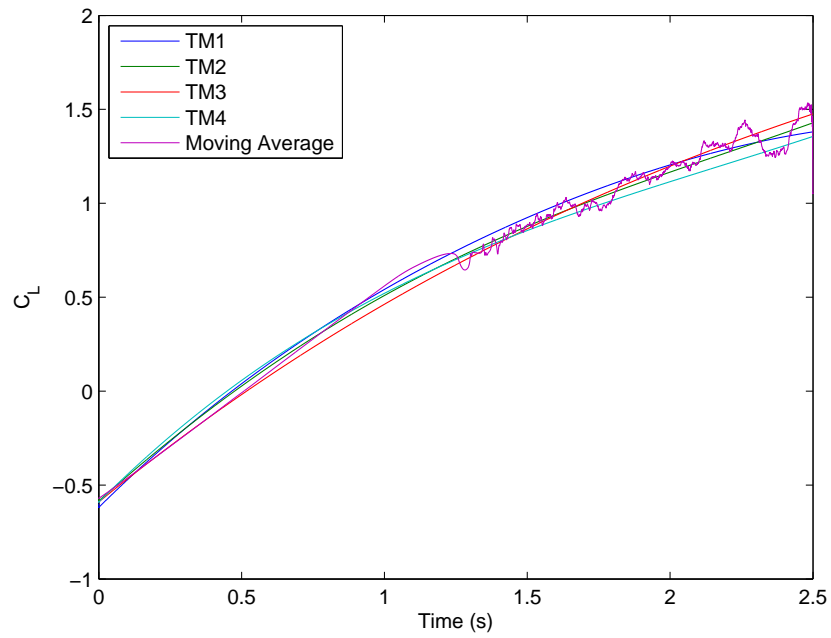
Figure 37. Model results COM1b C_L

64
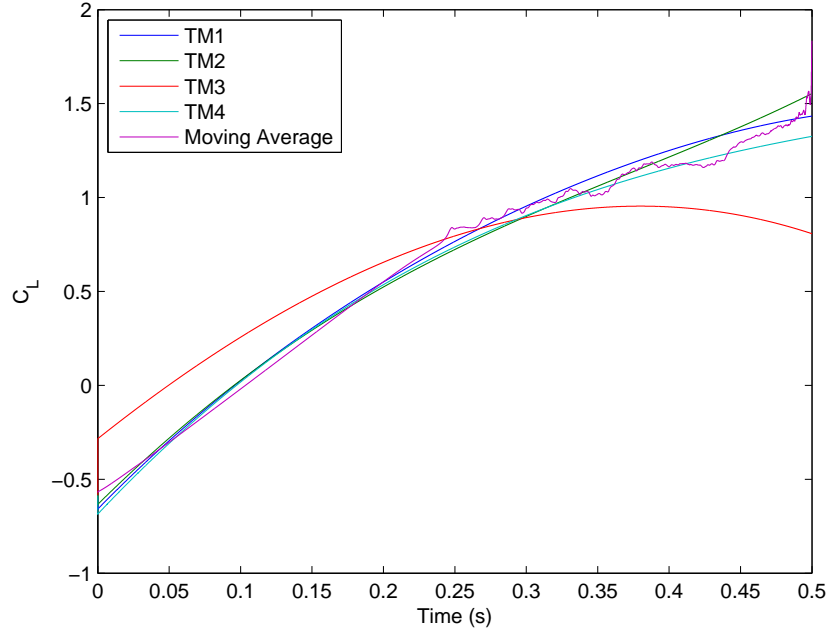
Figure 38. Model results COM1c C_L

omission is due to the highly inaccurate curve that TM3 produced which distracted from the rest of the results. Also consider that curve TM4 is essentially showing the fit of the model to the input data, rather than prediction data. TM1 and TM2 are both accurate throughout the maneuver; however, TM2 comes through as being more accurate in the metrics. This is surprising as the only RSP in which TM2 is better than TM1 is percent of points on the boundary. The success of TM2 would suggest that for at least C_L, hitting the boundaries is very important.

For the positive Q exponential maneuver, COM3, shown in Figure 40, all of the TMs provided good results through the course of the maneuver. However, this is the first instance where there is a display of error at the edge of the regressor space. This error by TM3 occurs because that portion of the regressor space tested by COM3 is outside the bounds of TM3. This error will be discussed in full further in the document. Fitting with the pattern from the previous maneuvers, TM2 returned the
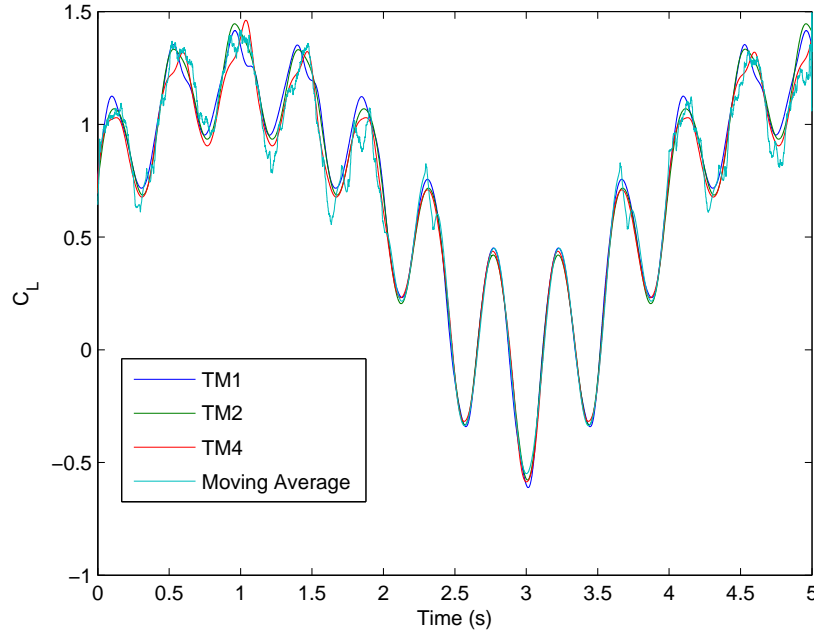
Figure 39. Model results COM2 C_L

best values while TM1 returned the second best values as shown in Table 8. These results do not immediately point to any link between the metrics and RSPs.

The results for COM4 shown in Figure 41 are similar to those from the previous maneuver. The models all line up well in the linear portion, but there is a small spread in the results in the unstable regime. Since this maneuver spends a longer time in the unsteady regime, the metrics are lower overall than the previous maneuver. From the results it can be seen that TM3 is close but not accurate in the high alpha low Q portion of the maneuver, while every other result is fairly accurate. TM3 also had the lowest standard deviation value for the low Q metric cells. This could indicate a focus point of not having a well spread data. Looking at the tabular results, TM4 has better metrics than TM2 for the most accurate maneuver.

For the several step pitch and hold maneuver, COM5, all the models seem to predict the zero Q values to a relatively high degree of accuracy. The accuracy of the models is reflected in the metrics; however, TM1 and TM2 beat the other maneuvers

66
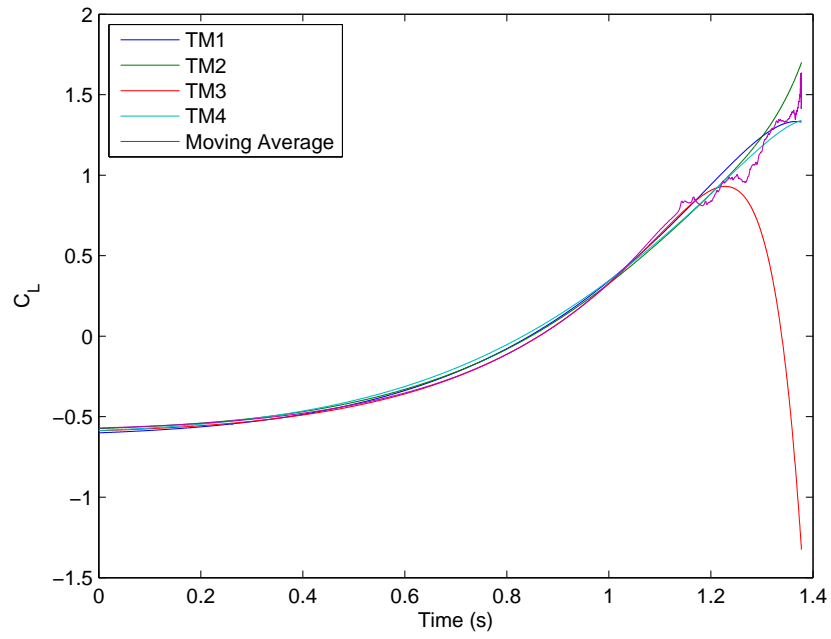
Figure 40. Model results COM3 C_L
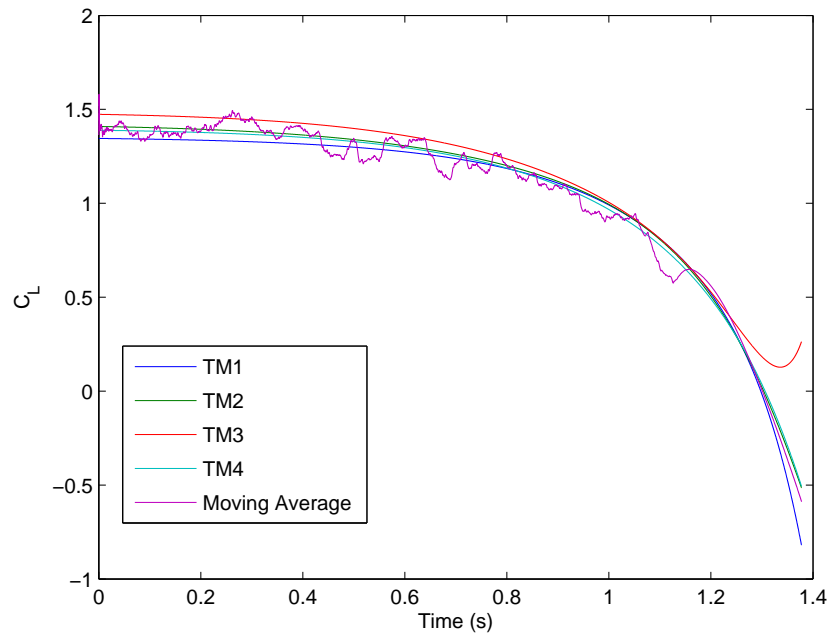
Figure 41. Model results COM4 C_L

for the best values and TM2 returns better values than TM1. It is worth noting that TM3 loses some value at the end of the maneuver, where AoA is 20 degrees, likely due the fact that maximum AoA for that training maneuver is around 18 degrees. Despite the large difference in zero Q RSP values, there does not seem to be a link to the metrics.
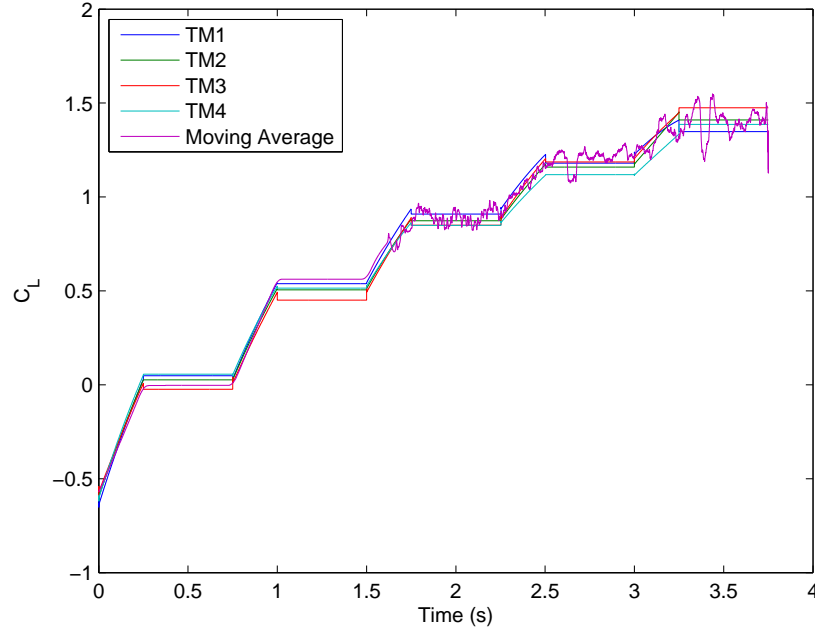
Figure 42. Model results COM5 C_L

4.3.2 Coefficient of Drag

The results for C_D can be seen in Table 9. On the whole, the results for C_D were less accurate than the results seen for C_L. There is also a larger distinction between the different training maneuvers than was seen for the previous coefficient.

Looking at the results displayed on Figure 43, it is easily seen that TM1 and TM4 best represent the data. It would seem that now that the data is not as well organized as lift was, the 'bad' models are now having a hard time accurately predicting the output. TM4 resulted in the largest R^2 and lowest NRMSD as shown in Table 9.

68

Table 9. R^2 and NRMSD for all C_D models vs a moving average

COM	TM1		TM2		TM3		TM4	
	R^2	NRMSD	R^2	NRMSD	R^2	NRMSD	R^2	NRMSD
COM1a	0.9869	0.0349	0.9152	0.1133	0.8671	0.0993	0.9905	0.0267
COM1b	0.9884	0.0343	0.8975	0.1413	0.9239	0.0950	0.9861	0.0351
COM1c	0.9742	0.0417	0.9533	0.0633	0.7549	0.2264	0.9750	0.0398
COM2	0.9809	0.0430	0.9115	0.1146	0.6048	0.5714	-	-
COM3	0.7732	0.0787	0.8569	0.0866	0.7705	0.0973	0.9629	0.0324
COM4	0.9668	0.0621	0.8475	0.1567	0.5973	0.8259	0.9836	0.0414
COM5	0.9850	0.0410	0.9103	0.1313	0.9179	0.1056	0.9825	0.0429

TM4 has the largest values in RSP1 and RSP2 which could suggest these factors are important for C_D models.

At the low-Q AoA sweep, it was expected that TM3 would still do well, but that proved to not be the case as seen in Figure 44. Both TM3 and TM2 seem to have a problem predicting the linear stage, whereas in the unsteady stage they are much closer. The inability of these two maneuvers to predict the two different stages could be due to lack of a variety in the training maneuvers themselves. From the metrics in Table 9, TM1 returns better values than TM4 in both R^2 and NRMSD. TM1 has better low Q RSP values, and since this is low Q maneuver, it suggests that the low Q values have an impact on the metrics.

As expected for the high Q sweep, TM3 does not produce very good results as seen in Figure 45. The inaccuracy makes the model pretty much useless in these conditions. TM1 and TM4 again display good values throughout the majority of the maneuver, only beginning to separate from the comparison coefficient at the high-alpha values. This could be due to there being no input data at the max alpha, at a positive Q value. In the training maneuvers at the max alpha the maneuvers are generally at a near-zero or negative Q to resulting in a decrease in AoA. TM4 returns the best values for this comparison maneuver. TM4 also has the best high Q RSPs.
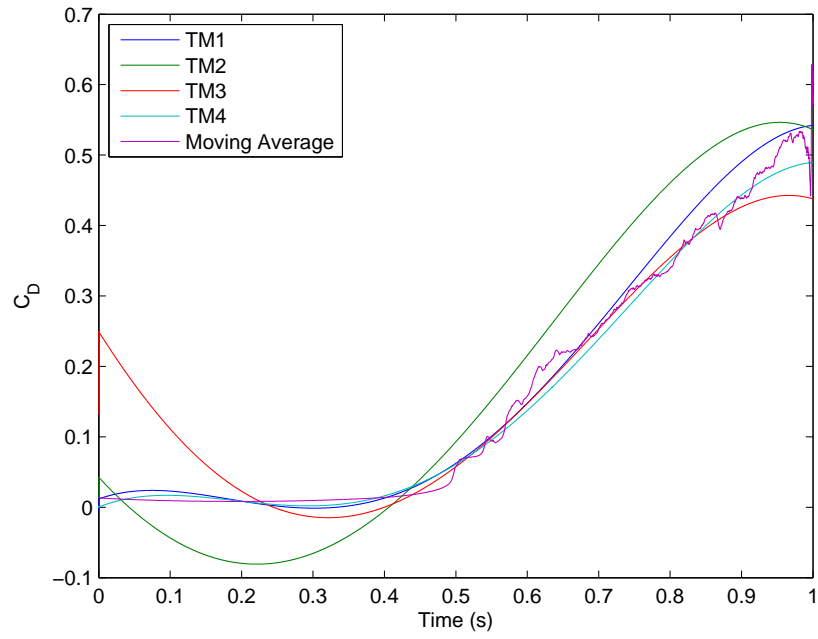
Figure 43. Model results COM1a C_D
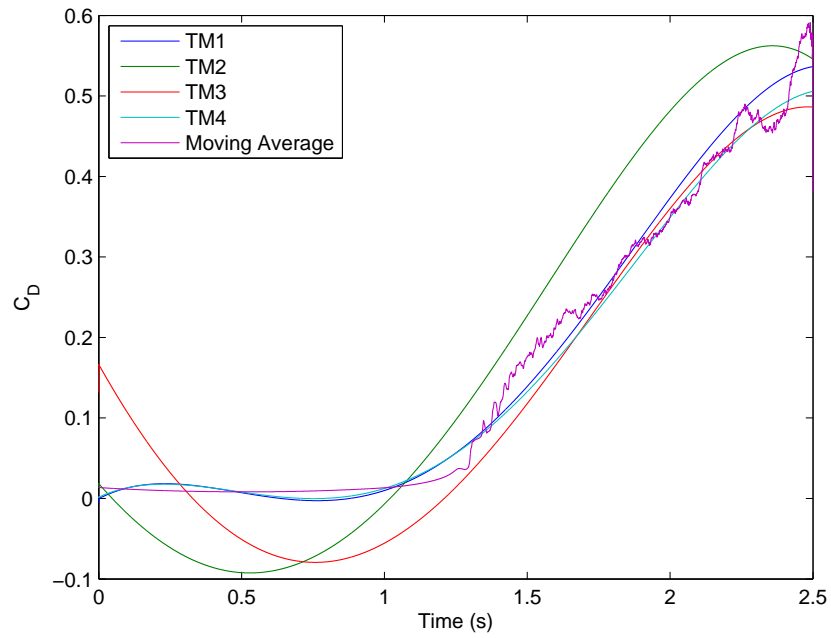
Figure 44. Model results COM1b C_D
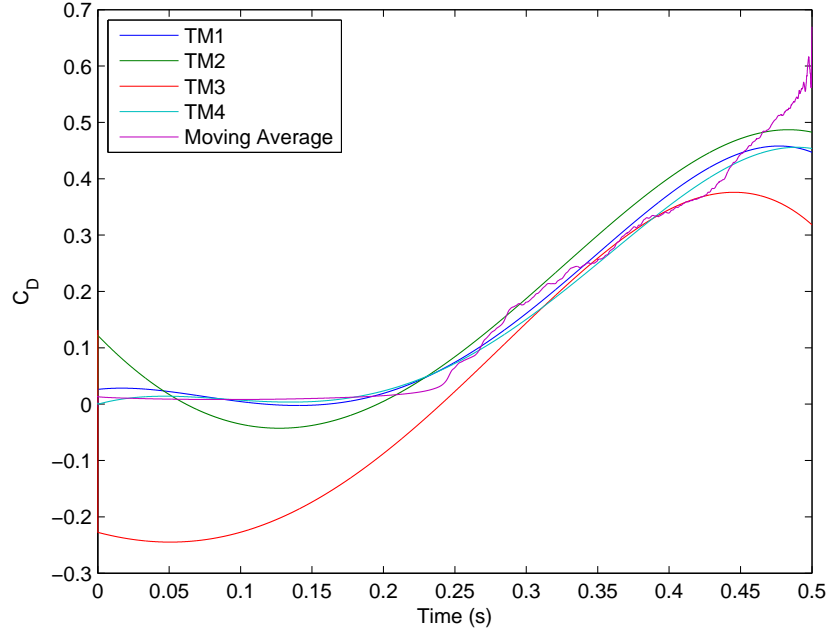
Figure 45. Model results COM1c C_D

For the COM2 maneuver shown in Figure 46, TM3 again was so inaccurate that the results are not shown. These inaccuracies likely due to the high Q nature of this maneuver that TM3 simply does not have the data for. The inaccuracy of TM3 should help to solidify the importance of covering the boundaries of the regressor space. TM4 also is not taken into account for this maneuver, although it is displayed on the figure. From Figure 46 and Table 9 it is shown that TM1 is the most accurate. TM1 does have better high Q values than TM2 and TM3, but it is hard to suggest that these factors alone are why it does better for this maneuver.

In the COM3 maneuver shown in Figure 47, there is a large spread in the results. TM2 and TM3 have problems in the low alpha and low Q sections of the maneuver. TM2 continues to display inaccuracy at the high alpha and high Q portion of the maneuver. TM1 and TM4 display good results throughout the course of the maneuver. By the tabular results, TM1 has a smaller NRMSD but TM4 has a larger R^2 value. The results are very close in magnitude. TM1 and TM4 have better low Q and high

71
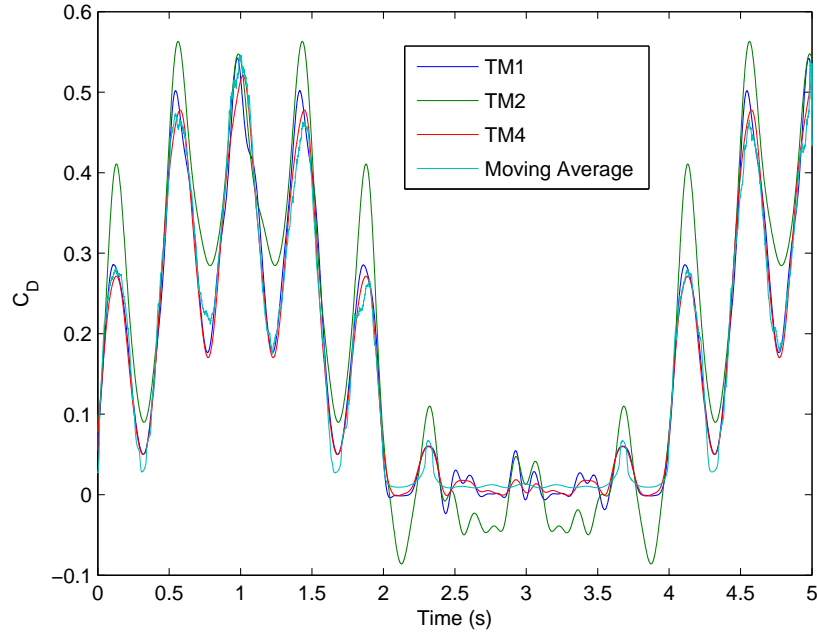
Figure 46. Model results COM2 C_D

Q RSP values than TM2 and TM3, but TM3 still manages to do well for a bit of the maneuver at high Q. There is no clear link between the RSPs and metrics for this maneuver.

For the COM4 maneuver shown in Figure 48, at the high alpha, low Q section of the maneuver both TM2 and TM3 were inaccurate. TM3 retains some precision during the ramp up Q; however, it again becomes inaccurate at the higher Q portion of the maneuver. TM1 and TM4 both retain a good degree of accuracy throughout the course of the maneuver. The only lack of precision being the very minor changes in drag at low angles of attack. According to Table 9, TM4 has the best values for R^2 and NRMSD. As with the previous maneuver, it is hard to base conclusions on the RSPs from this result.

For the last comparison maneuver, which is the step maneuver COM5, the results are similar to the previous maneuvers. TM2 and TM3 have trouble at the lower alpha values. TM2 continues to stay inaccurate while TM3 is relatively accurate at
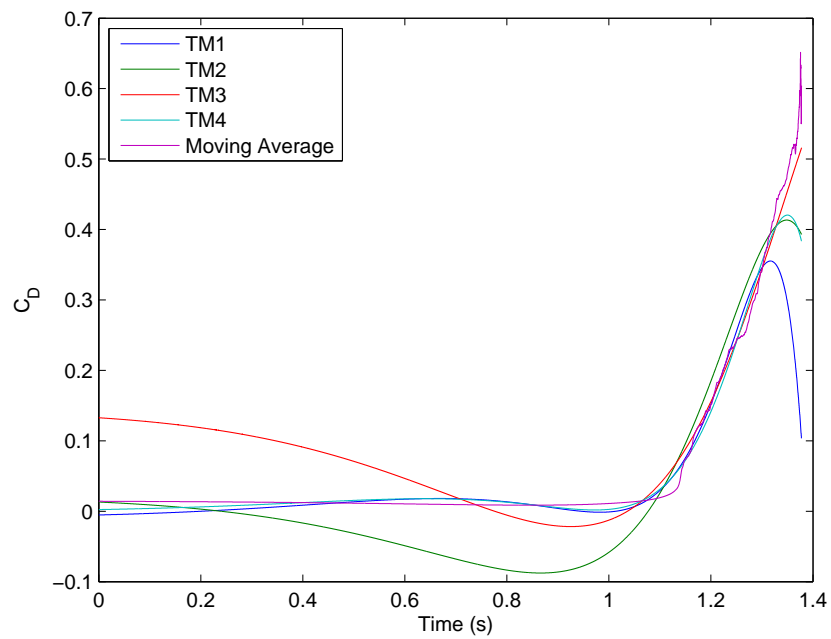
Figure 47. Model results COM3 C_D
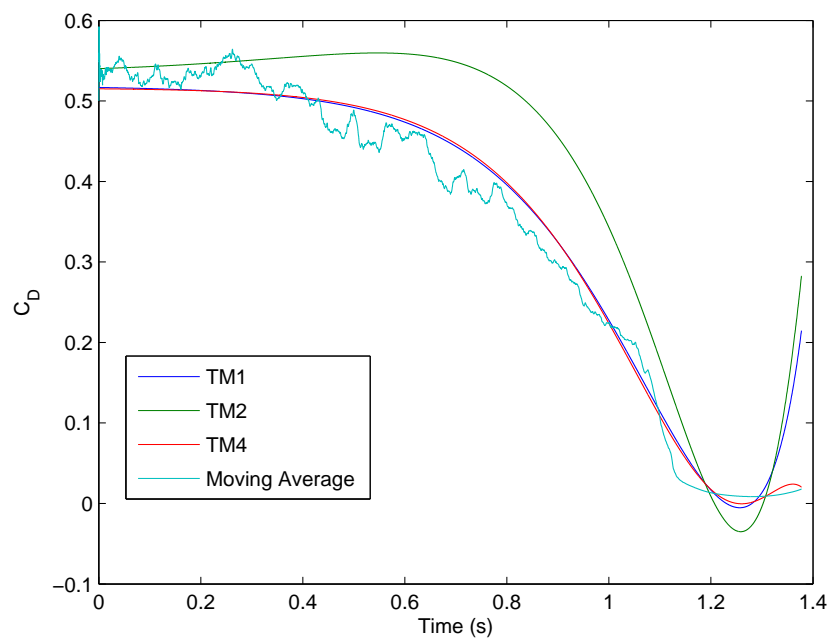
Figure 48. Model results COM4 C_D

15 degrees AoA. TM1 and TM4 show relative accuracy throughout the duration of the maneuver. Table 9 shows that TM1 was the most accurate maneuver. TM1 does have the best zero Q RSP results for percent and per cell but TM4 has a better standard deviation number.
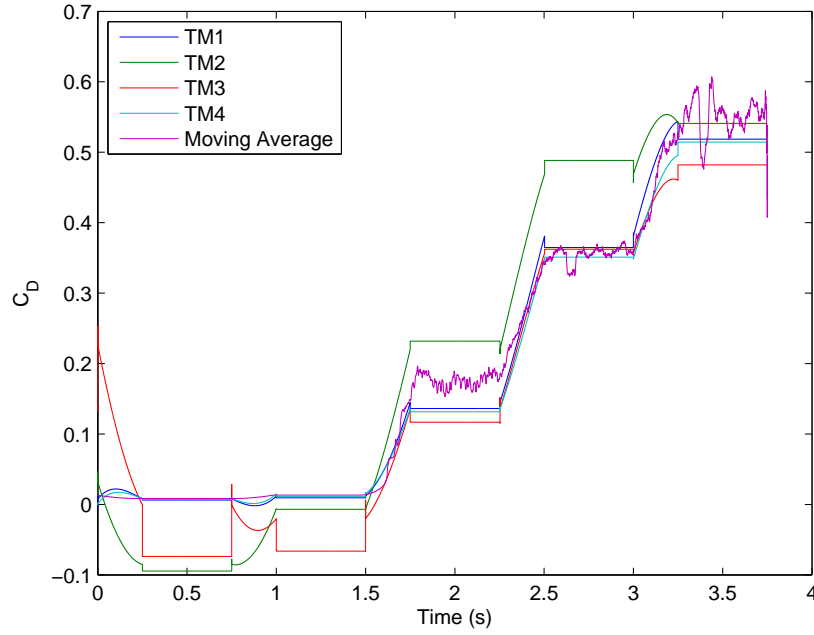
Figure 49. Model results COM5 C_D

4.3.3 Moment Coefficient

The results for the moment coefficient models can be seen in Table 10. The prediction of results for the moment coefficient fluctuated for the models. Overall, the values for R^2 and NRMSD are lower than the values seen for C_D and C_L. TM1 and TM4 have the best RSP1 and RSP2 values.

For the first alpha sweep, COM1a, TM3 was wildly off course for most of the maneuver, whereas TM1, TM2 and TM4 were relatively accurate. TM1 is a bit inaccurate at the higher AoAs. Per the metrics, TM1 has the largest R^2 while TM4 has the lowest NRMSD.

Table 10. R^2 and NRMSD for all C_M models vs a moving average

COM	TM1		TM2		TM3		TM4	
	R^2	NRMSD	R^2	NRMSD	R^2	NRMSD	R^2	NRMSD
COM1a	0.9487	0.0556	0.9096	0.0624	0.4612	0.4436	0.9434	0.0504
COM1b	0.9366	0.0871	0.8642	0.1073	0.6078	0.5391	0.9182	0.0902
COM1c	0.7634	0.1351	0.9106	0.0854	0.4263	1.4006	0.8825	0.0879
COM2	0.9138	0.0762	0.8862	0.0716	0.5020	0.2786	-	-
COM3	0.4243	0.2198	0.9252	0.0589	0.4668	2.1220	0.8438	0.0641
COM4	0.8286	0.1194	0.8679	0.0880	0.5548	1.0631	0.9050	0.0777
COM5	0.9118	0.1015	0.8960	0.0954	0.6196	0.5177	0.8851	0.1108
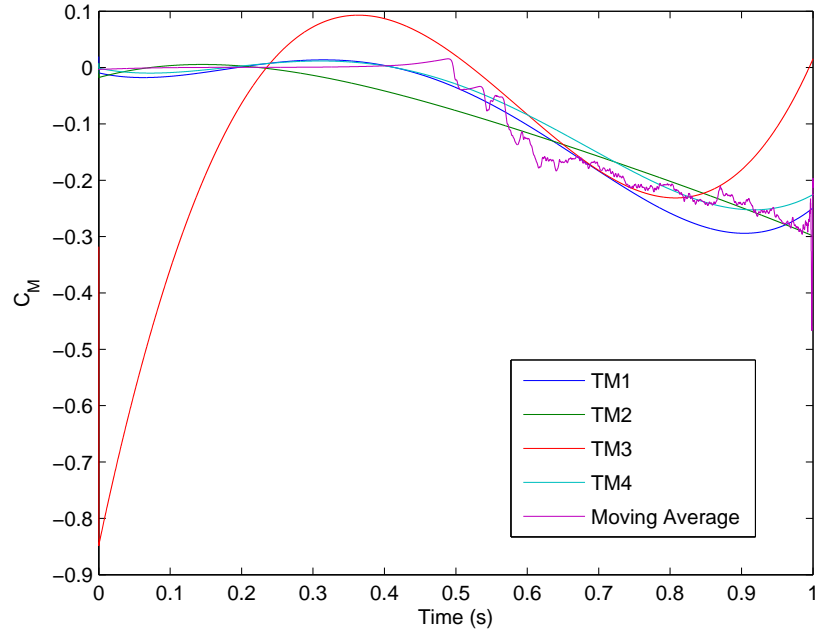
Figure 50. Model results COM1a C_M

75

For the next alpha sweep, COM1b, TM3 is again not very accurate. TM1 and TM4 show the same trend as seen in the previous maneuver, and TM2 also seems to follow the same line as before. According to Table 10, for this maneuver TM1 has the best metrics. As seen in the previous coefficient, TM1 has the best metrics and also has the better low Q RSPs. Also note the sharp decrease in moment coefficient. This would appear to correspond to separation. While there is a discussion to be had on the ability of CFD to accurately predict separation, the MVP models are not able to capture the phenomena that is predicted by the CFD.
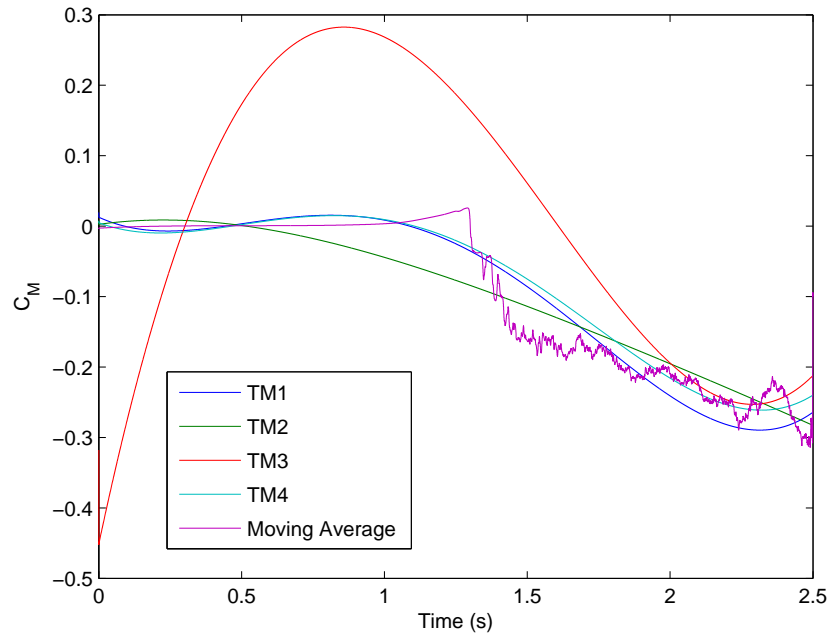
Figure 51. Model results COM1b C_M

For the final alpha sweep, COM1c, it is not surprising that TM3 is even more inaccurate, as it was expected to be for the high Q maneuvers. Because of TM3s inaccuracy it is removed from Figure 52 as it was distracting from the other maneuvers. As it can be seen, both TM4 and TM1 have a sharp rise at the high AoA values. Per Table 10, TM2 has the best output metrics. Much of the inaccuracy for TM1 and TM4 seems to happen in the last 0.1 seconds of the maneuver; without this section

TM1 and TM4 would likely result in a better prediction. Between TM1 and TM4, TM4 presents the better metrics and has better RSP values at high Q.
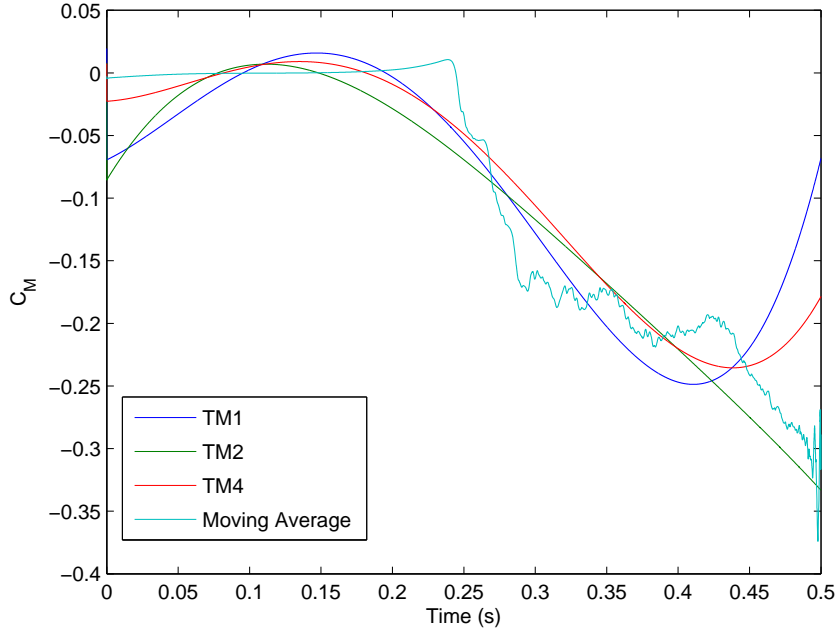
Figure 52. Model results COM1c C_M

For COM2, TM4 should not be considered for comparison although it is displayed in Figure 53. It can be seen that TM1 and TM2 both overestimate some peaks in the unsteady regime while overestimating oscillations in the linear regime. According to Table 10, TM1 is the most accurate maneuver. TM1 does have better high Q values than TM2 and TM3, but it is hard to suggest that these factors alone are why it does better for this maneuver.

For COM3, the exponential maneuver shown in Figure 54, TM3 is not shown due to gross inaccuracy. TM1 and TM4 seem to capture the linear regime better; however, TM2 seems to capture the non-linear regime better. In the metrics, TM4 is the most accurate maneuver. There is no obvious link between RSPs and output metrics from this maneuver.

For the negative exponential maneuver, COM4, shown in Figure 55, TM3 is accu-

77
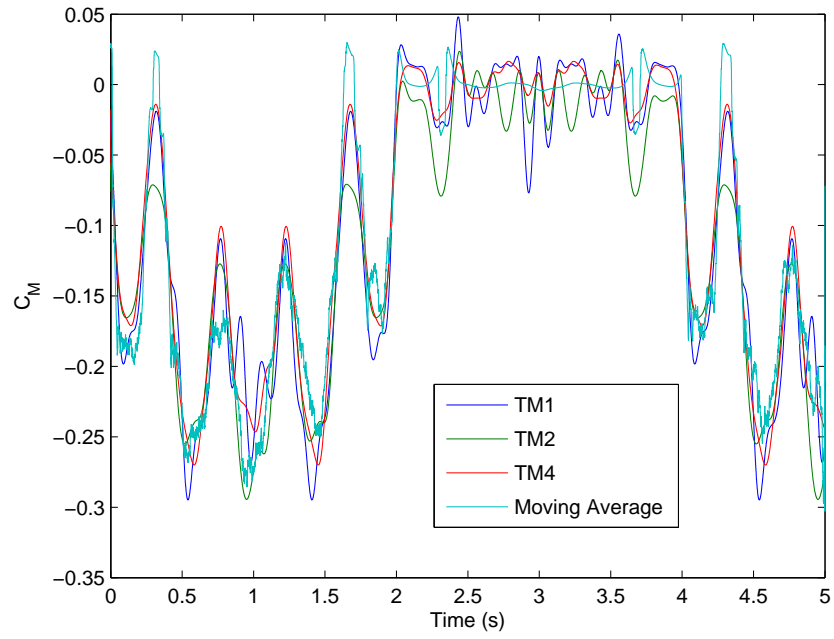
Figure 53. Model results COM2 C_M
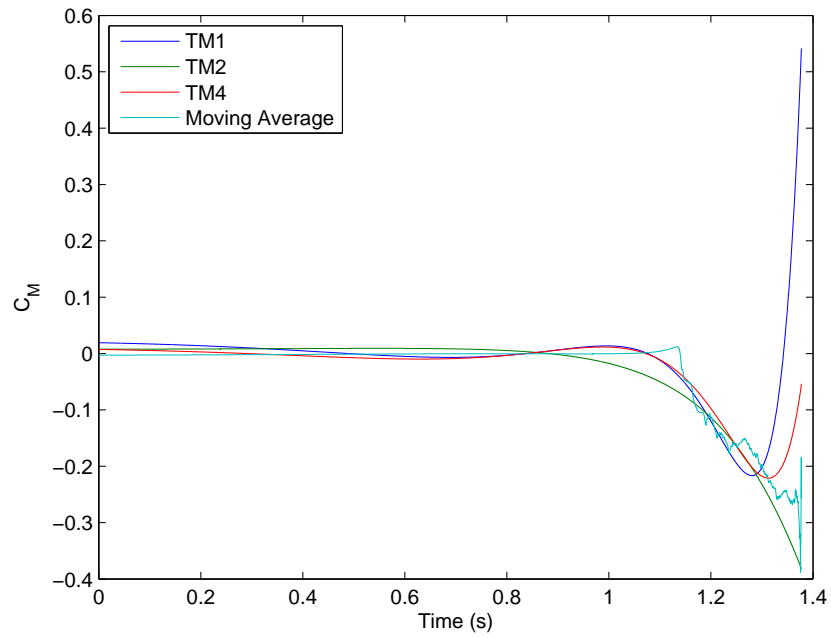
Figure 54. Model results COM3 C_M

rate in the low Q and high alpha region. However, once the Q value increases, TM3 is inaccurate. TM1 and TM4 are again closely linked, while TM2 is on track but seems to follow the trend of the data less closely. In Table 10, TM4 has the largest R^2 while NRMSD has the lowest NRMSD. Once again, this maneuver provides no obvious insight into the link between RSPs and the metrics.
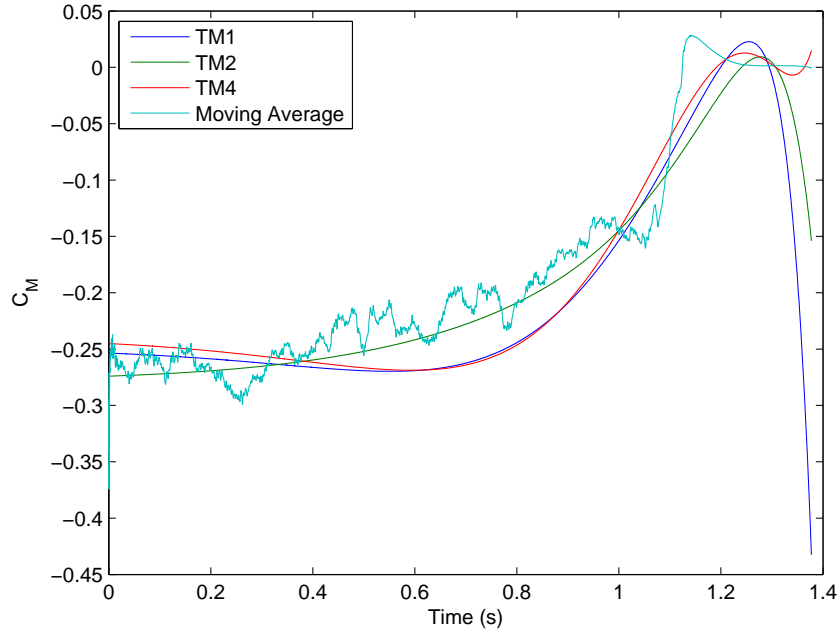
Figure 55. Model results COM4 C_M

The pitch and hold maneuver shown in Figure 56 does not display TM3. The results of TM3 were so inaccurate that it was difficult to distinguish between the other results. With TM3 removed, it can be seen that TM4 and TM1 do well at the low angles of attack, have trouble around 10 degrees, but then are strangely are better at 15 and 20 degrees. TM2 is inaccurate for the low AoAs but does well at larger angles. Referencing Table 10, TM1 has the best metrics for this maneuver, and as before, has the best zero Q RSP values.
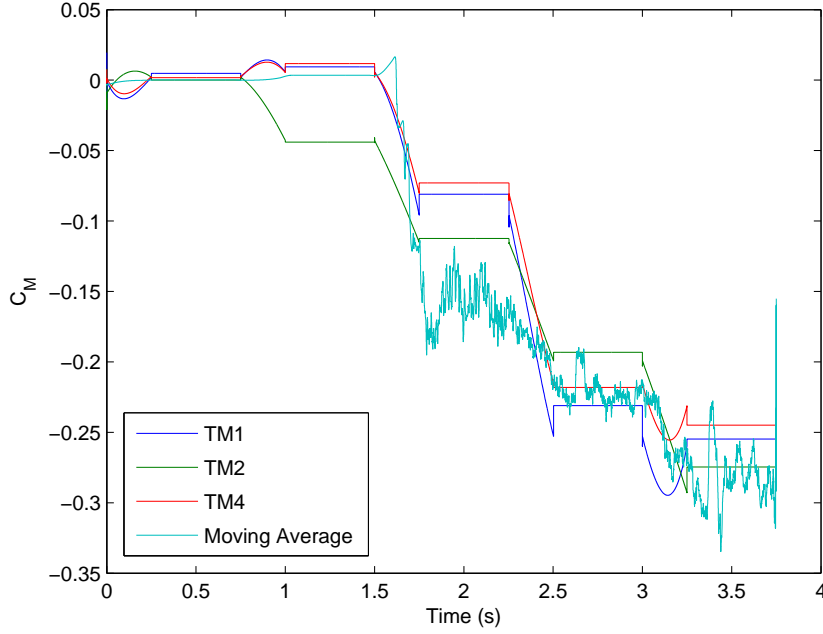
Figure 56. Model results COM5 C_M

4.4 Statistical Analysis of Initially Proposed RSPs

The results of this section and the results of Section 4.5.1 are colored using the same scale; however, each coefficient is colored using a different scale. The different coloring is due to the large discrepancy between the correlation values for each coefficient. The discrepancy is likely due to the scale of differences between R^2 and NRMSD values when examining coefficients. For C_L, most of the models returned a R^2 value around 0.99, while for C_M a high R^2 value was approximately 0.90, while a low value was approximately 0.5. The correlation values are then smaller for C_L as opposed to C_M as the change in each RSP reflects only a minor at best difference in R^2 and NRMSD values. Table 11 shows the coloring for the correlation values based on coefficient.

Table 12 shows the colored correlation value chart. The most obvious conclusion is that the RSPs are not consistently correlated. Despite the differing ranges to provide

80

Table 11. Correlation value coloring

Color	Correlation Value (Absolute Value)		
	C_L	C_D	C_M
red	$x < 0.5$	$x < 0.4$	$x < 0.6$
yellow	$0.5 < x < 0.6$	$0.4 < x < 0.55$	$0.6 < x < 0.8$
green	$x > 0.6$	$x > 0.55$	$x > 0.8$

adequate contrast, the correlation values are not consistent across coefficients. That is, a good RSP for one coefficient does not necessarily lead to being a good RSP for another coefficient. Another condition of note is that the standard deviation values seem to have one of the largest impacts across most the coefficients. Looking at RSP_3 and RSP_4, it appears that Q is a larger factor than AoA. Therefore, for the regressor space subsets (low Q and high Q) it may be beneficial to split the standard deviation calculation into AoA and Q standard deviation as is done with the whole regressor space in previous RSPs.

Table 12. Initial RSP correlations for all comparison maneuvers

RSP	Description	C_L		C_D		C_M	
		R^2	NRMSD	R^2	NRMSD	R^2	NRMSD
RSP_1	% Whole	0.3872	-0.3738	0.6027	-0.4702	0.4762	-0.4220
RSP_2	% Boundary	0.5279	-0.5248	0.5370	-0.4268	0.7129	-0.5682
RSP_3	α std	0.2821	-0.2630	0.4636	-0.3824	0.2873	-0.3037
RSP_4	Q std	0.4913	-0.4694	0.5860	-0.5006	0.5471	-0.5230
RSP_5	0Q %	0.3739	-0.3562	0.5742	-0.4619	0.4271	-0.4045
RSP_6	0Q per cell	-0.3010	0.3044	-0.0785	0.0906	-0.4105	0.3144
RSP_7	0Q std	0.4713	-0.4625	0.6321	-0.4902	0.6168	-0.5123
RSP_8	LQ %	0.3135	-0.2957	0.5190	-0.4180	0.3435	-0.3396
RSP_9	LQ per cell	-0.4685	0.4655	-0.2803	0.2598	-0.6040	0.4934
RSP_{10}	LQ std	0.4519	-0.4386	0.6445	-0.5063	0.5641	-0.4906
RSP_{11}	HQ %	0.3966	-0.3852	0.6065	-0.4685	0.5025	-0.4330
RSP_{12}	HQ per cell	0.2440	-0.2334	0.4931	-0.3707	0.3020	-0.2710
RSP_{13}	HQ std	0.5960	-0.5828	0.7018	-0.5661	0.7524	-0.6414

The most surprising fact is that none of the values for C_L or C_M are very strong. While there are some values that are larger than others, when the scale is held con-

81

sistent between the two sections (Section 4.4 and 4.5.1), there are no green cells for those two coefficients. C_L is easy to predict, causing the changes in RSPs for the different training maneuvers to have little effect on metrics. C_M is difficult for all the models to accurately predict. This leads to the impression for reformulation of the RSPs.

The first reformulation deals with how these standard deviations are calculated. For the initial RSPs, the distribution is filled with a count of which cells are hit. A different approach is to use the total number of points in a cell, rather than binary 1 or 0 method.

Since measuring the shape of the distribution seems to be important, additional means to measure the distribution might provide more favorable results.

4.5   Proposed RSPs

After the analysis conducted in Section 4.4, new RSPs were created and existing RSPs were modified. There were also several changes to the implementation of the programming, which in some cases caused a small difference in RSP values for RSPs that were otherwise not changed.

RSP_1 is unchanged from Equation (3.4.1) and RSP_2 is unchanged from Equation (3.4.2). RSP_3 no longer uses the maximum value as a standardization and takes into account how many times a value is hit. This is in order to conform more with a

standard statistical cumulative distribution function. The revised RSP_3 is shown in Equation (4.5.1).

$$RSP_3 = std \left[\begin{pmatrix} \# \ of \ hits \ at \ first \ AoA \\ \# \ of \ hits \ at \ second \ AoA \\ \vdots \\ \# \ of \ hits \ at \ last \ AoA \end{pmatrix} \div \# \ of \ AoA \ columns \right] \qquad (4.5.1)$$

RSP_4 makes the same changes in regards to Q as RSP_3 did in regards to AoA. The revised RSP_4 is given in Equation (4.5.2).

$$RSP_4 = std \left[\begin{pmatrix} \# \ of \ hits \ at \ first \ Q \\ \# \ of \ hits \ at \ second \ Q \\ \vdots \\ \# \ of \ hits \ at \ last \ Q \end{pmatrix} \div \# \ of \ Q \ rows \right] \qquad (4.5.2)$$

RSP_5 is unchanged from how it is presented in Equation (3.4.5) and RSP_6 is unchanged from how it is presented in Equation (3.4.6).

RSP_7, as with the previous standard deviation RSPs, divides by the number of AoA columns as shown in Equation (4.5.3).

$$RSP_7 = std \left(\frac{cell_1, \ cell_2, \ cell_3, ...last \ cell}{\# \ AoA \ columns} \right)_{@ \ 0 \ Q} \qquad (4.5.3)$$

RSP_8 is unchanged from how it is presented in Equation (3.4.8), and RSP_9 is unchanged from its presentation in Equation (3.4.9). However RSP_{10}, is where the RSPs begin to lose numbering from the previous iteration of RSPs. RSP_{10} is now broken up into two RSPs, which collapse the low Q data into AoA and Q cumulative distribution functions much like done for the new RSP_3 and RSP_4 above. The new

RSP_{10} is given by Equation (4.5.4), and the new RSP_{11} is given by Equation (4.5.5).

$$RSP_{10} = std \left[\begin{pmatrix} \# \, of \, hits \, at \, first \, \alpha \\ \# \, of \, hits \, at \, second \, \alpha \\ \vdots \\ \# \, of \, hits \, at \, last \, \alpha \end{pmatrix} \div \# \, of \, \alpha \, columns \right]_{@ \, low \, (not \, 0) \, Q} \tag{4.5.4}$$

$$RSP_{11} = std \left[\begin{pmatrix} \# \, of \, hits \, at \, first \, Q \\ \# \, of \, hits \, at \, second \, Q \\ \vdots \\ \# \, of \, hits \, at \, last \, Q \end{pmatrix} \div \# \, of \, Q \, rows \right]_{@ \, low \, (not \, 0) \, Q} \tag{4.5.5}$$

The high Q RSPs are set up the same as the new low Q RSPs; however, the numbering from the previous iteration of RSPs no longer lines up. The new RSP_{12} is equivalent to Equation (3.4.11) and the new RSP_{13} is equivalent to Equation (3.4.12). As with low Q, the standard deviation is now split into two different standard deviations, given in Equations (4.5.6) and (4.5.7).

$$RSP_{14} = std \left[\begin{pmatrix} \# \, of \, hits \, at \, first \, \alpha \\ \# \, of \, hits \, at \, second \, \alpha \\ \vdots \\ \# \, of \, hits \, at \, last \, \alpha \end{pmatrix} \div \# \, of \, \alpha \, columns \right]_{@ \, high \, Q} \tag{4.5.6}$$

$$RSP_{15} = std \left[\begin{pmatrix} \# \, of \, hits \, at \, first \, Q \\ \# \, of \, hits \, at \, second \, Q \\ \vdots \\ \# \, of \, hits \, at \, last \, Q \end{pmatrix} \div \# \, of \, Q \, rows \right]_{@ \, high \, Q} \tag{4.5.7}$$

All further RSPs presented are completely unrelated to any previous RSPs pre-

sented. RSP_{16} is an attempt to measure how closely and completely the training maneuver approaches the boundary. For the RSP calculations, points that are outside of bounds ($\pm$ 75 deg/s Q and -5 to 20 deg α) are not considered. Since, the maneuver may go outside the bounds, and RSP_16 aims to capture how many points are "wasted". RSP_{16} is shown in Equation (4.5.8).

$$RSP_{16} = \frac{\#\ of\ data\ points\ used}{Total\ \#\ of\ points} \qquad (4.5.8)$$

The next two RSPs aim to quantify how efficiently a maneuver captures the data. This maneuver takes into account how much of the regressor space was covered and the length of the maneuver. RSP_{17} is given by Equation (4.5.9) and RSP_{18} is given by Equation (4.5.10). RSP_{18} is an attempt to normalize the values depending on the time step used during simulation of the TMs.

$$RSP_{17} = \frac{RSP_1}{Length\ of\ Maneuver} \qquad (4.5.9)$$

$$RSP_{18} = \frac{RSP_1 * dt}{Length\ of\ Maneuver} \qquad (4.5.10)$$

The next three RSPs are similar to the previous two RSPs, but these three look to the how much of each subset is covered per the total duration (length) of the maneuver as shown in Equations (4.5.11) - (4.5.13).

$$RSP_{19} = \frac{RSP_5}{Length\ of\ Maneuver} \qquad (4.5.11)$$

$$RSP_{20} = \frac{RSP_8}{Length\ of\ Maneuver} \qquad (4.5.12)$$

$$RSP_{21} = \frac{RSP_{12}}{Length\ of\ Maneuver} \qquad (4.5.13)$$

The remaining RSPs are different from the previous RSPs in that they are gener-

ally considered higher order descriptions of data. Three different higher order statistics will be looked at; kurtosis, skewness and Pearson product-moment correlation coefficient.

Kurtosis is a measure of the "peakness" of a data set. A normal distribution returns a kurtosis value of 3. Kurtosis is defined in Equation (4.5.14) and the equation used to calculate kurtosis from a data set is shown in Equation (4.5.15). [22]

$$k = \frac{E(x - \mu)^4}{\sigma^4} \tag{4.5.14}$$

$$k = \frac{\frac{1}{n}\sum_{i=1}^{n}(x_i - \bar{x})^4}{\left(\frac{1}{n}\sum_{i=1}^{n}(x_i - \bar{x})^2\right)^2} \tag{4.5.15}$$

where x is the independent variable, $\bar{x}$ is the sample mean, μ is the population mean, n is the number of data points, and σ is the standard deviation.

Skewness is a measure of the asymmetry of the data around the mean. A positive skewness represents data that is spread out more to the right of the mean. Skewness is defined by Equation (4.5.16) and is calculated in Equation (4.5.17).

$$s = \frac{E(x - \mu)^3}{\sigma^3} \tag{4.5.16}$$

$$s = \frac{\frac{1}{n}\sum_{i=1}^{n}(x_i - \bar{x})^3}{\left(\sqrt{\frac{1}{n}\sum_{i=1}^{n}(x_i - \bar{x})^2}\right)^3} \tag{4.5.17}$$

The Pearson product-moment correlation coefficient (Pearson r) is a measure of linearity between two data sets. A value of 1 means positively correlated and a value

of -1 means negatively correlated. The equation to calculate the Pearson r is given in Equation (4.5.18). [26]

$$r = \frac{\sum\limits_{i=1}^{n}((x_i - \bar{x})(y_i - \bar{y}))}{\sqrt{\sum\limits_{i=1}^{n}(x_i - \bar{x})^2 \sum\limits_{i=1}^{n}(y_i - \bar{y})^2}} \tag{4.5.18}$$

Using the above statistics, the data was analyzed in the various subsets as was done previously. The data is organized into two different distribution curves, one for AoA and one for Q. Those distributions are also partitioned into four different intervals: whole, 0 Q, low (non-0) Q and high Q. RSP_{22} and RSP_{23} look at the kurtosis of the entire regressor space in Equation (4.5.19) and Equation (4.5.20).

$$RSP_{22} = Kurtosis \begin{pmatrix} \# \, of \, hits \, at \, first \, AoA \\ \# \, of \, hits \, at \, second \, AoA \\ \vdots \\ \# \, of \, hits \, at \, last \, AoA \end{pmatrix} \tag{4.5.19}$$

$$RSP_{23} = Kurtosis \begin{pmatrix} \# \, of \, hits \, at \, first \, Q \\ \# \, of \, hits \, at \, second \, Q \\ \vdots \\ \# \, of \, hits \, at \, last \, Q \end{pmatrix} \tag{4.5.20}$$

The next two RSPs look at the skewness of the entire regressor space and are shown in Equation (4.5.21) and Equation (4.5.22).

$$RSP_{24} = Skewness \begin{pmatrix} \# \, of \, hits \, at \, first \, AoA \\ \# \, of \, hits \, at \, second \, AoA \\ \vdots \\ \# \, of \, hits \, at \, last \, AoA \end{pmatrix} \tag{4.5.21}$$

$$RSP_{25} = Skewness \begin{pmatrix} \# \ of \ hits \ at \ first \ Q \\ \# \ of \ hits \ at \ second \ Q \\ \vdots \\ \# \ of \ hits \ at \ last \ Q \end{pmatrix} \tag{4.5.22}$$

The next RSP is the Pearson r between AoA and Q for the maneuver and is shown by Equation (4.5.23).

$$RSP_{26} = r = \frac{\sum\limits_{i=1}^{n}((AoA_i - \overline{AoA})(Q_i - \overline{Q}))}{\sqrt{\sum\limits_{i=1}^{n}(AoA_i - \overline{AoA})^2 \sum\limits_{i=1}^{n}(Q_i - \overline{Q})^2}} \tag{4.5.23}$$

The next set of RSPs looks at the kurtosis and skewness at 0 Q. The kurtosis RSP is given by Equation (4.5.24) and the skewness RSP is given by Equation (4.5.25).

$$RSP_{27} = Kurtosis \begin{pmatrix} \# \ of \ hits \ at \ first \ AoA \\ \# \ of \ hits \ at \ second \ AoA \\ \vdots \\ \# \ of \ hits \ at \ last \ AoA \end{pmatrix}_{@\,0\,Q} \tag{4.5.24}$$

$$RSP_{28} = Skewness \begin{pmatrix} \# \ of \ hits \ at \ first \ AoA \\ \# \ of \ hits \ at \ second \ AoA \\ \vdots \\ \# \ of \ hits \ at \ last \ AoA \end{pmatrix}_{@\,0\,Q} \tag{4.5.25}$$

The next set of equations looks at the kurtosis and skewness for Q and AoA at low but not 0 Q. Kurtosis for AoA is given in Equation (4.5.26), and Q is given in

Equation (4.5.27). Skewness for AoA is given in Equation (4.5.28), and Q is given in Equation (4.5.29).

$$RSP_{29} = Kurtosis \begin{pmatrix} \# \ of \ hits \ at \ first \ AoA \\ \# \ of \ hits \ at \ second \ AoA \\ \vdots \\ \# \ of \ hits \ at \ last \ AoA \end{pmatrix}_{@ \ low \ (not \ 0) \ Q} \tag{4.5.26}$$

$$RSP_{30} = Kurtosis \begin{pmatrix} \# \ of \ hits \ at \ first \ Q \\ \# \ of \ hits \ at \ second \ Q \\ \vdots \\ \# \ of \ hits \ at \ last \ Q \end{pmatrix}_{@ \ low \ (not \ 0) \ Q} \tag{4.5.27}$$

$$RSP_{31} = Skewness \begin{pmatrix} \# \ of \ hits \ at \ first \ AoA \\ \# \ of \ hits \ at \ second \ AoA \\ \vdots \\ \# \ of \ hits \ at \ last \ AoA \end{pmatrix}_{@ \ low \ (not \ 0) \ Q} \tag{4.5.28}$$

$$RSP_{32} = Skewness \begin{pmatrix} \# \ of \ hits \ at \ first \ Q \\ \# \ of \ hits \ at \ second \ Q \\ \vdots \\ \# \ of \ hits \ at \ last \ Q \end{pmatrix}_{@ \ low \ (not \ 0) \ Q} \tag{4.5.29}$$

The next set of RSPs measures the kurtosis and skewness of the high Q data. Equation (4.5.30) measures the kurtosis of AoA and Equation (4.5.31) measures the

kurtosis of Q. Equation (4.5.32) measures the skewness of AoA and Equation (4.5.33) measures the skewness of Q.

$$RSP_{33} = Kurtosis \begin{pmatrix} \# \, of \, hits \, at \, first \, AoA \\ \# \, of \, hits \, at \, second \, AoA \\ \vdots \\ \# \, of \, hits \, at \, last \, AoA \end{pmatrix}_{@ \, high \, Q} \qquad (4.5.30)$$

$$RSP_{34} = Kurtosis \begin{pmatrix} \# \, of \, hits \, at \, first \, Q \\ \# \, of \, hits \, at \, second \, Q \\ \vdots \\ \# \, of \, hits \, at \, last \, Q \end{pmatrix}_{@ \, high \, Q} \qquad (4.5.31)$$

$$RSP_{35} = Skewness \begin{pmatrix} \# \, of \, hits \, at \, first \, AoA \\ \# \, of \, hits \, at \, second \, AoA \\ \vdots \\ \# \, of \, hits \, at \, last \, AoA \end{pmatrix}_{@ \, high \, Q} \qquad (4.5.32)$$

$$RSP_{36} = Skewness \begin{pmatrix} \# \, of \, hits \, at \, first \, Q \\ \# \, of \, hits \, at \, second \, Q \\ \vdots \\ \# \, of \, hits \, at \, last \, Q \end{pmatrix}_{@ \, high \, Q} \qquad (4.5.33)$$

RSP_{36} concludes the RSPs considered for this research. The MATLAB®function created for the calculation of these RSPs is given in Appendix A.4 for the reader's reference.

4.5.1 Proposed RSP Results

Following the discussion in Section 4.5, the additional RSPs were calculated in two groups. First, the 'first order' statistics are given in Table 13. The first thing to note is the different standard deviation values. While it was expected for the values to change as the normalization was changed, the change in switching to total hits instead of cells has changed the trend of the data. The change is most evident in RSPs 3, 4 and 7. In Table 6, TM1 has the largest AoA standard deviation, while in Table 13 it has the third largest. The implications of these different results may be seen later on with the correlation results.

Table 13. First set of revised RSP values

RSP	Description	TM1	TM2	TM3	TM4
RSP_1	% Whole	3.6573	0.8851	0.6880	5.0024
RSP_2	% Boundary	3.4897	11.556	0.0000	15.046
RSP_3	α std	3.6625	1.3754	4.3837	4.9181
RSP_4	Q std	0.0861	0.0098	0.2083	0.0935
RSP_5	0Q %	4.8000	0.8000	0.8000	4.4000
RSP_6	0Q per cell	0.8720	0.1280	0.9880	0.7640
RSP_7	0Q std	0.0178	0.0057	0.0488	0.0160
RSP_8	LQ %	4.9560	0.8120	1.3050	4.2230
RSP_9	LQ per cell	0.9473	0.1311	1.3432	0.8761
RSP_{10}	LQ α std	2.9953	1.3198	4.4692	4.4361
RSP_{11}	LQ Q std	0.2047	0.0024	1.1168	0.0158
RSP_{12}	HQ %	3.1866	0.9115	0.4650	5.2843
RSP_{13}	HQ per cell	0.8153	0.1874	0.3845	1.1357
RSP_{14}	HQ α std	1.9957	0.6853	1.1915	2.6407
RSP_{15}	HQ Q std	0.1285	0.0142	0.1935	0.1456
RSP_{16}	Effectiveness	0.9964	0.8082	1.0000	0.9999
RSP_{17}	Time1	0.9143	0.8851	0.2293	1.0005
RSP_{18}	Time2	1.142e-05	1.106e-05	2.866e-06	1.251e-05
RSP_{19}	Time Eff 0Q	1.2000	0.8000	0.2667	0.8800
RSP_{20}	Time Eff LQ	1.2390	0.8120	0.4350	0.8446
RSP_{21}	Time Eff HQ	0.7966	0.9115	0.1550	1.0569

Another note is the switch from one standard deviation value for the low Q and

high Q ranges to one for AoA and one for Q. In Table 13, it can be seen that there are different trends in AoA and Q.

A final note concerns the trends seen in RSPs 19, 20 and 21, these RSPs are far different than the percentage RSPs (RSPs 5,8 and 12) that form the basis. The result of this can be seen in the magnitude of the correlation values.

Table 14 shows the correlation values for the 'first order' statistics. The positive outlook is now we can see green start to cover more of the table. Some statistics are starting to reveal themselves as more useful than others.

Table 14. First set of revised RSPs - correlation values

RSP	Description	C_L		C_D		C_M	
		R^2	NRMSD	R^2	NRMSD	R^2	NRMSD
RSP_1	% Whole	0.3838	-0.3648	0.6001	-0.4666	0.4626	-0.4166
RSP_2	% Boundary	0.4889	-0.4827	0.4920	-0.3862	0.6644	-0.5253
RSP_3	α std	-0.2577	0.2610	-0.0015	0.0502	-0.3242	0.2649
RSP_4	Q std	-0.6034	0.5936	-0.4752	0.4207	-0.7563	0.6386
RSP_5	0Q %	0.3716	-0.3503	0.5721	-0.4595	0.4181	-0.4009
RSP_6	0Q per cell	-0.3660	0.3686	-0.1534	0.1538	-0.4923	0.3845
RSP_7	0Q std	-0.6474	0.6346	-0.5691	0.4901	-0.8098	0.6874
RSP_8	LQ %	0.3117	-0.2910	0.5189	-0.4166	0.3370	-0.3369
RSP_9	LQ per cell	-0.4728	0.4707	-0.2851	0.2641	-0.6141	0.4985
RSP_{10}	LQ α std	-0.3760	0.3740	-0.1462	0.1717	-0.4591	0.3912
RSP_{11}	LQ Q std	-0.6634	0.6484	-0.6405	0.5384	-0.8311	0.7068
RSP_{12}	HQ %	0.3930	-0.3754	0.6036	-0.4648	0.4872	-0.4271
RSP_{13}	HQ per cell	0.2405	-0.2241	0.4903	-0.3672	0.2863	-0.2653
RSP_{14}	HQ α std	0.2069	-0.1911	0.4622	-0.3427	0.2441	-0.2297
RSP_{15}	HQ Q std	-0.4483	0.4463	-0.2409	0.2357	-0.5731	0.4708
RSP_{16}	Effectiveness	-0.2523	0.2584	-0.0067	0.0397	-0.3457	0.2615
RSP_{17}	Time1	0.6652	-0.6472	0.6883	-0.5745	0.8218	-0.7096
RSP_{18}	Time2	0.6652	-0.6472	0.6883	-0.5745	0.8218	-0.7096
RSP_{19}	Time Eff 0Q	-0.3520	0.3310	-0.5577	0.4466	-0.3932	0.3802
RSP_{20}	Time Eff LQ	-0.6577	0.6435	-0.5909	0.5094	-0.8153	0.6983
RSP_{21}	Time Eff HQ	-0.2936	0.2731	-0.5024	0.4032	-0.3128	0.3175

The first statistic in this group is the time statistics. For this research a constant time step, Δt was used, hence, RSP_{17} and RSP_{18} have the same correlation values.

It is interesting that these RSPs would be more significant than RSP_1, which they are based on.

The zero Q standard deviation has become much more useful due to the restructuring of calculation. The thought behind the zero Q data was that it might be important how long a maneuver spends in each cell, hence the creation of RSP_6. However, by calculating the standard deviation based on the amount of the points at that AoA as opposed to by a cell count, that 'length of hover' is now incorporated into the statistic as well as the spread across the AoA regime.

The separation of AoA and Q for the standard deviation calculations and the overall switch to number of total hits versus number of cell hits, seems to have done well for the low Q metrics. With the revised setup, low-Q standard deviation of Q has been shown to be a significant factor, whereas low Q AoA standard deviation as been shown as insignificant. This implies Q is a greater consideration than AoA for the investigated conditions

While the next system seemed to work well for the low Q values, the high Q values do not seem to have improved. Neither the AoA or the Q standard deviation has an improved correlation to the old system of calculation.

The second set of RSPs is shown in Table 15. One interesting statistic is that RSP_{26} is nearly zero for all cases. Another interesting, or at least promising trend, is that for each subsection there is a difference in the values. This should insure that there are some different correlations.

The correlation values for the second set of RSPs is shown in Table 16. The first thing to notice is the chart has much more yellow and green correlations than red. The change in coloring shows the revised RSPs have been determined to be more useful when compared to the previous set of RSPs. Kurtosis for AoA, LQ skewness

Table 15. Second set of final RSP values

RSP	Description	TM1	TM2	TM3	TM4
RSP_{22}	Kurtosis α	8.8673	45.752	44.091	12.483
RSP_{23}	Kurtosis Q	27.190	7.1970	108.31	29.246
RSP_{24}	Skewness α	2.0055	5.4952	4.9727	2.6874
RSP_{25}	Skewness Q	3.0550	2.0665	8.4767	3.7456
RSP_{26}	Pearson	0.0000	0.0000	0.0000	0.0458
RSP_{27}	Kurtosis 0Q	56.051	123.01	197.99	34.044
RSP_{28}	Skewness 0Q	6.6218	11.046	13.700	5.5731
RSP_{29}	Kurtosis LQ α	9.0705	70.075	48.588	17.429
RSP_{30}	Kurtosis LQ Q	39.463	1.2336	68.916	3.4526
RSP_{31}	Skewness LQ α	2.3732	7.8303	5.6304	3.7178
RSP_{32}	Skewness LQ Q	4.9504	0.4401	7.5377	-0.2166
RSP_{33}	Kurtosis HQ α	2.4077	2.8856	1.6763	4.1160
RSP_{34}	Kurtosis HQ Q	24.574	5.7243	120.328	21.999
RSP_{35}	Skewness HQ α	0.3376	0.4104	-0.4953	1.0433
RSP_{36}	Skewness HQ Q	2.9407	1.7515	8.0510	3.1100

of AoA, high Q kurtosis of AoA and high Q skewness of Q are all determined to be significant for each coefficient.

The task now remains to reduce the list of 36 RSPs to an easier to manage list of RSPs from which to motivate a maneuver. From Section 4.3 it was determined the zero Q, low Q and high Q results trended towards more accurate maneuvers in those areas. Thus, it tracks that at least one RSP to be maximized for the 'ideal' maneuver. RSP_{17} has some of the highest correlation values across the board and is a measure of how fast that space is covered. Therefore, it is fitting RSP_{17} is the primary RSP to use in designing a maneuver.

The next step is to determine which low Q RSP to use. RSP_{31} and RSP_{11} return very high correlation values, and seem to be strong measures of maneuver effectiveness. However, RSP_{11} has slightly higher correlation values for most of the metrics, and is therefore selected to go forward.

For the high Q RSP selection, the choice is equally as tough. RSP_{33} and RSP_{36}

Table 16. Second set of revised RSPs - correlation values

RSP	Description	C_L		C_D		C_M	
		R^2	NRMSD	R^2	NRMSD	R^2	NRMSD
RSP_{22}	Kurtosis α	-0.6548	0.6401	-0.5826	0.5065	-0.8051	0.6946
RSP_{23}	Kurtosis Q	0.2123	-0.2055	0.3994	-0.2758	0.3126	-0.2371
RSP_{24}	Skewness α	-0.5723	0.5513	-0.7033	0.5715	-0.6936	0.6140
RSP_{25}	Skewness Q	-0.5180	0.4968	-0.6794	0.5476	-0.6214	0.5569
RSP_{26}	Pearson	-0.1751	0.1569	-0.4088	0.3189	-0.1676	0.1923
RSP_{27}	Kurtosis 0Q	-0.5696	0.5617	-0.5189	0.4261	-0.7496	0.6081
RSP_{28}	Skewness 0Q	-0.1207	0.1032	-0.3461	0.2717	-0.0918	0.1334
RSP_{29}	Kurtosis LQ α	-0.5328	0.5260	-0.5038	0.4054	-0.7123	0.5704
RSP_{30}	Kurtosis LQ Q	0.4829	-0.4724	0.5739	-0.4429	0.6448	-0.5215
RSP_{31}	Skewness LQ α	-0.6650	0.6500	-0.6170	0.5272	-0.8250	0.7069
RSP_{32}	Skewness LQ Q	0.5852	-0.5700	0.6665	-0.5326	0.7494	-0.6286
RSP_{33}	Kurtosis HQ α	-0.6585	0.6441	-0.5930	0.5113	-0.8155	0.6992
RSP_{34}	Kurtosis HQ Q	0.5959	-0.5743	0.6383	-0.5480	0.6930	-0.6335
RSP_{35}	Skewness HQ α	0.5375	-0.5160	0.5792	-0.5045	0.6072	-0.5703
RSP_{36}	Skewness HQ Q	0.6499	-0.6345	0.6655	-0.5491	0.8202	-0.6943

correlated to the metrics better than any of the other high Q RSPs. RSP_{36} has larger correlation values than RSP_{33}, so it was chosen to be optimized.

The next step is to look at which zero Q RSP to optimize. RSP_7 returned the highest correlation values by a good margin, so it was selected to be optimized.

Finally, it must be decided which RSP will be most important. There are a lot of parameters to vary and it seems unlikely there is one maneuver that will have the best values for all these parameters. RSP_{17} has very high correlation values and is a measure of the entire maneuver it is the most important. However, since low Q values are more difficult to predict, RSP_{11} is selected as the next parameter. High Q values are a very large subset of the total regressor space so RSP_{36} is next. Finally, since zero Q data is the smallest subset of the regressor space, it is the least important.

4.6 RSP Motivated Training Maneuver

Following the discussion in Section 4.5.1, RSPs 17, 11, 36, and 7 were decided to be used to motivate a training maneuver. The training maneuver was first attempted as an expansion of the "chirp" maneuver. However, it was found to be difficult to improve the RSPs using a "chip" type maneuver. Therefore, a training maneuver similar to TM4 was adopted. TM4 is the training maneuver adopted from COM2 in order to provide another set of RSPs for the statistical analysis. The simularity can be seen in Figure 57. In order to increase RSP_{17}, the length of the maneuver was shortened. While TM5 looks similar to TM4, is it quite different. The difference can be seen most clearly in Figure 58. TM4 utilizes changes in both amplitude and frequency for both sinusoids, whereas TM4 has constant amplitude and frequency for both sinusoid functions. Lastly note the large spread of data across the regressor space shown in Figure 59. It was also quickly determined that finding a maneuver which has the best value for each of the selected RSPs is extremely difficult.

The selected RSPs are calculated for each training maneuver and shown in Table 17. The table also shows whether the RSP should be maximized or minimized. From the table, it can be seen that TM5 ranks the best RSP_{17}, the third best RSP_{11}, the second best RSP_{36} and the second best RSP_7. If the RSPs are truely and indication of future training maneuver performance, these RSP values would point to TM5 producing accurate results.

Table 17. RSP motivated TM and RSP values

RSP	Description	Max or Min	TM1	TM2	TM3	TM4	TM5
RSP_{17}	Time	Max	0.9143	0.8851	0.2293	1.0005	1.2660
RSP_{11}	LQ Q std	Min	0.2047	0.0024	1.1168	0.0158	0.0234
RSP_{36}	Skewness HQ Q	Min	2.9407	1.7515	8.0510	3.1100	2.3560
RSP_7	0Q std	Min	0.0178	0.0057	0.0488	0.0160	0.0116
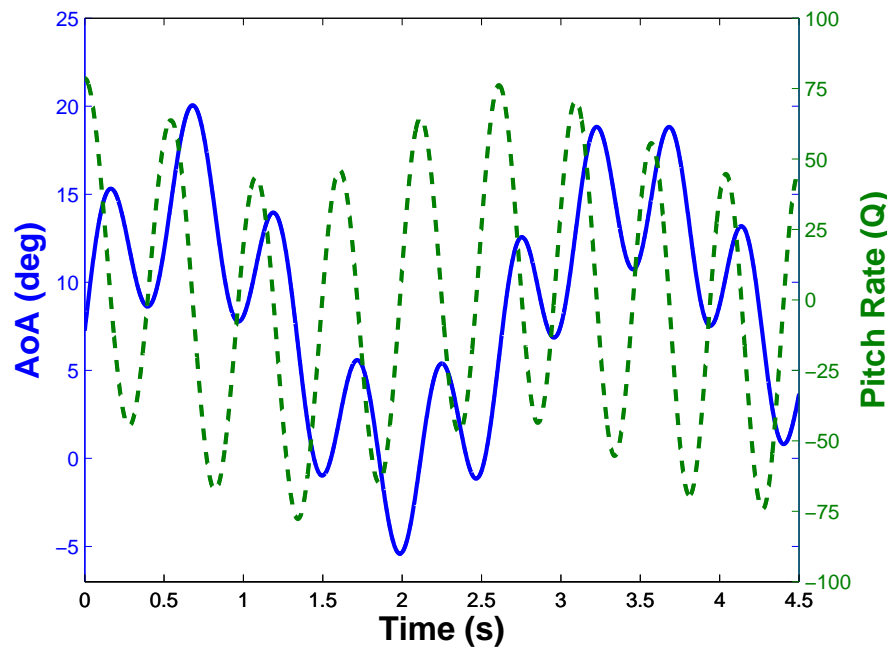
Figure 57. Training maneuver 5: AoA and Q vs time
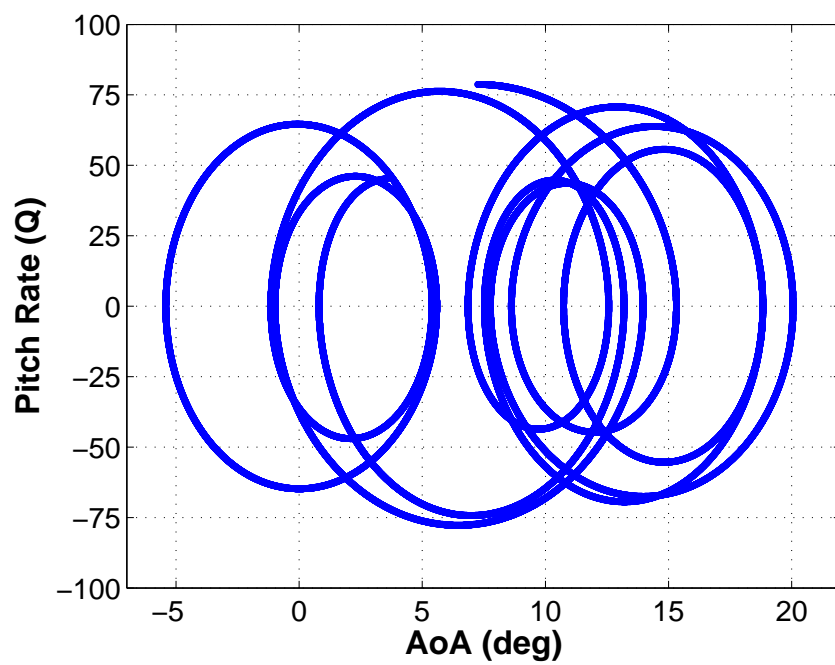
Figure 58. Training maneuver 5: Q vs AoA

97
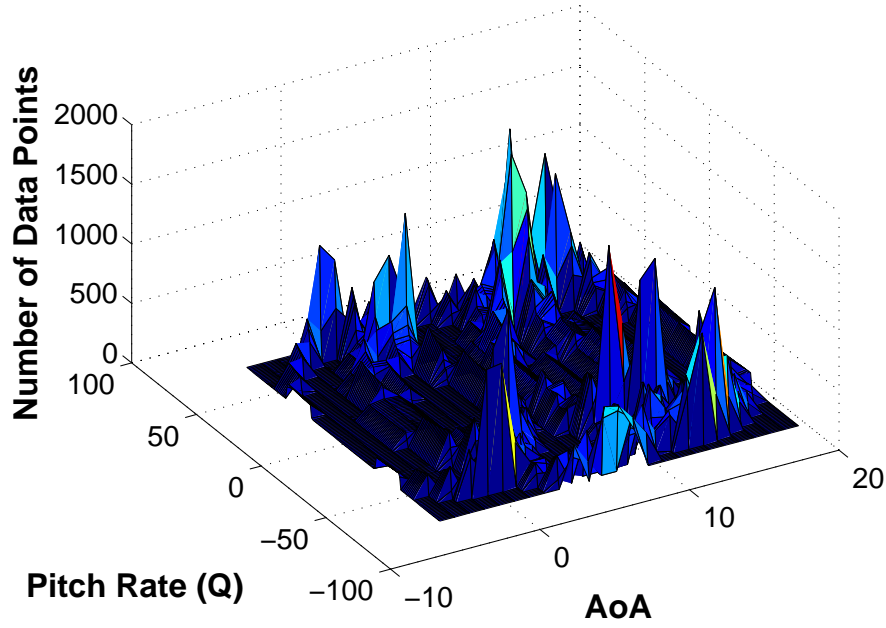
Figure 59. Training maneuver 5: discretized regressor space

4.6.1 RSP Motivated Maneuver Results

In an effort to reduce presentation of redundant information, the metrics for TM5 are not presented next to the metric information for the other training maneuvers. Instead the data will be presented for all comparison maneuvers and all coefficients for just TM5. The chart is color-coded podium style, with gold symbolizing the 'best' comparison metrics when compared to the other four models, silver second and bronze third. This data is represented in Table 18.

In another effort to reduce the amount of redundant information presented, only charts deemed important to the understanding of TM5 model performance will be presented here. However, the charts for each coefficient and comparison maneuver with TM5 plotted are included in Appendix B.

As can be seen from Table 18, TM5 does very well for some maneuvers, accurate for some others and then comparably for the rest. There are no points at which TM5

98

Table 18. TM5 model metrics

| COM | C_L | | C_D | | C_M | |
	R^2	NRMSD	R^2	NRMSD	R^2	NRMSD
COM1a	0.9875	0.0292	0.9878	0.0301	0.9182	0.0592
COM1b	0.9843	0.0325	0.9785	0.0435	0.8674	0.1145
COM1c	0.9873	0.0264	0.9640	0.0456	0.8088	0.1050
COM2	0.9862	0.0279	0.9869	0.0337	0.9236	0.0778
COM3	0.9950	0.0185	0.8927	0.0516	0.5881	0.1123
COM4	0.9824	0.0280	0.9865	0.0370	0.9200	0.0658
COM5	0.9784	0.0354	0.9755	0.0512	0.8371	0.1364

is a terrible maneuver. Looking at the cells that are not colored at all, we see that the R^2 values are large and NRMSD values are small, indicating that all models were extremely accurate for those maneuvers, and the difference among all the models is slight. Just because TM5 did not get the best values in those cases does not mean it is an unsuitable TM.

The results for COM1b for C_L are shown in Figure 60. While TM5 did not place in the top three results, it produces highly accurate results throughout the range AoAs.

Figure 61 shows the high accuracy of the TM5 model. While most of the other models had trouble resolving the low AoA high Q aspect of COM4, TM5 was able to retain its fidelity. This ability seems to suggest the favorable value of RSP_{36} leads to good high Q results.

The one area of concern, which is a consistent area of concern for all the models, is COM3 for C_M. TM5 returns a R^2 value of 0.5881. The model is shown in Figure 62. The reason for the low R^2 value is the high Q, high alpha portion of COM3. While the model has high Q and high alpha data points, it does not have a good representation of both of them. Thinking back to the regressor space figures in Section 4.6, there is very little, or no data, in the corners of the regressor space. When the model is then
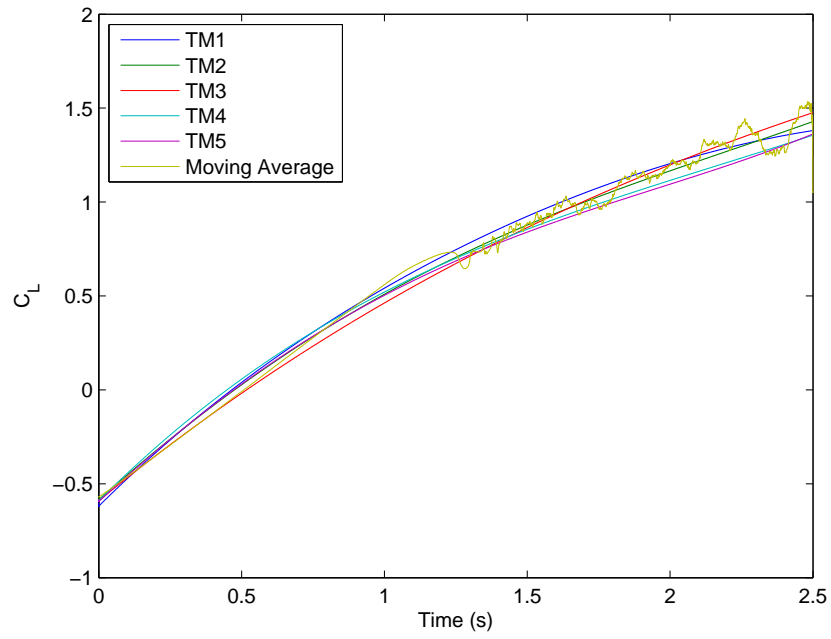
Figure 60. Model results COM1b C_L with TM5
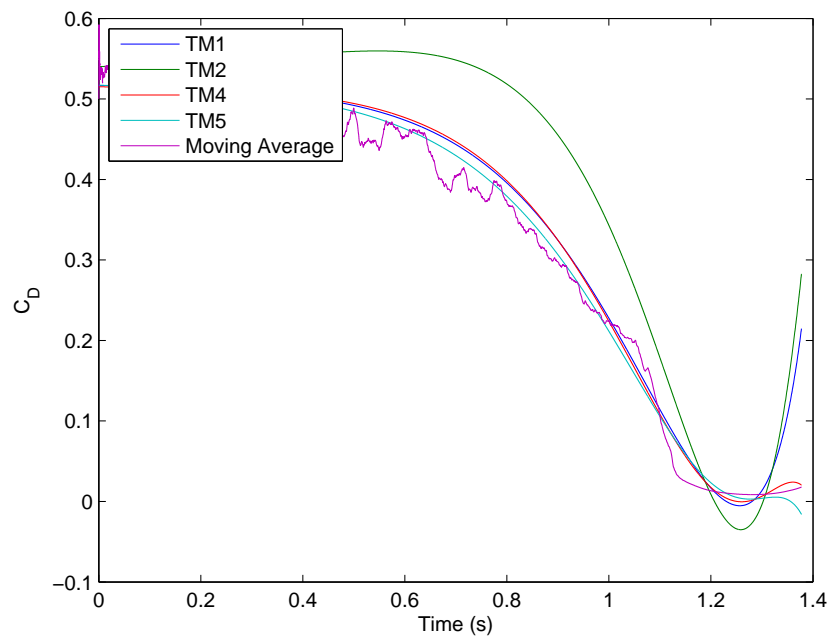
Figure 61. Model results COM4 C_D with TM5

mapped to the resulting data of the training maneuver, this subset of data is outside the bounds of the training maneuver, and the polynomial functions fall off.
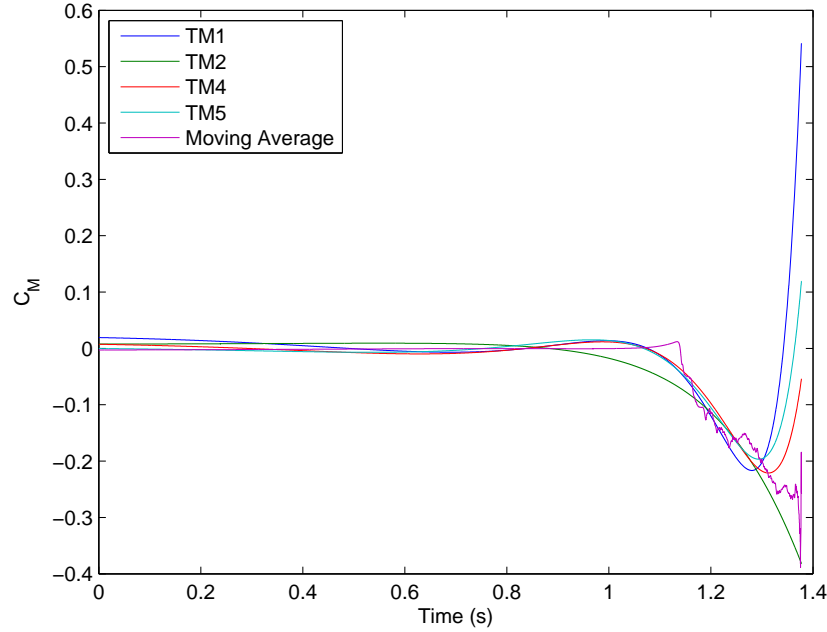
Figure 62. Model results COM3 C_M with TM5

At this point, it has been shown using statistical measures to gain greater insight into actions of a training maneuver, the maneuver can be better tailored to a particular need. However, with there being some time left an additional maneuver may be able to solidify or expand the knowledge of these RSPs and the output metrics. From the experience gained over the course of this research, the author has decided a series of actions that can help with the system identification process. First, the results from TM5 should be appended to the statistical analysis to better determine which RSPs are important. Applying the results of TM5 to the data set and recalculating the correlation values gives the chart shown in Table 19.

Comparing the results, most of the important RSPs from before are decidedly still useful to predicting TM accuracy. However, the values of the correlations have changed. From the results, RSP_{11} now has stronger correlation values than RSP_{17},

Table 19. Correlation values with TM5 included

RSP	Description	C_L		C_D		C_M	
		R^2	NRMSD	R^2	NRMSD	R^2	NRMSD
RSP_1	% Whole	0.4002	-0.3740	0.6153	-0.4891	0.4223	-0.4358
RSP_2	% Boundary	0.4520	-0.4498	0.4240	-0.3421	0.6487	-0.4841
RSP_3	α std	-0.2534	0.2572	-0.0006	0.0483	-0.3217	0.2619
RSP_4	Q std	-0.6166	0.6043	-0.4994	0.4466	-0.7492	0.6547
RSP_5	0Q %	0.3917	-0.3637	0.5955	-0.4846	0.3756	-0.4247
RSP_6	0Q per cell	-0.3532	0.3574	-0.1347	0.1412	-0.4980	0.3716
RSP_7	0Q std	-0.6595	0.6431	-0.5970	0.5199	-0.7927	0.7025
RSP_8	LQ %	0.3418	-0.3139	0.5499	-0.4464	0.3067	-0.3715
RSP_9	LQ per cell	-0.4775	0.4748	-0.2917	0.2738	-0.6228	0.5049
RSP_{10}	LQ α std	-0.3948	0.3901	-0.1860	0.2035	-0.4614	0.4141
RSP_{11}	LQ Q std	-0.6741	0.6553	-0.6636	0.5660	-0.8099	0.7199
RSP_{12}	HQ %	0.4113	-0.3863	0.6232	-0.4919	0.4539	-0.4480
RSP_{13}	HQ per cell	0.2858	-0.2634	0.5378	-0.4154	0.2952	-0.3141
RSP_{14}	HQ α std	0.2627	-0.2394	0.5174	-0.3976	0.2603	-0.2901
RSP_{15}	HQ Q std	-0.4595	0.4561	-0.2621	0.2556	-0.5813	0.4849
RSP_{16}	Effectiveness	-0.2433	0.2504	0.0018	0.0323	-0.3562	0.2532
RSP_{17}	Time1	0.6244	-0.5995	0.6867	-0.5767	0.7121	-0.6700
RSP_{18}	Time2	0.6244	-0.5995	0.6867	-0.5767	0.7121	-0.6700
RSP_{19}	Time Eff 0Q	0.5737	-0.5459	0.6512	-0.5586	0.5956	-0.6140
RSP_{20}	Time Eff LQ	0.5070	-0.4789	0.5922	-0.5099	0.4987	-0.5430
RSP_{21}	Time Eff HQ	0.6284	-0.6060	0.6793	-0.5662	0.7439	-0.6746
RSP_{22}	Kurtosis α	-0.3828	0.3553	-0.5933	0.4824	-0.3648	0.4149
RSP_{23}	Kurtosis Q	-0.6688	0.6508	-0.6183	0.5389	-0.7915	0.7124
RSP_{24}	Skewness α	-0.3270	0.2992	-0.5355	0.4343	-0.2869	0.3558
RSP_{25}	Skewness Q	-0.6669	0.6491	-0.6062	0.5332	-0.7818	0.7094
RSP_{26}	Spearman	0.2083	-0.2021	0.3790	-0.2683	0.3263	-0.2311
RSP_{27}	Kurtosis 0Q	-0.5685	0.5416	-0.7127	0.5876	-0.6289	0.6121
RSP_{28}	Skewness 0Q	-0.5106	0.4830	-0.6817	0.5573	-0.5488	0.5513
RSP_{29}	Kurtosis LQ α	-0.2312	0.2064	-0.4709	0.3753	-0.1734	0.2534
RSP_{30}	Kurtosis LQ Q	-0.5811	0.5671	-0.5622	0.4675	-0.7416	0.6232
RSP_{31}	Skewness LQ α	-0.1844	0.1601	-0.4187	0.3350	-0.1050	0.2028
RSP_{32}	Skewness LQ Q	-0.5473	0.5340	-0.5497	0.4494	-0.7111	0.5884
RSP_{33}	Kurtosis HQ α	0.4410	-0.4349	0.4935	-0.3908	0.6148	-0.4741
RSP_{34}	Kurtosis HQ Q	-0.6757	0.6570	-0.6419	0.5554	-0.8005	0.7204
RSP_{35}	Skewness HQ α	0.5812	-0.5668	0.6424	-0.5262	0.7374	-0.6233
RSP_{36}	Skewness HQ Q	-0.6699	0.6519	-0.6193	0.5400	-0.7923	0.7135

and shifting from previous results, RSP_{34} has a greater correlation than RSP_{36}. Therefore, the decided new order of RSP importance is RSP_{11}, RSP_{17}, RSP_{34} and RSP_7.

Second, the phenomena discussed above were observed for many models. Figure 63 illustrates the corners of the regressor space are not covered. It is not just that there are not data points there. At 10 deg AoA and 25 deg/s pitch rate, there are not data points either, but there is not a huge inaccuracy in the comparison maneuvers at that value. The predictions are still accurate because of the data points that bound it. It would make sense then in order to ensure the entire regressor space is covered, the training maneuver should encompass the regressor space. While it seems to be common practice in the literature [15] to constrain the training maneuver within the same regressor space as the model prediction space, there is no reason why the training maneuver can not be extended beyond that.
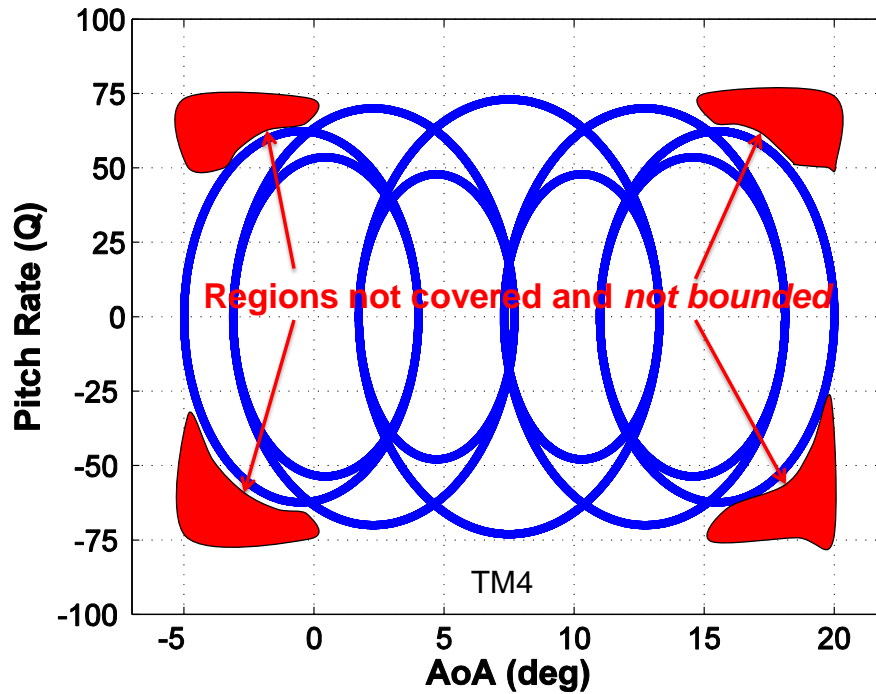

Figure 63. Edge problem shown in TM4 regressor space

4.7 Lessons Learned Maneuver

In consideration of the results from Section 4.6.1, a decidedly different approach was taken for the final maneuver. Most of the previous research has pointed towards completing training maneuvers within specified regressor space bounds. At the very least, the literature [17] [15] makes the claim to stay within the ranges of the training maneuver, which could be taken to mean that staying within max/min Q and AoA would be sufficient. Unfortunately, it is entirely possible, as this research can show, that it is possible to fill the regressor space and still overextend the models within the chosen regressor space. By extending the training maneuver outside of the regressor space 'box', there is a much better opportunity to ensure model accuracy in the entirety of the regressor space

The addition of a single sine oscillation to the beginning of the maneuver will allow for a guaranteed inclusion of the entire regressor space by the training maneuver. A single sine oscillation at constant amplitude and frequency forms a circle on the Q vs AoA regressor map. Hitting the four corners of the regressor space ensures there will be data points constraining the fit in the entire regressor space. Then, the "best practice" DC chirp maneuver is used to fill the space to desirable levels. Figures 64 and 65 illustrate TM6.

4.7.1 Lessons Learned Maneuver Results

The RSP values for TM6 versus the other maneuvers are shown in Table 20. While TM6 does not return the best values when compared against the other maneuvers, it does have values in the same range as the other 'good' maneuvers. As was discovered with TM5, it is hard to individually manipulate a single RSP. A best effort has to be made to observe changes with changing inputs. The results from the sixth
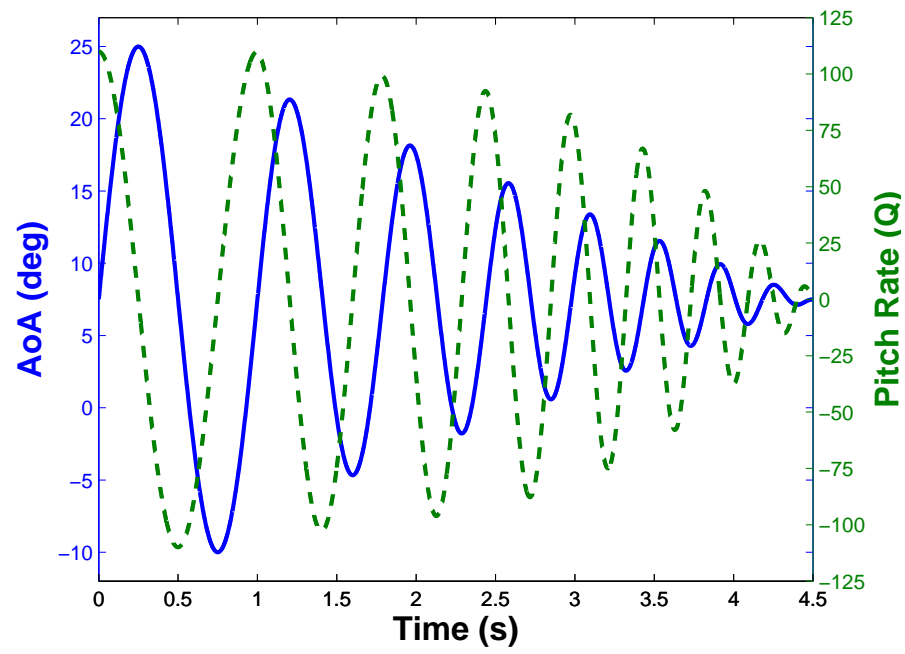
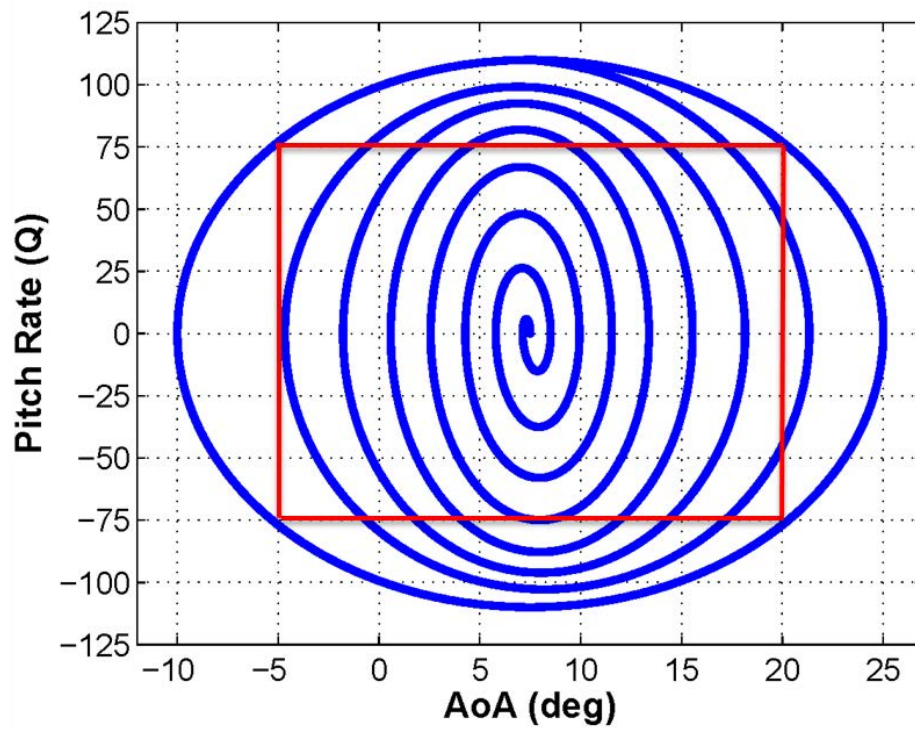104

Figure 64. Training maneuver 6: AoA and Q vs time

Figure 65. Training maneuver 6: Q vs AoA

Table 20. RSP values for all TMs

RSP	Description	Max or Min	TM1	TM2	TM3	TM4	TM5	TM6
RSP_{11}	LQ Q std	Min	0.2047	0.0024	1.1168	0.0158	0.0234	0.1842
RSP_{17}	Time	Max	0.9143	0.8851	0.2293	1.0005	1.2660	0.9670
RSP_{34}	Kurtosis HQ Q	Min	24.574	5.7243	120.33	21.999	12.396	37.5211
RSP_7	0Q std	Min	0.0178	0.0057	0.0488	0.0160	0.0116	0.0128

training maneuver are shown in Table 21, which shows the raw TM6 results color coded 'podium style.'

Table 21. TM6 model metrics

COM	C_L		C_D		C_M	
	R^2	NRMSD	R^2	NRMSD	R^2	NRMSD
COM1a	0.9823	0.0334	0.9748	0.0430	0.8716	0.0755
COM1b	0.9721	0.0419	0.9624	0.0562	0.8198	0.1328
COM1c	0.9880	0.0247	0.9812	0.0351	0.8817	0.0890
COM2	0.9740	0.0371	0.9729	0.0484	0.8722	0.1038
COM3	0.9911	0.0244	0.9735	0.0284	0.9074	0.0568
COM4	0.9328	0.0525	0.9871	0.0377	0.9349	0.0699
COM5	0.9594	0.0466	0.9682	0.0590	0.8250	0.1452

From the table, it can be seen that TM6 did very well at the high Q values. However, TM6 seemed to struggle with the low Q maneuvers. The reason for this can be seen in Figure 66. The fit to the data is good in the high Q range; however, the fit drops off, by the end of the maneuver which is in the middle of the regressor space.

The Kestrel MVP in Figure 67 was constructed using the same SIDPAC software as used in this research. However, due to the organized fashion of the coefficient results when an entire aircraft is taken into consideration, compared to a 1 ft chord airfoil, the constructed model is much more accurate to the training data. The difference is likely the major contributor to the error seen by TM6. The choice of the desired regressor space may have been too ambitious for an airfoil from the start of the current research.

At the very large AoAs and Qs generated in the sixth maneuver, the difference in flow phenomena could be too large for the model to be able to fit the entire maneuver. It would be interesting to contrast the use of a RBF (radial basis function) model in this situation. RBF models have the characteristic of exactly matching the training data. However, the theory behind the generation of TM6 should still stand, if applied to a more applicable problem.
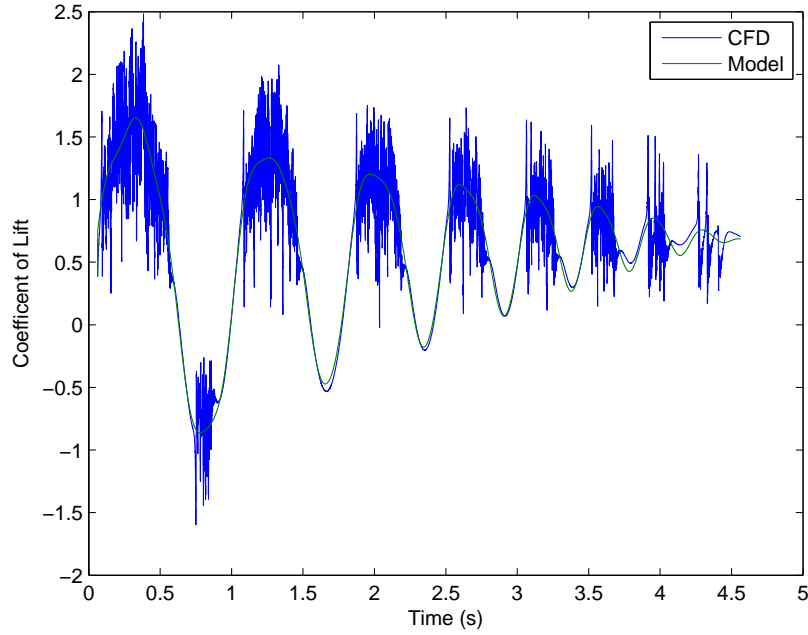

Figure 66. Fit problem shown in TM4 regressor space

Despite TM6 not performing as well as hoped, there is a lesson learned. Referencing Figure 68, it can clearly be seen the edge of the regressor space error is removed. TM6 is very accurate in that region, where the other models are inaccurate. However, TM6 has problems predicting the low Q, low AoA region at the beginning of the comparison maneuver.
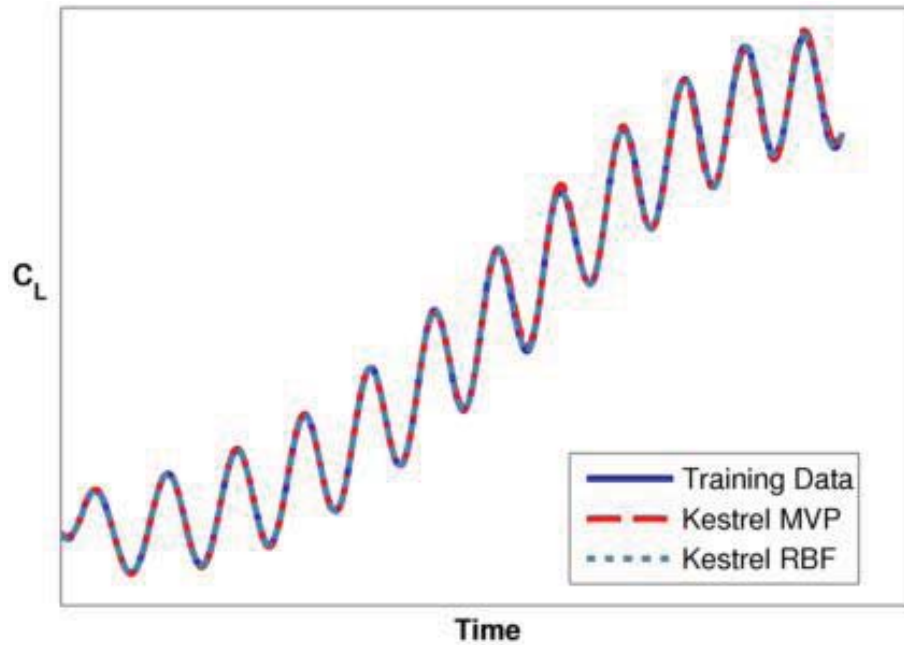
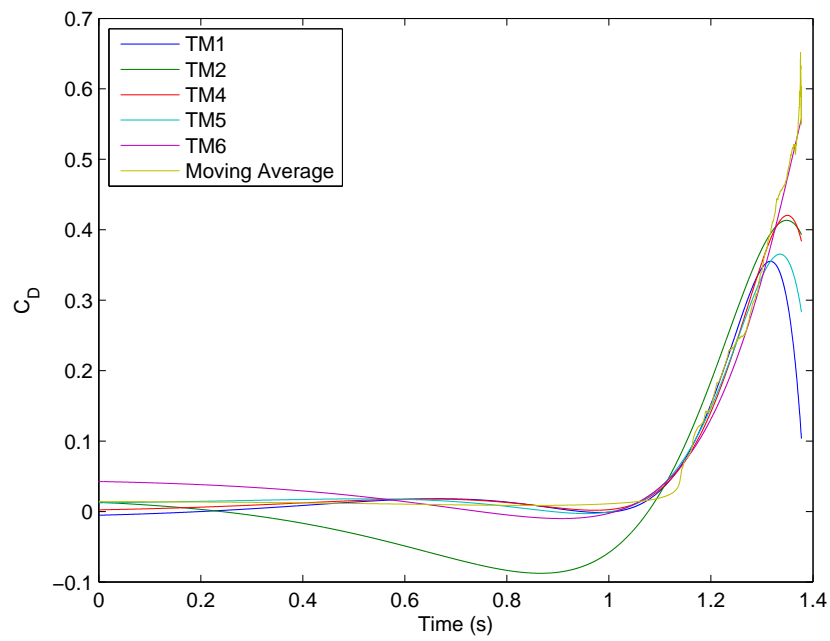**Figure 67. Fit for an F-16 training maneuver completed by AFSEO [11]**

Figure 68. Model results COM3 C_D with TM6

V. Conclusions and Future Work

5.1 Overview

Identification of stability issues early during the design process is an immediate need for the Air Force. The inability to detect these issues has led to costly overruns and late design changes for several aircrafts. Late design changes lead to *ad hoc* fixes that are not ideal for the aircraft function. CFD has been proposed as a tool for engineers to get high-fidelity static and dynamic results. CFD has a large computational cost associated with it, and for CFD to identify these trouble areas, requires an immense amount of simulations in a variety of conditions. System identification has recently been introduced as a method to bring CFD and S&C together by reducing the computational cost. The CFD SID process hinges upon the decision of an appropriate training maneuver. The results of this research allow engineers to make smarter decisions in the training maneuver development.

This research includes a variety of topics including: CFD, system identification, S&C and statistics. The methods and actions required to solve the Navier-Stokes equations with turbulence models to get high-fidelity solutions was discussed. The need for accurate stability and control parameters has been demonstrated. Previous research was considered, and the lessons herein were presented and applied to the current work.

A C-Grid topology was applied to a NACA 64A010 airfoil, and a method for determining grid and time step independence was presented and completed. The grid was determined to be time and grid density independent, and the resulting grid and timestep were selected to move forward. When dynamic maneuvers were simulated, the grid was in need of further refinement to eliminate stability issues.

Several different training and comparison maneuvers were created and simulated

109

using CREATE-AV's flow solver Kestrel and were evaluated using regressor space parameters. Multivariate polynomial models were created from the training maneuver data. The coefficient predictions made by these models were compared against coefficients obtained from the full CFD simulation of comparison maneuvers and suitable metrics were calculated. Those metrics and the regressor space parameters were fed into the statistical analysis program JMP®and correlation values were calculated. Those correlation values were used to refine the regressor space parameters and shape an additional training maneuver. Lessons learned from conducting the above evaluation led to the creation of a six training maneuver.

5.2 Conclusions

The goal of this research was to investigate methods by which to measure training maneuvers before the full CFD computational simulation and to link the results of this evaluation process to future performance. Fulfilling this goal would create a greater understanding of how to devise and create training maneuvers. While the results from this research do not point to a definitive rules for creating a accurate training maneuver, the results are suggestive of techniques. Using visual methods, there is a noticeable difference between training maneuvers with better high Q RSPs and high Q performance, as was the case with TM1 and TM4 for C_L in the high Q comparison maneuver COM1c. For the low Q maneuver, this link was demonstrated with TM1 providing the best results for C_D.

Correlation values between the metrics and RSPs were calculated to determine which RSPs were most predictive of favorable TM performance. The analysis showed that the way in which the points were distributed, as measured by standard deviation, was important. The results of this analysis led to the creation of a total of 36 RSPs. A large number of those set up to measure how the points are distributed in the

regressor space. RSP_{17}, RSP_{11}, RSP_{36} and RSP_7 were determined to provide insight into future maneuver performance. RSP_{17} is a measure of the rate at which the training maneuver covers unique area of the regressor space. RSP_{11} is a measure of the low pitch rate standard deviation in pitch rate. RSP_{36} is a measure of skewness in high pitch rate in pitch rate. RSP_7 is a measure of zero pitch rate standard deviation.

Using the selected regressor space parameters, a fifth training maneuver (TM5) was created with specific RSPs in mind. The creation of this maneuver proved that it is hard to modify all these RSPs via one maneuver. For many of the RSPs it is abstract to think how modifying the training maneuver motion will result in the desired changes in the RSPs. TM5 was generated such that the selected RSPs indicated favorable results. The results TM5 were favorable, with TM5 producing the best comparison metrics for several comparison maneuvers and coefficients; however, it did not return the best metrics for every coefficient and every maneuver. A type of error due to the edge of the regressor space was observed even for TM5.

Lessons learned over the course of this research provided the needed insight for the creation of TM6. Rather than restrict the training maneuver to the confines of the defined regressor space, providing data to bound the extremes of the box was decided to be an avenue worth pursuing. TM6 did not return the best overall model; however, it does shed light on the limitations of MVP models. The choice of a regressor space for this project may have been overly ambitious, with much of the regressor space being highly unsteady. Extending that range of AoA and Q experienced by the airfoil even further may have resulted in the poor fit to the training data shown in Chapter IV.

From this research it has been shown that RSPs are important. Using selected RSPs as a guide, an additional maneuver (TM5) was created that was able to outperform maneuvers generated without the RSPs in a variety of comparison scenarios.

This research has shown it is important how the the data is distributed in the regressor space through RSPs that measure distribution of data as opposed to quantity of data. This research has also shown that pitch rates, such as Q are as important, if not more than the angles such as angle of attack through the RSPs.

5.3 Future Work

While much ground has been covered in this work, there are always more avenues that could be explored. The first possible avenue is to apply the higher order statistics using the previous system of calculating distribution RSPs, using cells instead of number of hits. While the author tried to use a variety of methods and statistics for quantifying the training maneuvers, it was not an exhaustive effort. Continued research into methods and statistics could be fruitful. Further, utilizing RBF models particularly in regions where MVP models have trouble fitting the training data, as in TM6, could produce more accurate results.

A further area of research could be implementing a optimization routine to the RSPs. The first step would be to identify a cost function. Time would be an appropriate choice. Then the RSPs would need to be set up as constraints. The best choice would likely to be determine an 'acceptable' level for the RSPs and set append the RSPs as inequality constraints. Additional constraints would be angle and rate constrictions. Second derivative constraints may be necessary to ensure a continuous path. The challenging piece would be including abstract concepts like standard deviation and skewness into the mix.

The next step then is to progress into 3 dimensions. The lessons learned from this research should be applied for the lateral directional coefficients as well. Further, the results need to be extended for other flow conditions. This research was run at Mach

0.5 at 10,000 ft. What may be important for model prediction accuracy could depend on the flow conditions.

Grid generation is a topic that is brought up often in the CFD community and is acknowledged by practitioners to be exceedingly challenging. There are methods in the literature for producing a static grid; however, prescribed motion problems require a different process. While the technology for computing more advanced problems improves, methods for generating grids for those problems needs to keep pace.

The newest version of Kestrel, Version 3.1.1, offers the ability to use control surfaces in the flow solution. This offers an interesting opportunity to further integrate S&C and CFD. While it is possible to gain insight into stability and control using non-deflecting grids and problems, it would be an immense value to the S&C field to incorporate derivatives such as $C_{m_{\delta e}}$ which is change in pitch rate due to elevator deflection. Furthering CFD and SID interaction to include moving control surfaces is a very exciting prospect for future research.

This research has shown that there is merit to quantifying the pertinent characteristics of potential training maneuvers in order to allow for better informed training maneuver generation. While adopting a best practice maneuver may produce adequate results, by researching and defining what characteristics are needed for a training maneuver, this work represents a step forward toward introducing a standardized process.

TRAINING MANEUVER EVALUATION FOR REDUCED ORDER MODELING

OF STABILITY & CONTROL PROPERTIES USING COMPUTATIONAL

FLUID DYNAMICS

A. Matlab®Pre and Post processing Files

A.1 Spectral Analysis M-file

```
1  %2LT Craig C Porter
   %Frequency Analysis MATLAB File in Support of ROM Thesis Work
   %Derived from M-file provided by Dr. Keith Bergeron

   clear
6  clc
   close

   %...
       ************************************************************************%...

   %Factors that need to be changed
11
   file_name1 = 'CGRID3T1.coeff';
   cd ../Data/St %Change depending on location of data
   data1 = dlmread(file_name1,'',20,0);
   Iteration=data1(:,1);
16 Time=data1(:,2);
   AOA=data1(:,3);
   BETA=data1(:,4);
   CAXIAL  =data1(:,5);
   CNORMAL =data1(:,6);
21 CLIFT   =data1(:,7);
   CDRAG   =data1(:,8);
   CSIDE   =data1(:,9);
   CPITCH  =data1(:,10);
   CROLL   =data1(:,11);
26 CYAW=data1(:,12);
   N=max(Iteration);
   cutoff = 2000; %if desired removes startup iterations
   del_time = Time(N)-Time(N-1); %assumes constant delT
   %L2 = 2048;                   % Length of signal (truncated to a ...
       power of 2, i.e., 2048) THIS IS WHAT YOU NEED TO CHANGE
31
   %Default is CNORMAL for FFT, change below if neccesary
```

```matlab
%...
    ************************************************************************&...

%  Beware line below is correct , i.e., L2 = a power of 2!
i=1;
while (N-cutoff)>2^i
i=i+1;
end
L2=2^(i-1);

for i= 1:N-cutoff
    amplitude1(i)=CNORMAL(i+cutoff);
end

    amp_average1 = mean(amplitude1);

for i = 1:N-cutoff
        y2(i) = amplitude1(i)-amp_average1;
end


for i = 1:N-cutoff
        time(i) = (i-1)*del_time;
end

figure(1)
    plot(time, y2, 'color',[0 1 1],'Marker','square','LineWidth'...
        ,.5)
    hold on
    xlabel('Time (s)')
    ylabel('Amplitude')
    title('Normal Force')

%%%%%%%%%%%%%%%%%%%%%%%%%%%%%
% FFT
%%%%%%%%%%%%%%%%%%%%%%%%%%%%%%
        Fs2 = 1/del_time;                   % Sampling frequency
      NFFT2 = 2^nextpow2(L2);               % Next power of 2 from ...
        length of y
        n2 = NFFT2;
      yfft2 = fft(y2,NFFT2)/L2;
        f2 = Fs2/2*linspace(0,1,NFFT2/2+1);
    power2 = 2*abs(yfft2);

% Plot single-sided amplitude spectrum.
figure(2)
      plot(f2,2*abs(yfft2(1:NFFT2/2+1)))
      title('Single-Sided Amplitude Spectrum of Normal Force')
      xlabel('Frequency (Hz)')
      ylabel('Magnitude of Normal Force')
      axis([0 500 0 1])
      axis 'auto y'
```

```matlab
81
   % Identify dominant frequency
         temp2(1) = 0.0;
         temp2(2) = 0.0;
         temp_j2 = 1;
86       temp_power2 = power2;
         max_pwr2(1:n2/2) = 0.0;
         max_freq2(1:n2/2) = 0.0;
   for i = 1:n2/2
         for j = 1:n2/2
91           if (temp_power2(j) > temp2(1))
                 temp2(1)  = temp_power2(j);
                 temp2(2)  = f2(j);
                 temp_j2 = j;
             end;
96           max_pwr2(i)  = temp2(1);
             max_freq2(i) = temp2(2);
         end;
         temp2(1) = 0.0;
         temp2(2) = 0.0;
101       temp_power2(temp_j2)=0.0;
   end

   %Print top 6 frequency's to screen

106   for i = 1: 6;
        i, Amplitude = max_pwr2(i), Frequency = max_freq2(i)
       end
        disp('')
        disp('Average Ampltidue')
111      disp(amp_average1)
```

116

A.2 Model Generation Script

```matlab
%Craig Porter TM Model Creation Scipt
%% Load Data
clc
clear all
close all

File='TM6';
file_name1 = strcat(File, '.coeff');
%file_name2 = strcat(File, '.flow');
file_name3 = strcat(File, '.motion');
cd /home/afiten1/gae13m/cporter/Thesis/TM/TM6b/ %Change depending ...
    on location of data

% %If using v2
% data1 = dlmread(file_name1,'',5519,0);
% %data2 = dlmread(file_name2,'',5519,0);
% data3 = dlmread(file_name3,'',5519,0);

%If using 3.1.1
data1 = dlmread(file_name1,'',5520,0);
data3 = dlmread(file_name3,'',5522,0);

TIME=data1(:,2);

%For 3.1.1 Runs, refernce frame screwup Q is actually -R
Q=-data3(:,13);

% %For v2 runs
% Q=data3(:,12);

AOA=data1(:,3);
CLIFT=data1(:,7);
CDRAG=data1(:,8);
CPITCH  =data1(:,10);
ITERATION=data1(:,1);
dt=1.25e-5;
QDOT=deriv(Q,dt);
AOADOT=deriv(AOA,dt);

clear data1 data3

%% Create Model

close all
clc

x(:,1)=AOA; %ALPHA
x(:,2)=Q; %Q
x(:,3)=QDOT;
z=CLIFT;
```

```
   NORD =5;
   nord =[ NORD  NORD  NORD ];
   maxord =5;
53 sig2 =0;
   auto =1;
   Iplot =1;
   ivar =0;
   bvar =0;
58 maxopt =0;

   [y ,p ,ip ,crb ,pse ,xp ,a ,ia ,psi ]= mof (x ,z ,nord ,maxord ,sig2 ,auto ,Iplot ,...
       ivar ,bvar ,maxopt );
   [xr ,xlab ]= polygen (x ,ip );

63 figure (2)
   plot ( TIME ,z ,TIME ,y )
   xlabel ('Time  (s)')
   ylabel ('Coefficent  of  Lift ')
   legend ('CFD ','Model ')
```

A.3   Initial RSP M-file[5]

```matlab
function [metric metrica metricq as qs z]=Metric...
    (pos2,rate2,bounds,steps,metricsteps,maxN0,pm0)
%extract AoA and Q bounds of regressor space
aextrema=bounds(1,:);qextrema=bounds(2,:);

%extract step sizes for AoA and Q for regressor space ...
    discretization
astep=steps(1);qstep=steps(2);

%Debugging variables
ametstep=metricsteps(1);qmetstep=metricsteps(2);

%All AoA values
arange=aextrema(1):astep:aextrema(2);

%All Q values
qrange=qextrema(1):qstep:qextrema(2);

%Create 2D Mesh for discretized regressor space
[as,qs]=meshgrid(...
    mean(arange(1:2)):astep:mean(arange(length(arange)-1:length(...
        arange))),...
    mean(qrange(1:2)):qstep:mean(qrange(length(qrange)-1:length(...
        qrange))));

%Z-axis of 3D plot of regressor map (number of data points per ...
    cell)
z=zeros(size(as));

%Make AoA's (pos variables) and Q values same length
pos3=zeros(1,length(pos2)-1);
for i=2:length(pos2)
    pos3(i-1)=mean(pos2(i-1:i));
end

%Loop through AoA's to mark which cell each point lies
for i=1:length(rate2)
    if rate2(i)>qextrema(1) && rate2(i)<qextrema(2);
        %Find which AoA cell
        for j=1:length(arange)-1
            apos=j;
            if pos3(i)<=arange(j+1)
                break
            end
        end
        %Find which Q cell
        for j=1:length(qrange)-1
            qpos=j;
            if rate2(i)<=qrange(j+1)
                break
```

```matlab
47                    end
                  end
                  %Increment "number of data points per cell" counter
                  z(qpos,apos)=z(qpos,apos)+1;
              end
52  end
      asteps=size(z,2)/ametstep;

      %Examine the evenness of the data in AoA
      counta=zeros(asteps,1);
57  totala=zeros(asteps,1);
      totala(1)=size(z,1)*ametstep;
      for i=1:size(z,1)
          k=1;
          for j=1:size(z,2)
62            if z(i,j)~=0
                  counta(k)=counta(k)+1;
              end
              if mod(j,ametstep)==0
                  totala(k)=totala(1);
67                k=k+1;
              end
          end
      end
      metrica=counta./totala;
72
      %Examine the evenness of the data in Q
      qsteps=size(z,1)/qmetstep;
      countq=zeros(qsteps,1);
      totalq=zeros(qsteps,1);
77  totalq(1)=size(z,2)*qmetstep;
      for i=1:size(z,2)
          k=1;
          for j=1:size(z,1)
              if z(j,i)~=0
82                countq(k)=countq(k)+1;
              end
              if mod(j,qmetstep)==0
                  totalq(k)=totalq(1);
                  k=k+1;
87            end
          end
      end
      metricq=countq./totalq;
      %***** Metric 1 - total percentage of cells with data points *****
92  metric(1)=100*sum(countq)/sum(totalq);

      %Examine the data points on the boundaries
      count=0;
      total=0;
97  j=size(z,2);
      for i=1:size(z,1)
```

```matlab
        if z(i,1)~=0
            count=count+1;
        end
102     total=total+1;
        if z(i,j)~=0
            count=count+1;
        end
        total=total+1;
107 end
    j=size(z,1);
    for i=2:size(z,2)-1
        if z(1,i)~=0
            count=count+1;
112     end
        total=total+1;
        if z(j,i)~=0
            count=count+1;
        end
117     total=total+1;
    end

    %Find the location of zero pitch rate
    for i=1:length(qrange)-1
122     zeroqpos=i;
        if 0<=qrange(i+1)
            break
        end
    end
127 %***** Metric 2 - total percentage of boundary cells with data ...
        points *****
    metric(2)=100*count/total;

    %***** Metrics 3 & 4 - Evenness of data in AoA and Q respectively ...
        *****
    metric(3:4)=[std(metrica/max(metrica)) std(metricq/max(metricq))];
132
    %Isolate the data points at 0 Q
    zsteps=size(z,2)/qmetstep;
    countz=zeros(zsteps,1);
    k=1;
137 i=zeroqpos;
    for j=1:size(z,2)
        if z(i,j)~=0
            countz(k)=countz(k)+z(i,j);
        end
142     if mod(j,qmetstep)==0
            k=k+1;
        end
    end
    %Cap max number of data points in a given cell (if desired)
147 countz12=0;
    for i=1:length(countz)
```

```matlab
            if countz(i)>maxN0
                countz(i)=maxN0;
            end
152         if countz(i)>0
                countz12=countz12+1;
            end
        end
        %***** Metric 5 - total percentage of 0 Q cells with data points ...
            *****
157 metric(5)=100*countz12/length(countz);

        %***** Metric 6 - Avg # data points per cell at 0 Q *****
        metric(6)=mean(countz);

162 %***** Metric 7 - evenness of data at 0 Q *****
    metric(7)=std(countz/max(countz));

        %Now isolate region of "low" Q (excluding region of 0Q)
        countz22=0;
167 for mi=1:length(pm0)
        countz2=[z(zeroqpos-pm0(mi):zeroqpos-1,:);z(zeroqpos+1:...
            zeroqpos+pm0(mi),:)];
        %Cap max number of data points per cell (if desired)
        for i=1:size(countz2,1)
            for j=1:size(countz2,2)
172             if countz2(i,j)>maxN0
                    countz2(i,j)=maxN0;
                end
                if countz2(i,j)>0
                    countz22=countz22+1;
177             end
            end
        end
    %***** Metric 8 - total percentage of "low" Q cells with data ...
        points *****
        metric(6+2*mi)=100*countz22/(size(countz2,1)*size(countz2,2));
182
    %***** Metric 9 - Avg # data points per cell at "low" Q *****
        metric(7+2*mi)=mean(mean(countz2));

        %There may be NaN's in metric calculation after normalization ...
            - change
187     %these to 0
        for i=1:size(countz2,1)
            met8(i)=std(countz2(i,:)/max(countz2(i,:)));
        end
        j=1;
192     for i=1:length(met8)
            if isnan(met8(i))
                met82(i)=0;
            else
                met82(i)=met8(i);
```

```matlab
197             end
        end
    %***** Metric 10 - evenness of data at "low" Q *****
        metric(8+2*mi)=mean(met82);
    end
202
    %Isolate region of "high" Q
    mll=9+2*mi;
    countz3=[z(1:zeroqpos-pm0(mi),:);z(zeroqpos+pm0(mi):size(z,1),:)];
    countz32=0;
207 for i=1:size(countz3,1)
        for j=1:size(countz3,2)
            if countz3(i,j)>0
                countz32=countz32+1;
            end
212     end
    end
    %***** Metric 11 - total percentage of "high" Q cells with data ...
        points ****
    metric(mll)=100*countz32/(size(countz3,1)*size(countz3,2));

217 %***** Metric 12 - Avg # data points per cell at "high" Q *****
    metric(mll+1)=mean(mean(countz3));

    %There may be NaN's in metric calculation after normalization - ...
        change
    %these to 0
222
    for i=1:size(countz3,1)
        met10(i)=std(countz3(i,:)/max(countz3(i,:)));
    end
    j=1;
227 for i=1:length(met10)
        if isnan(met10(i))
            met102(i)=0;
        else
            met102(i)=met10(i);
232     end
    end

    %***** Metric 13 - evenness of data at "high" Q *****
    metric(mll+2)=mean(met102);
237 end
```

A.4   Final RSP calculation M-file

```matlab
function [rsp,as,qs,z]=RSP(pos2,rate2,that,dt,bounds,steps,maxN0,...
    pm0)

%extract AoA and Q bounds of regressor space
aextrema=bounds(1,:);
qextrema=bounds(2,:);

%extract step sizes for AoA and Q for regressor space ...
    discretization
astep=steps(1);
qstep=steps(2);

%All AoA values
arange=aextrema(1):astep:aextrema(2);

%All Q values
qrange=qextrema(1):qstep:qextrema(2);

%Create 2D Mesh for discretized regressor space
[as,qs]=meshgrid(...
    mean(arange(1:2)):astep:mean(arange(length(arange)-1:length(...
        arange))),...
    mean(qrange(1:2)):qstep:mean(qrange(length(qrange)-1:length(...
        qrange))));

%Z-axis of 3D plot of regressor map (number of data points per ...
    cell)
z=zeros(size(as));
NOBS=0;

%Make AoA's (pos variables) and Q values same length
pos3=zeros(1,length(pos2)-1);

for i=2:length(pos2)
    pos3(i-1)=mean(pos2(i-1:i));
end

%Loop through AoA's to mark which cell each point lies
for i=1:length(rate2)
    if rate2(i)>=qextrema(1) && rate2(i)<=qextrema(2);
        if pos3(i)>=aextrema(1) && pos3(i)<=aextrema(2);

            %Find which AoA cell it is in
            for j=1:length(arange)-1
                if pos3(i)<=arange(j+1)
                    apos=j;
                    break
                end
            end
            %Find which Q cell
```

124

```matlab
            for j=1:length(qrange)-1
                if rate2(i)<=qrange(j+1)
                    qpos=j;
                    break
                end
            end
            %Increment "number of data points per cell" counter
            z(qpos,apos)=z(qpos,apos)+1;
            NOBS=NOBS+1;
            end
        end
    end

    asteps=size(z,2);
    qsteps=size(z,1);

    %Examine the evenness of the data in AoA and Q and count
    rspa=zeros(asteps,1);
    rspq=zeros(qsteps,1);
    counth=0;
    for i=1:asteps
        for j=1:qsteps
        %For every loop sum the number of hits for each AoA
        rspa(i)=rspa(i)+z(j,i);
        %Every loop sum the number of hits for each Q
        rspq(j)=rspq(j)+z(j,i);
        %Keeping track of how many cells are hit
        if z(j,i)>0
            counth=counth+1;
        end
        end
    end

    %Examine the data points on the boundaries
    countb=0;
    total=0;
    j=asteps;

    %Left and right boundaries
    for i=1:qsteps
        if z(i,1)~=0
            countb=countb+1;
        end
        total=total+1;
        if z(i,j)~=0
            countb=countb+1;
        end
        total=total+1;
    end
    j=qsteps;
```

```matlab
    %Top and bottom boundaries , making sure to not double count the ...
        corners
 98 for i=2:asteps-1
        if z(1,i)~=0
            countb=countb+1;
        end
        total=total+1;
103     if z(j,i)~=0
            countb=countb+1;
        end
        total=total+1;
    end
108
    %Find the location of zero pitch rate
    for i=1:qsteps
        if 0<=qrange(i+1)
            zeroqpos=i;
113         break
        end
    end

    %Count the total number of data points at 0 Q
118 countz=zeros(asteps,1);
    j=zeroqpos;
    for i=1:asteps
            countz(i)=z(j,i);
    end
123
    %Cap max number of data points in a given cell (if desired)
    countz12=0;
    for i=1:asteps
        if countz(i)>maxN0
128         countz(i)=maxN0;
        end
        if countz(i)>0
            countz12=countz12+1;
        end
133 end

    %Isolate region of "low" Q (excluding region of 0Q)
    countlq=0;
        countlq2=[z(zeroqpos-pm0:zeroqpos-1,:);z(zeroqpos+1:zeroqpos+...
            pm0,:)];
138     %Cap max number of data points per cell (if desired)
        for i=1:size(countlq2,2)
            for j=1:size(countlq2,1)
                if countlq2(j,i)>maxN0
                    countlq2(j,i)=maxN0;
143             end
                if countlq2(j,i)>0
                    countlq=countlq+1;
                end
```

```matlab
                end
148     end
    sizelq=size(countlq2,1)*size(countlq2,2);

    %Isolate region of "high" Q
    counthq2=[z(1:zeroqpos-pm0,:);z(zeroqpos+pm0:size(z,1),:)];
153 counthq=0;
    for i=1:size(counthq2,2)
        for j=1:size(counthq2,1)
            if counthq2(j,i)>maxN0
                counthq2(j,i)=maxN0;
158         end
            if counthq2(j,i)>0
                counthq=counthq+1;
            end
        end
163 end
    sizehq=size(counthq2,1)*size(counthq2,2);

    %RSP calcs
    rspalq=zeros(size(countlq2,2),1);
168 rspqlq=zeros(size(countlq2,1),1);
    rspahq=zeros(size(counthq2,2),1);
    rspqhq=zeros(size(counthq2,1),1);
    for j=1:size(countlq2,1)
        for i=1:size(countlq2,2)
173         rspalq(i)=rspalq(i)+countlq2(j,i);
        %Every loop is summing the number of hits for each Q
            rspqlq(j)=rspqlq(j)+countlq2(j,i);
        end
    end
178 for j=1:size(counthq2,1)
        for i=1:size(counthq2,2)
            rspahq(i)=rspahq(i)+counthq2(j,i);
        %Every loop is summing the number of hits for each Q
            rspqhq(j)=rspqhq(j)+counthq2(j,i);
183     end
    end

    %Pearson Calc
    rho1=zeros(length(pos3),1);
188 rho2=zeros(length(pos3),1);
    rho3=zeros(length(pos3),1);
    mean3=mean(pos3);
    mean2=mean(rate2);
    for i=1:length(pos3)
193     rho1(i)=(pos3(i)-mean3)*(rate2(i)-mean2);
        rho2(i)=(pos3(i)-mean3)^2;
        rho3(i)=(rate2(i)-mean2)^2;
    end

198 %***** RSP 1 - total percentage of cells with data points *****
```

```matlab
    rsp (1) =100* counth /( asteps * qsteps );

    %***** RSP 2 - total percentage of boundary cells with data points...
        *****
    rsp (2) =100* countb / total ;
203
    %***** RSP 3 & 4 - Evenness of data in AoA and Q respectively ...
        *****
    rsp (3:4) =[ std ( rspa /( asteps )) std ( rspq /( qsteps ))];

    %***** RSP 5 - total percentage of 0 Q cells with data points ...
        *****
208 rsp (5) =100* countz12 / asteps ;

    %***** RSP 6 - Avg # data points per cell at 0 Q *****
    rsp (6) =mean ( countz );

213 %***** RSP 7 - evenness of data at 0 Q *****
    rsp (7) =std ( countz / asteps );

    %***** RSP 8 - total percentage of "low" Q cells with data points ...
        *****
    rsp (8) =100* countlq /( sizelq );
218
    %***** RSP 9 - Avg # data points per cell at "low" Q *****
    rsp (9) =mean ( mean ( countlq2 ));

    %***** RSP 10 & 11 - evenness of data at "low" Q *****
223 rsp (10:11) =[ std ( rspalq / size ( countlq2 ,2)) std ( rspqlq / size ( countlq2...
        ,1))];

    %***** RSP 12 - total percentage of "high" Q cells with data ...
        points *****
    rsp (12) =100* counthq /( sizehq );

228 %***** RSP 13 - Avg # data points per cell at "high" Q *****
    rsp (13) =mean ( mean ( counthq2 ));

    %***** RSP 14 & 15 - evenness of data at "high" Q *****
    rsp (14:15) =[ std ( rspahq / size ( counthq2 ,2)) std ( rspqhq / size ( counthq2...
        ,1))];
233
    %***** RSP 16 - Training Maneuver Effectiveness *****
    rsp (16) =NOBS / length ( rate2 );

    %***** RSP 17 - Time Effectiveness1 *****
238 rsp (17) =rsp (1) /max ( that );

    %***** RSP 18 - Time Effectiveness2 *****
    rsp (18) =rsp (1) *dt /max ( that );

243 %***** RSP 19 & 20 & 21 Time Eff 0Q, LQ, HQ ****
```

```matlab
    rsp(19:21)=[rsp(5)/max(that) rsp(8)/max(that) rsp(12)/max(that)];

    %***** RSP 22 & 23 - Kurtosis Alpha & Q *****
    rsp(22:23)=[kurtosis(rspa) kurtosis(rspq)];
248
    %***** RSP 24 & 25 - Skewness Alpha & Q *****
    rsp(24:25)=[skewness(rspa) skewness(rspq)];

    %***** RSP 26 - Pearson product-moment correlation coefficient
253 rsp(26)=sum(rho1)/sqrt(sum(rho2)*sum(rho3));

    %***** RSP 27 & 28 Kurtosis and Skewness OQ *****
    rsp(27:28)=[kurtosis(countz) skewness(countz)];

258 %***** RSP 29 & 30 Kurtosis LQ AoA / Q ****
    rsp(29:30)=[kurtosis(rspalq) kurtosis(rspqlq)];

    %***** RSP 31 & 32 Skewness LQ AoA / Q ****
    rsp(31:32)=[skewness(rspalq) skewness(rspqlq)];
263
    %***** RSP 33 & 34 Kurtosis HQ AoA / Q ****
    rsp(33:34)=[kurtosis(rspahq) kurtosis(rspqhq)];

    %***** RSP 35 & 36 Skewness HQ AoA / Q ****
268 rsp(35:36)=[skewness(rspahq) skewness(rspqhq)];


    end
```

B. Figures with TM5 included
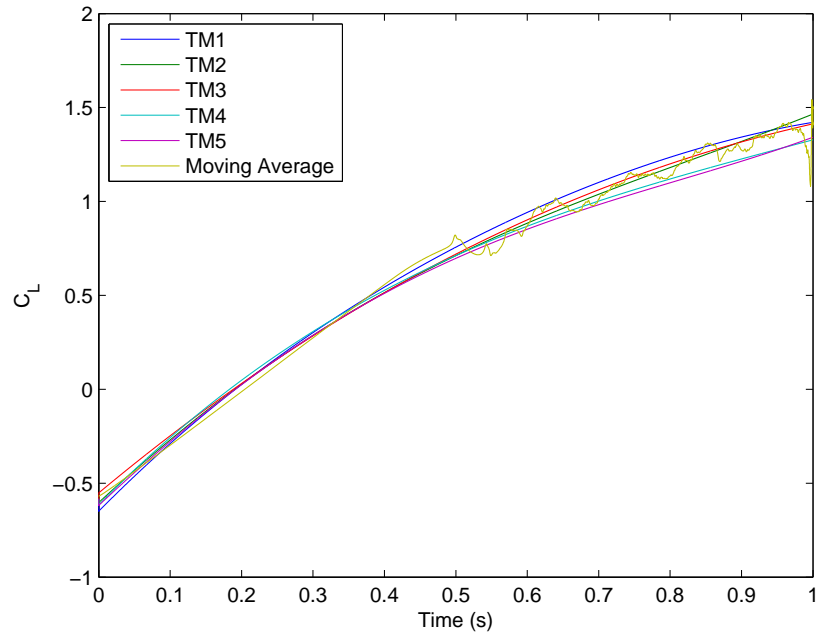
Figure 69. Model Results COM1a C_L
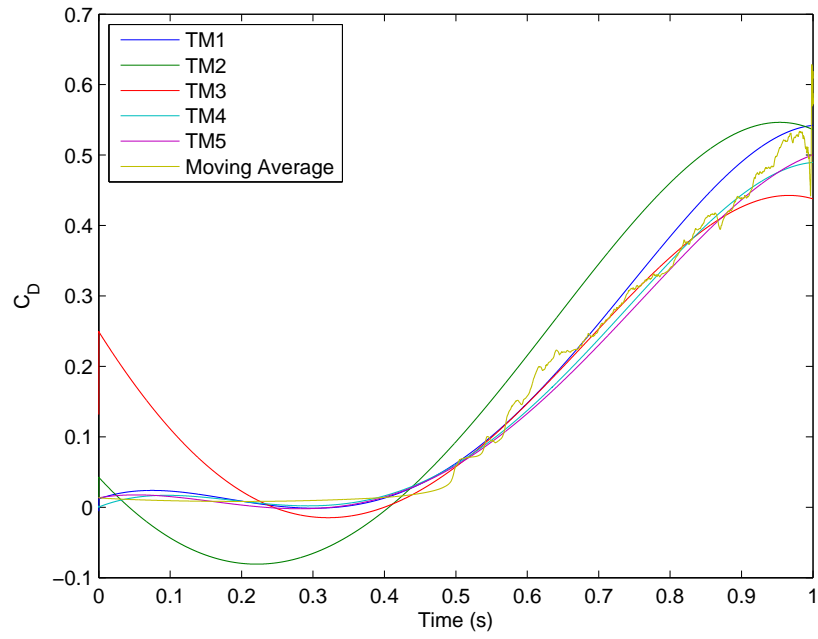
Figure 70. Model Results COM1a C_D
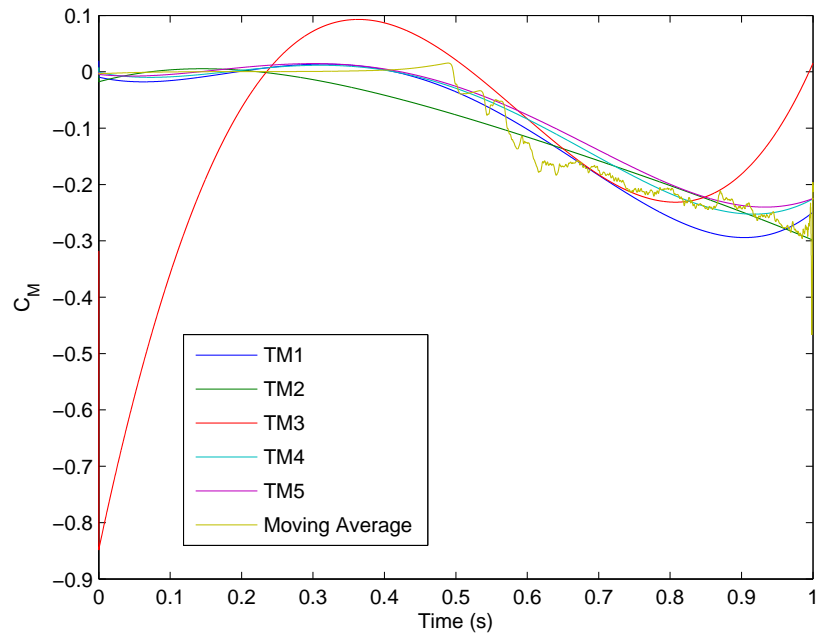
Figure 71. Model Results COM1a C_M

Figure 72. Model Results COM1b C_L
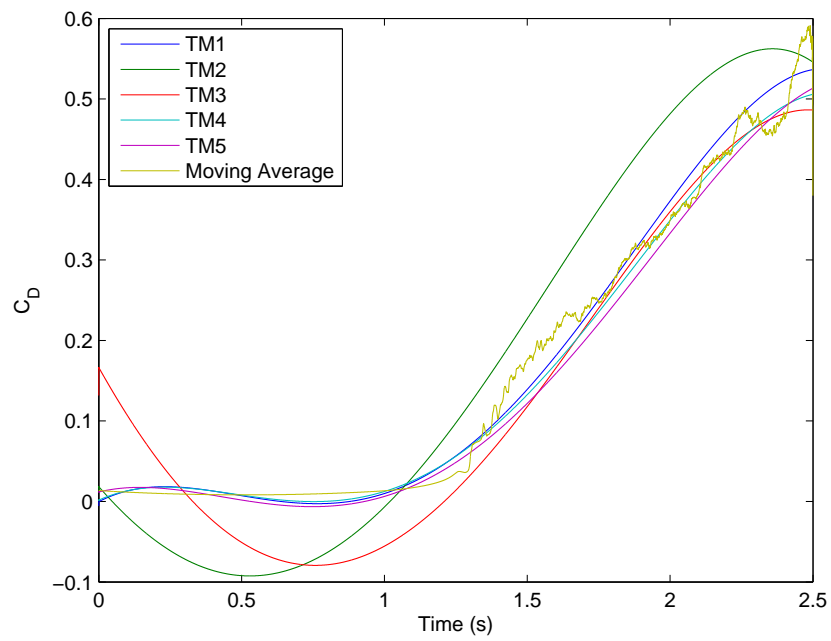
Figure 73. Model Results COM1b C_D
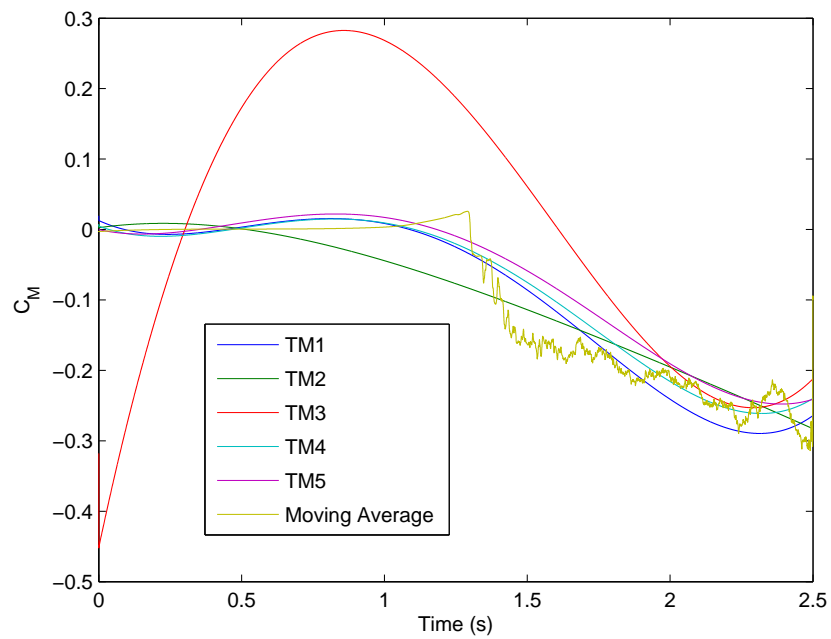
Figure 74. Model Results COM1b C_M
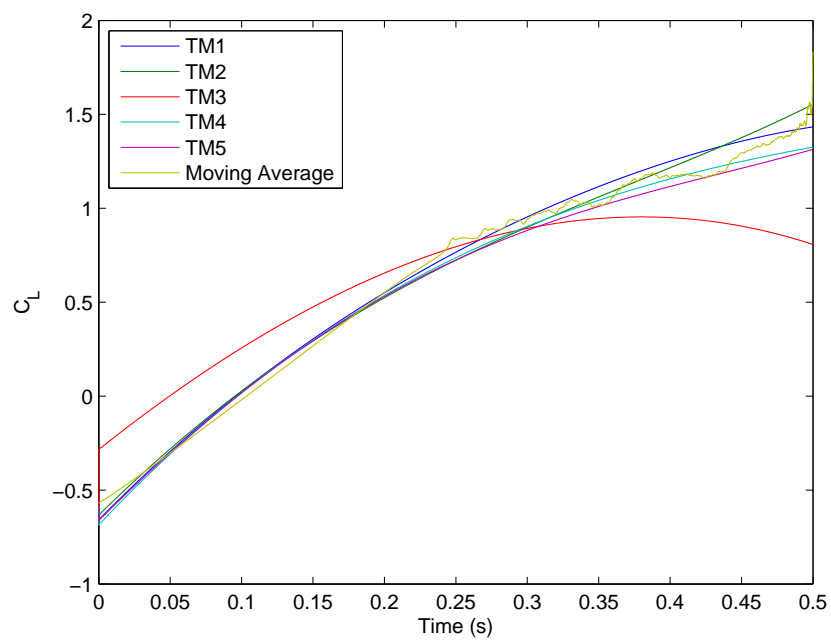
Figure 75. Model Results COM1c C_L

133
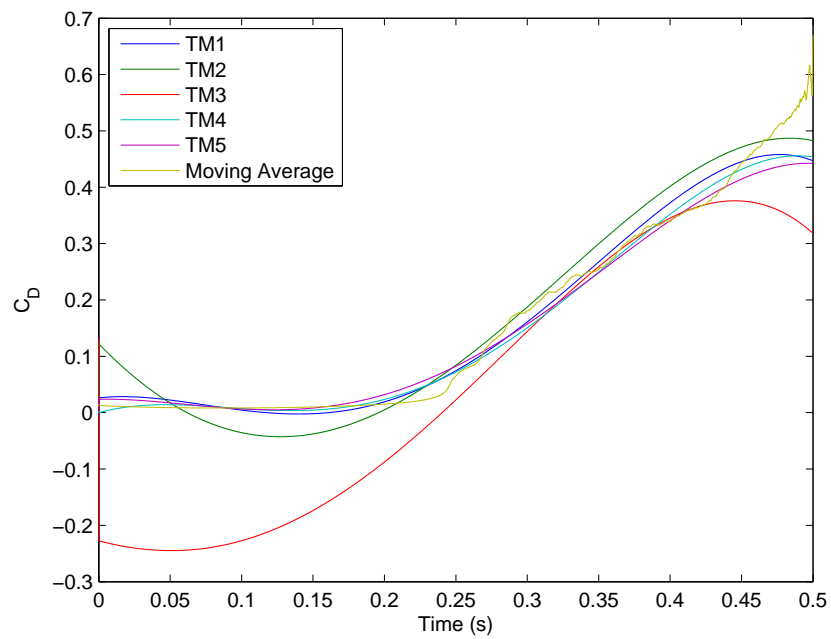
Figure 76. Model Results COM1c C_D
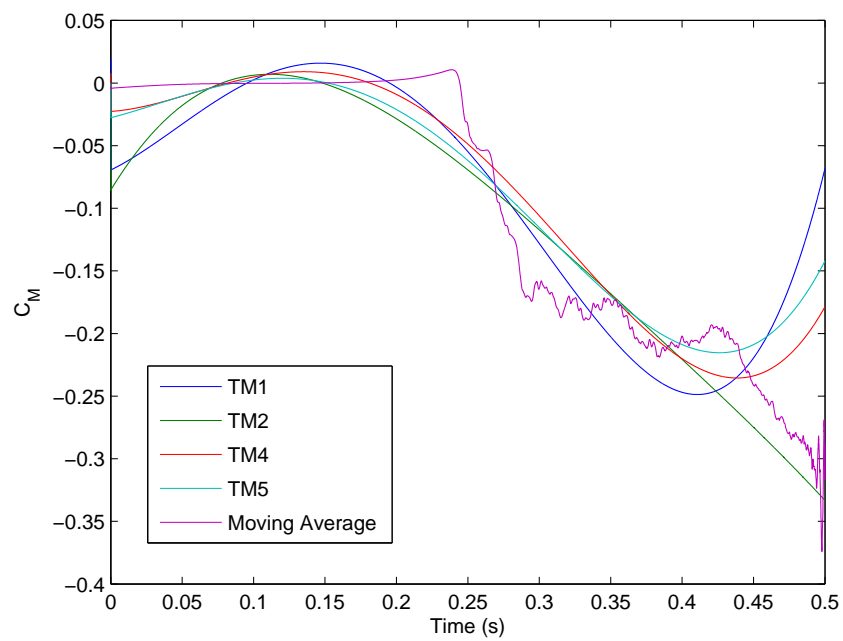
Figure 77. Model Results COM1c C_M

134
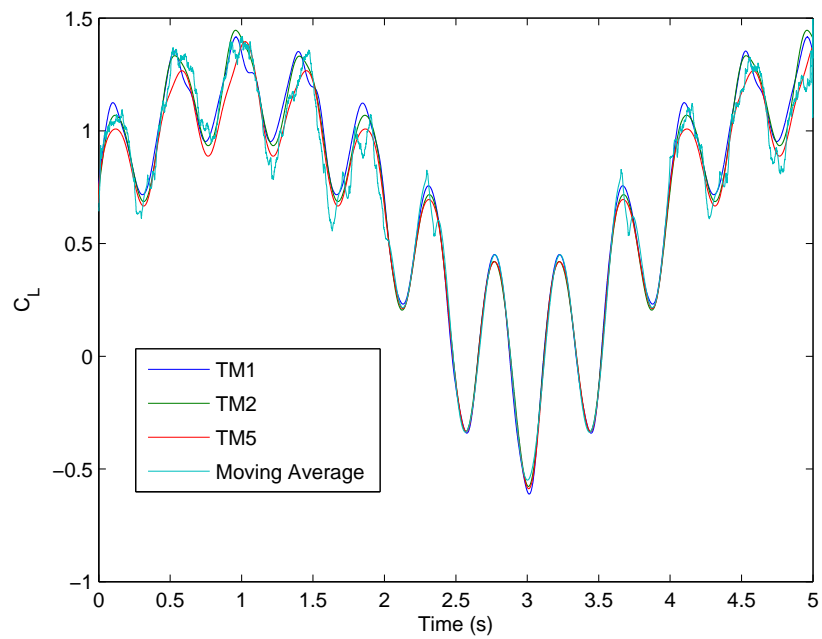
Figure 78. Model Results COM2 C_L
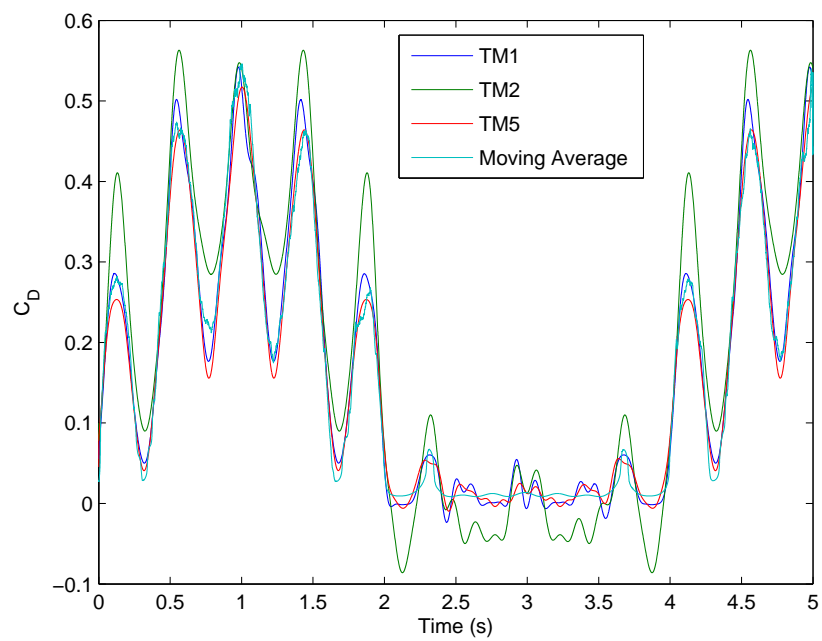
Figure 79. Model Results COM2 C_D

135
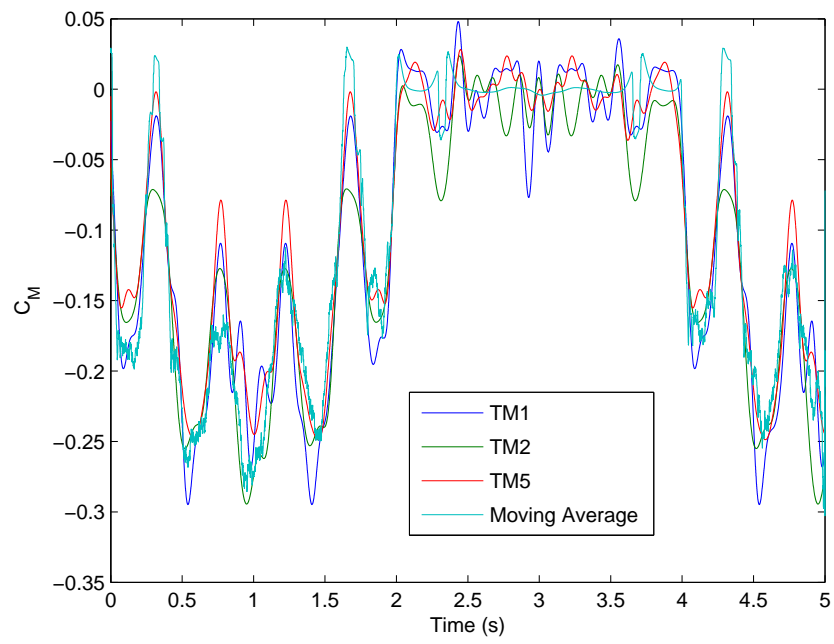
Figure 80. Model Results COM2 C_M
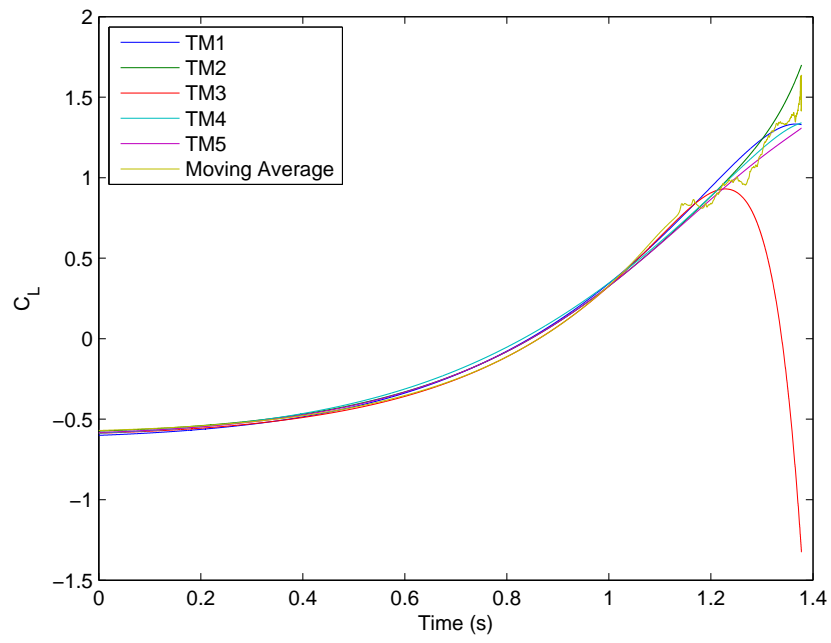
Figure 81. Model Results COM3 C_L
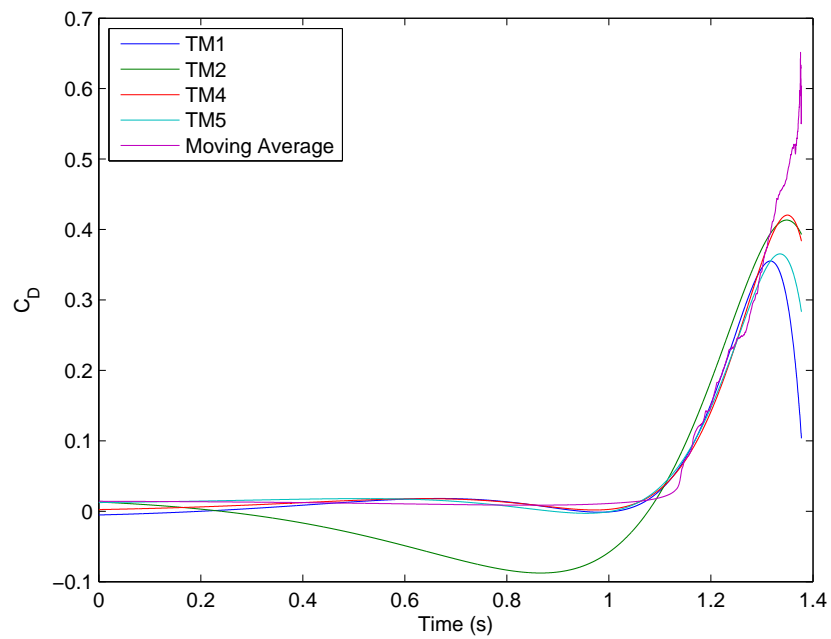
Figure 82. Model Results COM3 C_D
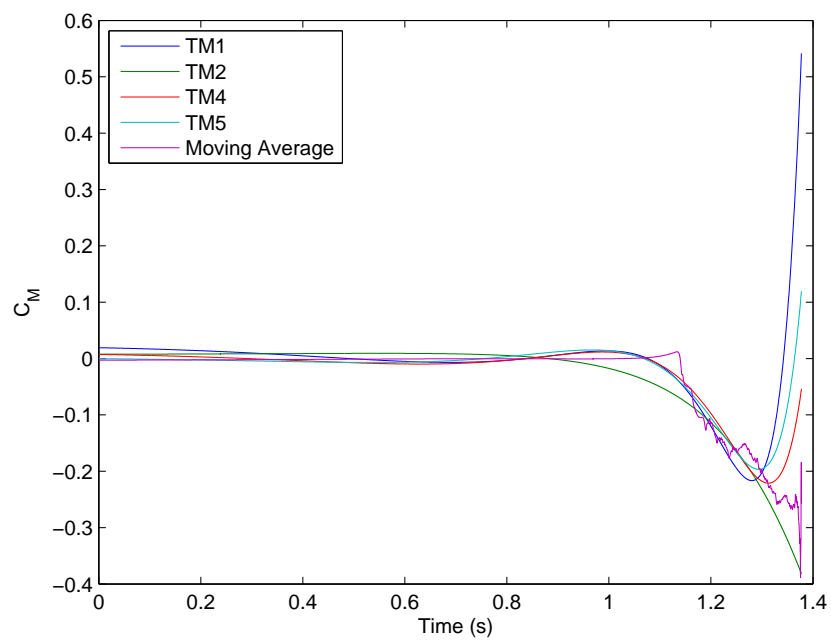
Figure 83. Model Results COM3 C_M

138
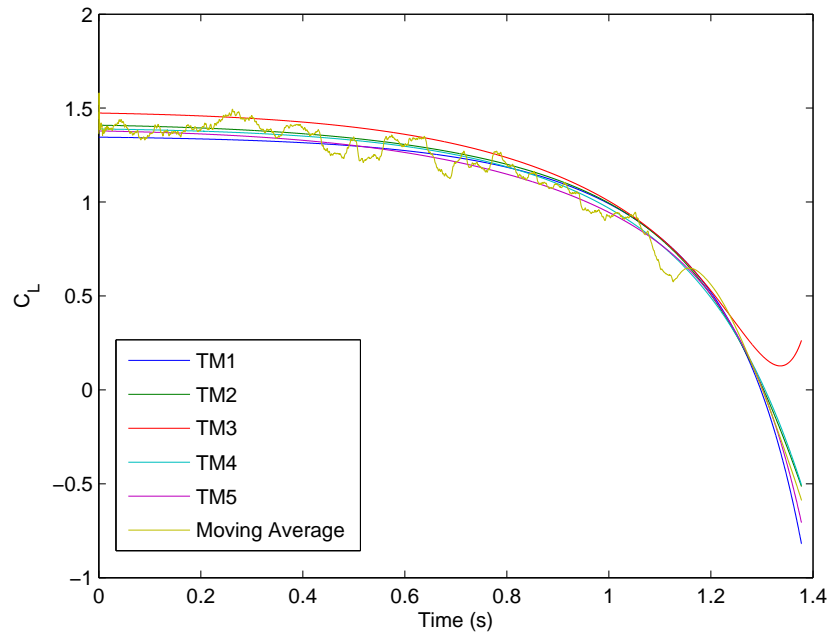
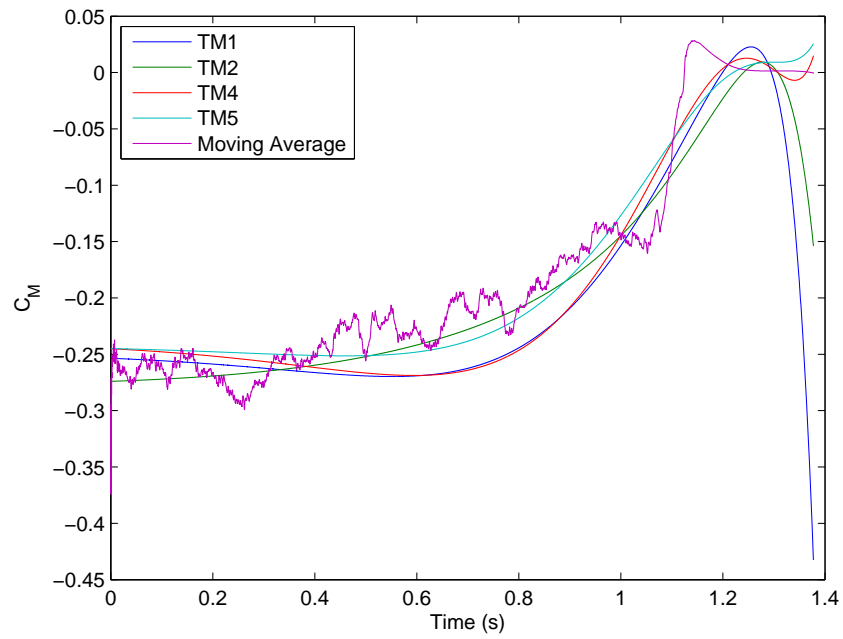**Figure 84. Model Results COM4 C_L**
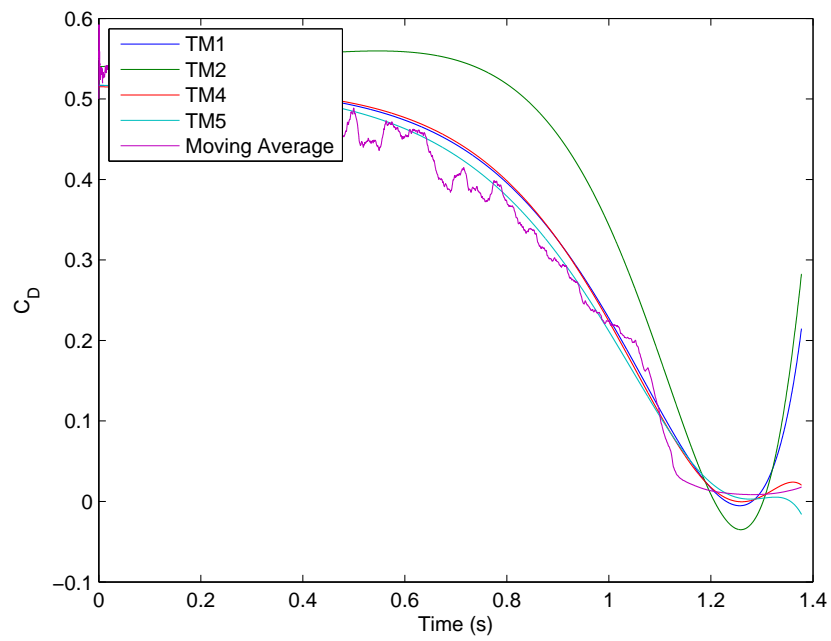
Figure 85. Model Results COM4 C_D
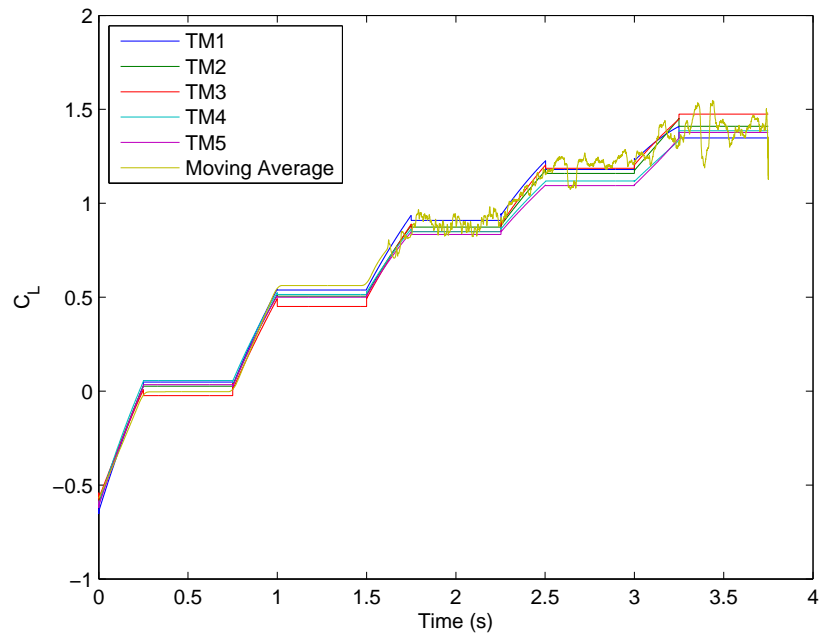
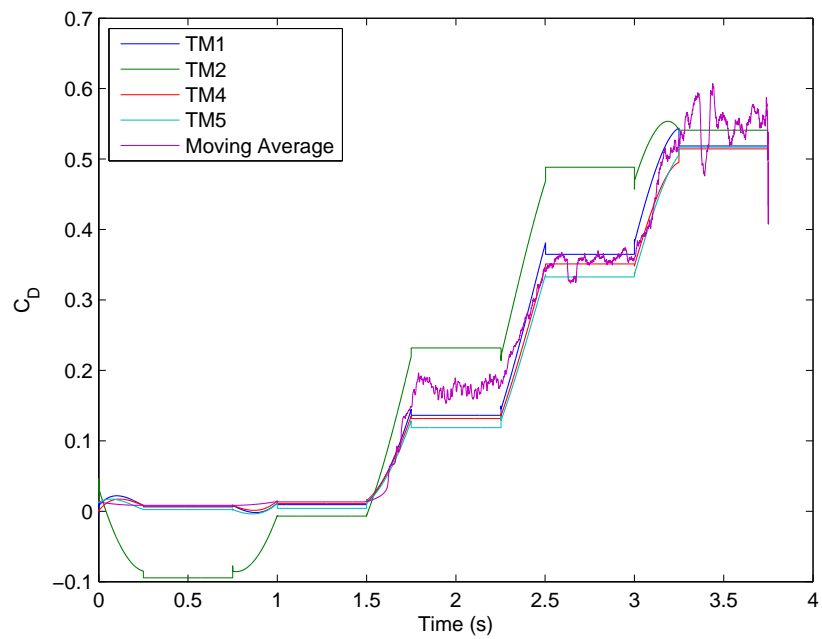**Figure 86. Model Results COM4** C_M

Figure 87. Model Results COM5 C_L
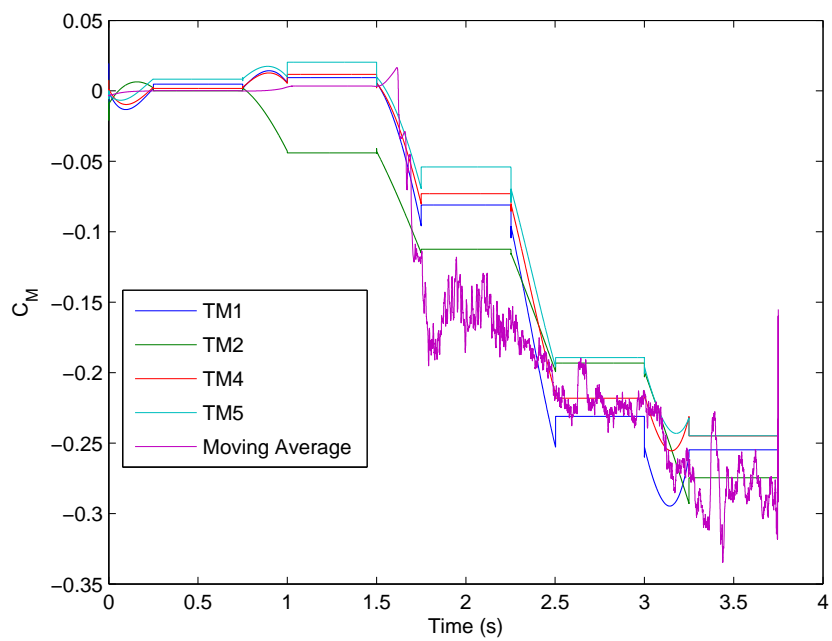
Figure 88. Model Results COM5 C_D

Figure 89. Model Results COM5 C_M

141

Bibliography

[1] "DEPARTMENT OF AERONAUTICS AND ASTRONAUTICS DEPART-MENT BROCHURE". Wright-Patterson Air Force Base, Ohio, 2012.

[2] AFRL. "Cray XE6 (Raptor) User Guide". Online, October 2012.

[3] Army, US. "Fixed-Wing Aerodynamics and Performance". Online.

[4] Blazek, Jiri. *Computational Fluid Dyanmics: Principles and Applications*. Elsevier, second edition, 2005.

[5] Butler, Jedediah H. *Accurate Modeling of Stability & Control Properties for Fighter Aircraft from CFD*. Master's thesis, Graduate School of Engineering, Air Force Institute of Technology (AETC), Wright-Patterson AFB OH, March 2012. AFIT/GAE/ENY/12-M04.

[6] Cebeci, T. and A.M.O Smith. "Analysis of Turbulent Boundary Layers".

[7] Chaderjian, N. M., S. Pandya J. Ahmad, and S. Murman. "Progress Toward Generation of a Navier-Stokes Database for a Harrier in Ground Effect". *AIAA*, 2002.

[8] CREATE-AV. *Kestrel User's Guide Version 3.0*. Department of Defense High Performance Computating Modernization Program, 2012.

[9] Cummings, R.M., S.A. Morton, D.R. McDaniel, J.R. Forsythe, and D.C. Blake. "Compuational Fluid Dynamics". Course Notes for AE 342, Department of Aeronautics, United States Air Force Academy.

[10] Cummings, Russell M., Scott A. Morton, and David R. McDaniel. "Experiences in accurately predicting time-dependent flows". *Progress in Aerospace Sciences*, 44(4):241–257, May 2008.

[11] Dean, John P., James D. Clifton, David J. Bodkin, and C. Justin Ratcliff. "High Resolution CFD Simulations of Maneuvering Aircraft Using the CREATE-AV/Kestrel Solver". *49th AIAA Aerospace Sciences Meeting including the New Horizons Forum and Aerospace Exposition*. American Institution of Aeronautics and Astronautics, Orlando, Florida, January 2011. CD Proceedings.

[12] Dean, John P., Scott A. Morton, James D. Clifton, and David J. Bodkin. "Aircraft Stability and Control Characteristics Determined by System Identification of CFD Simulations". *AIAA Atmospheric Flight Mechanics Conference and Exhibit*. American Institution of Aeronautics and Astronautics, Honolulu, Hawaii, August 2008. CD Proceedings.

[13] Dean, John P., Scott A. Morton, David R. McDaniel, and Stefan Görtz. "Efficient High Resolution Modeling of Fighter Aircraft with Stores for Stability and Control Clearance". *U.S. Air Force T&E Days.* American Institution of Aeronautics and Astronautics, Destin, Florida, February 2007. CD Proceedings.

[14] Fremaux, Michael C. and Robert M. Hal. "COMSAC: Computational Methods for Stability and Control". *NASA/CP-2004-213028/PT1.* NASA, Hampton, Virginia, April 2004. CD Proceedings.

[15] Görtz, Stephan, David R. McDaniel, and Scott A. Morton. "Towards an Efficient Aircraft Stability and Control Analysis Capability using High-Fidelity CFD". *45th AIAA Aerospace Sciences Meeting and Exhibit.* American Institution of Aeronautics and Astronautics, Reno, Nevada, January 2007. CD Proceedings.

[16] Jeans, Tiger L., Adam Jirasek, David R. McDaniel, Keith Bergeron, and Russell M. Cummings. "Modeling the Nonlinear Dynamic Roll of a Generic Fighter Using Delayed Detached-Eddy Simulation". *Journal of Aircraft*, 49(2), 2012.

[17] Jeans, Tiger L., David R. McDaniel, Russell M. Cummings, and Keith Bergeron. "Lower-Order Aerodynamic Loads Modeling of a Maneuvering Generic Fighter Using DDES Simulations". *47th AIAA Aerospace Sciences Meeting Including The New Horizons Forum and Aerospace Exposition.* American Institution of Aeronautics and Astronautics, Orlando, Florida, January 2009. CD Proceedings.

[18] Jirasek, Adam and Russell M. Cummings. "Reduced Order Modeling of X-31 Wind Tunnel Model Aerodyanmic Loads". *28th AIAA Applied Aerodynamics Conference.* AIAA, Chicago, Illinois, July 2010. CD Proceedings.

[19] Jirasek, Adam, Tiger L. Jeans, Matthew Martenson, Russell M. Cummings, and Keith Bergeron. "Improved Methodologies for Maneuver Design of Aircraft Stability and Control Simulations". *48th AIAA Aerospace Sciences Meeting Including the New Horizons Forum and Aerospace Exposition.* American Institution of Aeronautics and Astronautics, Orlando, Florida, January 2010. CD Proceedings.

[20] Klein, Vladislav and Eugene A. Morelli. *Aircraft System Identification: Theory and Practice.* AIAA, Reston, VA, 2006.

[21] Lillian, Chad S, Scott A. Morton, and David R. McDaniel. "Aircraft Loads Characteristics Determined by System Identification and Proper Orthogonal Decomposition of CFD Simulations". *28th AIAA Applied Aerodyanmics Conference.* American Institution of Aeronautics and Astronautics, Chicago, Illinois, July 2010. CD Proceedings.

[22] Mathworks®, Natick, MA. *Statistics Toolbox^{TM} Users Guide R2012b*, 2012.

[23] Morelli, Eugene A. "SYSTEM IDENTIFICATION PROGRAMS FOR AIR-CRAFT (SIDPAC)". *AIAA Atmospheric Flight Mechanics Conference and Exhibit.* American Institution of Aeronautics and Astronautics, Montery, California, August 2002. CD Proceedings.

[24] Morton, Scott A., David R. McDaniel, David R. Spears, Brett Tillman, and Todd R. Tuckey. "Kestrel - A Fixed Wing Virtual Aircraft Product of the CREATE Program". *47th AIAA Aerospace Sciences Meeting including the New Horizons Forum and Aerospace Exposition.* American Institution of Aeronautics and Astronautics, Orlando, Florida, January 2009. CD Proceedings.

[25] Press, William H., Saul A. Teukolsky, William T. Vetterling, and Brian P. Flannery. *Numerical Recipes.* Cambridge University Press, third edition, 2007.

[26] SAS Institute Inc. *JMP® 10 Modeling and Multivariate Methods.* SAS Institute Inc, Cary, NC, 2012.

[27] Spalart, P. R., S. Deck, M. L. Shur, K. D. Squires, M. Kh. Strelets, and A. Travin. "A new version of detached-eddy simulation, resistant to ambiguous grid densities". *Theor. Comput. Fluid Dyn*, 20:181–195, 2006.

[28] Spalart, Philippe R. *Young-Person's Guide to Detached-Eddy Simulation Grids.* Contractor Report NASA/CR-2001-211032, NASA, Boeing Commercial Airplanes, Seattle, Washington, July 2001.

[29] Spalart, P.R. and S.R. Allmaras. "A One-Equation Turbulence Model for Aerodynamic Flows". *30th AIAA Aerospace Sciences Meeting & Exhibit.* American Institution of Aeronautics and Astronautics, Reno, NV, 1992. CD Proceedings.

[30] Tomaro, R., W. Strang, and L.N. Sankar. "An Implicit Algorithm for Solving Time Dependent Flows on Unstructured Grids". *35th Aerospace Sciences Meeting and Exhibit.* Reno, NV, 1997.

[31] Yechout, Thomas R., Steven L. Morris, David E. Bossert, and Wayne F. Hallgren. *Introduction to Aircraft Flight Mechanics: Performance, Static Stability, Dynamic Stability, and Classical Feedback Control.* AIAA, 2003.

Vita

Second Lieutenant Craig Porter was born in Reston, Virginia and grew up in Mendon, New York. After graduating from Honeoye Falls-Lima High School, he studied aeronautical engineering at the United States Air Force Academy (USAFA). He graduated with his Bachelor's degree in Aeronautical Engineering and was commissioned into the United States Air Force in May of 2011. Following USAFA, he entered graduate school at the Air Force Institute of Technology (AFIT) in August of 2011 and he is currently completing his Master's degree. His anticipated follow-on assignment is with the 773d Test Squadron at Edwards AFB.

REPORT DOCUMENTATION PAGE

1. REPORT DATE *(DD–MM–YYYY)*	2. REPORT TYPE	3. DATES COVERED *(From — To)*
27–03–2013	Master's Thesis	Aug 2011 — Mar 2013

4. TITLE AND SUBTITLE

Training Maneuver Evaluation for Reduced Order Modeling of Stability & Control Properties Using Computational Fluid Dynamics

5a. CONTRACT NUMBER

5b. GRANT NUMBER

5c. PROGRAM ELEMENT NUMBER

6. AUTHOR(S)

Porter, Craig C., 2d Lt, USAF

5d. PROJECT NUMBER

5e. TASK NUMBER

5f. WORK UNIT NUMBER

7. PERFORMING ORGANIZATION NAME(S) AND ADDRESS(ES)

Air Force Institute of Technology
Graduate School of Engineering and Management (AFIT/EN)
2950 Hobson Way
WPAFB OH 45433-7765

8. PERFORMING ORGANIZATION REPORT NUMBER

AFIT-ENY-13-M-28

9. SPONSORING / MONITORING AGENCY NAME(S) AND ADDRESS(ES)

(intentionally left blank)

10. SPONSOR/MONITOR'S ACRONYM(S)

11. SPONSOR/MONITOR'S REPORT NUMBER(S)

12. DISTRIBUTION / AVAILABILITY STATEMENT

DISTRIBUTION A.: APPROVED FOR PUBLIC RELEASE; DISTRIBUTION UNLIMITED.

13. SUPPLEMENTARY NOTES

14. ABSTRACT

System identification has long been used as a tool for flight test engineers to characterize systems under test. There has been a recent effort to incorporate computational fluid dynamics (CFD) into the system identification process. An integral piece of the process is the simulation of training maneuvers utilizing CFD. This research strives to recommend a set of parameters to be used in determining whether a training maneuver will be suitable under a particular set of flow conditions. Regressor space parameters (RSPs) were proposed and evaluated for several maneuvers. Model-predicted coefficient values were compared to CFD simulations of comparison maneuvers, measured by a set of suitable statistical metrics. Using statistical analysis, the set of proposed RSPs were then analyzed in order to evaluate their utility in assessing the suitability of the training maneuvers. This research showed the reliable capability of certain RSPs to characterize training maneuver performance. Finally, lessons learned from this research were applied to improve on current best practice training maneuvers.

15. SUBJECT TERMS

System Identification, Reduced Order Modeling, Computational Fluid Dynamics

16. SECURITY CLASSIFICATION OF:

a. REPORT	b. ABSTRACT	c. THIS PAGE
U	U	U

17. LIMITATION OF ABSTRACT

U

18. NUMBER OF PAGES

162

19a. NAME OF RESPONSIBLE PERSON
Capt Christopher L. Martin

19b. TELEPHONE NUMBER *(include area code)*
(937) 785-3636, x4403 937-255-3636 x 4403